3D modeling and simulation of morphogenesis

Athanasios Lontos

UNIVERSITÉ DE GRENOBLE

THÈSE

Pour obtenir le grade de

DOCTEUR DE L'UNIVERSITÉ DE GRENOBLE

Spécialité : **Informatique**

Arrêté ministériel : 7 août 2006

Présentée par

Athanasios Lontos

Thèse dirigée par **Emmanuel Promayon** et
codirigée par **Jacques Demongeot**

préparée au sein du **Laboratoire TIMC IMAG**
dans **l'École Doctorale Mathématiques, Sciences et Technologie de l'Information et Informatique**

Modélisation et simulation 3D de la morphogenèse

Thèse soutenue publiquement le **« 6 décembre 2013 »**,
devant le jury composé de :

Mme. Danielle Dhouailly
Professeur Université Joseph Fourier, Président

Mme. Nadine Peyriéras
Directrice de Recherche CNRS Institut de Neurobiologie Alfred Fessard, Rapporteur

M. Vitaly Volpert
Directeur de Recherche CNRS Institut Camille Jordan, Rapporteur

M. Luis Almeida
Directeur de Recherche CNRS Laboratoire Jacques-Louis Lions, Examinateur

M. Emmanuel Promayon
Maître de Conférences Université Joseph Fourier, Directeur de Thèse

M. Jacques Demongeot
Professeur Université Joseph Fourier, Co-Directeur de Thèse

Acknowledgements

First of all, I would like to thank the members of my jury: Nadine Peyriéras and Vitaly Volpert for reading my manuscript and providing valuable corrections and suggestions, Luis Almeida for his questions and insight concerning future work and Danielle Dhouailly for accepting to preside over the presentation.

I would like to express my deepest gratitude to my two supervisors, Emmanuel Promayon and Jacques Demongeot. Mahnu, for always being there for me whenever I needed guidance or support (it helped that I was in the office next-door) and Jacques for providing the ideas and stimuli to keep going in this multi-disciplinary subject.

The two main frameworks used during the course of this work are SOFA and CamiTK. So, I would like to thank all the people whose work contributes to making these frameworks better, more sophisticated and friendlier to the user.

A big “thank you” to all the members of team GMCAO. We have created a wonderful working environment and I will miss working with you. The excellent ambience between the members of the team is one of the reasons I chose to do a PhD in this team and I don't regret it at all.

More in particular, I want to express my gratitude to all the people who helped me feel wellcome in Grenoble, although coming from a foreign country:
Xavi, my flatmate for the last 3 years and Kumai, flatmate for more than 2 years. Our conversations with Xavi are precious and Kumai, although not very talkative, was always there for me.
Yannick and Nico, the CamiTK engineers I've worked with, have helped me become familiar with the framework and facilitated my work.
Laure and Arnaud for organizing the basketball sessions and of course all the people in the basketball team. It was a wellcome break from everyday's routine.
All the coinche players from the lab, but especially my coinche partner, Sonia. Because playing cards is great and winning tournaments is even greater.
Johan, my workmate. We shared the same office for 1 year and he crashed his PC trying to help me create a video one day before defending. I am not sure he will feel the same for me though...
My friends and family from Greece who came for my defence and gave me the courage I needed to pull it off. They have also supported and tolerated me for all these years which is enough of a handfull on its own.

Finally, I want to thank you dear reader for taking the time to discover all the “treasures” hidden in the next pages.

Contents

Chapter 1

Introduction

Contents

Back in December 1942, C. H. Waddington made the following statement: "Recent years have seen considerable advances in our knowledge of chemical interactions between different parts of developing embryos, and of the metabolic processes by which the stimulating evocators are released. We have also acquired further information, on the biological level, of the correlations between parts which lead to the formation of units organized into definite patterns. On the other hand, the forces which actually bring about the changes in shape which are perhaps the salient feature of early development have remained almost unstudied." [Waddington 1942].

Morphogenesis is a general concept including all the processes which generate shapes and cellular organizations in a living organism. It originates from the combination of two greek words, "$\mu o \varrho \varphi \eta$" ("morphe", which stands for form, shape) and "$\gamma \varepsilon \nu \varepsilon \sigma \iota \varsigma$" ("genesis" which stands for principle, origin, birth). Consequently, morphogenesis refers to the "Birth of forms". Other terms that are in the same scope are embryogenesis ("Creation of the embryo") and organogenesis ("Creation of the organs"). The loosness of the definition of these terms has allowed them to be enthusiastically embraced by researchers examining the factors and parameters controlling the creation of tissues, organs and ultimately life.

Biological and genetic processes are controlled by numerous factors: protein signalling, gene expression, cell cycle, chemotaxis are some of them. Changes in cell shape and structural integrity also affect the processes in a decisive manner. The bridge that connects genetic and molecular-level events to tissue-level deformations that shape the developing embryo is biomechanical forces.

A favourite organism for biological research is the Drosophila melanogaster, a small, common fly. A very important stage of morphogenesis in the drosophila is gastrulation. The early embryo performs rapid nuclei divisions followed by cellularization until the formation of the blastula, a geometrically simple closed elongated sphere or "bean-shaped" structure that consists of a single cell layer enclosing the hollow blastocoel. Gastrulation includes mass movements of cells to form complex structures (e.g. tissues) from a simple initial shape (blastula).

Ventral Furrow Invagination is an early stage of gastrulation. The process starts after the flattening of the cells on the ventral midline. The myosin of the most ventrally located cells becomes concentrated at their apical sides. This excess of myosin causes the constriction of their apical surface and a simultaneous apico-basal elongation. As a result of these cell-shape changes, the blastoderm epithelium first forms an indentation, the ventral furrow, which is then completely internalized.

The modeling of the invagination of the ventral furrow of the embryo of the Drosophila Melanogaster has been a challenging topic for a long time. Alan Turing presented a mathematical formalism for morphogenesis in the 1950s while René Thom developed a general mathematical model relying on dynamical systems in the 1960s. More recently, the study of the physical aspects of morphogenesis has been of much interest to the scientific community. With the advances on computing power, technology and techniques, complex biomechanical models were produced in order to simulate morphogenetic processes. Biomechanical models offer the opportunity to predict the outcome of a process in a simple and rapid way by testing parameters that are normally difficult to be tested *in vivo* or *in vitro*. Once these predictions are made, biologists and geneticists are provided with insight and are able to control and carry out their experiments more efficiently.

The scope of this thesis combines the fields of biology, mechanics and computer science in order to study the forces that bring the cell shape changes that Waddington mentioned. The early morphogenetic process on which this thesis in focused is the invagination of the ventral furrow of the embryo of the Drosophila Melanogaster.

1.1 Contribution of the thesis

One contribution of this work focuses on the study of the relationship between the apical constriction of the ventral cells and the invagination. In [Martin *et al.* 2008], the in vivo monitoring of the invagination in the Drosophila Melanogaster, shows that the area where the apical constriction starts differs from the area where the invagination starts. In fact, the actin-myosin contractions occur first in the ventral medial area, while the invagination starts from the ventral curved extremities and then propagates to the medial area. So the first question addressed in this thesis is: "What makes the invagination start from the curved extremities?"

We hypothesized that this observation can be explained by the unique "bean-shaped" geometry of the embryo. To test this hypothesis, I created two biomechanical models, based on two popular methods: a physically based discrete model and a model based on the Finite Element Method. The models integrate the effect of the cytoskeleton of cells as elastic forces and the effect of the myosin contraction as active contracting forces. The interplay of these forces and how the embryo geometry explains the invagination, are the central topics studied in the framework of the model developed for the embryo of the Drosophila Melanogaster.

Although the discrete model simulates efficiently the process of internalization of the ventral cells, it cannot produce a "hard" mathematical proof, as it lacks a robust physical background. In order to have a strong physical basis, the physically based discrete model was replaced by a model based on the Finite Element Method. The velocity of invaginating cells positioned in different parts of the model is monitored along with a factor that is thought to predict the tendency of a cell to divide, the cell $surface/volume$ ratio. The effect of the geometry on the interplay of active and passive forces and invagination is studied by comparing the "bean-shaped" geometry of the Drosophila embryo to a spherical model following exactly the same principles.

While both discrete and continuous model efficiently simulate the internalization of the ventral cells, none were able to simulate the ventral closure. This led us to consider that there is another factor that needs to be taken into account and integrated in the models. We hypothesized that this new factor is the proliferation of the ventral cells once internalized [Grosshans & Wieschaus 2000]. To validate this hypothesis, a mesh division and refinement technique was developed for a Finite Element Mesh. This technique was then integrated in the Finite Element model of the Drosophila embryo.

1.2 Organization of the thesis manuscript

The manuscrit is organized in 6 chapters.

Chapter 2 presents the Biological Context of this work. First, the factors that affect cell shape, movement and behaviour are presented. The morphogenetic process of the Ventral Furrow Invagination in the embryo of the Drosophila Melanogaster, which is the main focus of this thesis, is analytically described. The processes of Posterior Midgut Invagination and Germ Band Extension, which are subjects of future work, are briefly described. The Chapter finishes by explaining the first question that gave birth to this thesis.

Chapter 3 presents the existing biomechanical methods used to model morphogenetic processes. The principles of Discrete and Continuum Mechanics are introduced and compared. The discrete method of Mass-Spring Network and the Finite Element Method are explained in detail. The contribution of the different biomechanical models simulating the Ventral Furrow Invagination, that have appeared in bibliography, is discussed.

Chapter 4 presents the work done during the course of this thesis concerning the Ventral Furrow Invagination of the Drosophila Melanogaster. The Chapter is organized according to the contributions of this work in scientific articles already published in International Conferences and Journals and an article that is going to be submitted in the Journal of BMC Bioinformatics. Initially, the physically based discrete model of the embryo of the Drosophila Melanogaster is presented.

The simulated process of Ventral Furrow Invagination is explained by focusing on the changes of the whole geometry, along with the monitoring of individual cell behaviour and shape. The replacement of the discrete model by the model based on the Finite Element Method is the next topic discussed. The results of the simulations with the Finite Element model are presented focusing on the changes of the whole geometry and the shape and behaviour of individual cells. The results obtained with the FEM model confirm the ones obtained with the discrete model. Finally, the Chapter finishes by discussing the inability of the two models to simulate the ventral closure and introducing the factor we will add in our model to try to better simulate ventral closure as well.

Chapter 5 presents the modeling of the cell division. The existing methods for mesh division and refinement are briefly presented and discussed. Then, the method developed during this thesis is explained using a very simple example. Finally, the integration of the cell division method in the Finite Element Mesh is presented and evaluated concerning its effect on the closure of the ventral furrow.

Chapter 6 sums up on the contributions of this thesis and concludes on the perspectives and future work.

Chapter 2

Biological Context

Contents

In this chapter we explain the biological context of this scientific work.

2.1 Introduction

The cell is the basic structural, functional and biological unit of all known living organisms. The distinction between prokaryotes and eukaryotes is considered to be the most important distinction among groups of organisms. In Table 2.1 we present the differences between an eukaryotic and a prokaryotic cell.

Table 2.1: *Eukaryotic and Prokaryotic Cell*

	Eukaryotic Cell	**Prokaryotic Cell**
Example	Animals and Plants	Bacteria and Archaea
Nucleus	Present	Absent
Cell Type	Multicellular	Usually monocellular (some cyanobacteria may be multicellular)
Microtubules	Present	Absent
Cytoskeleton	Always present	May be absent
Cell size	10-100 μm	1-10 μm

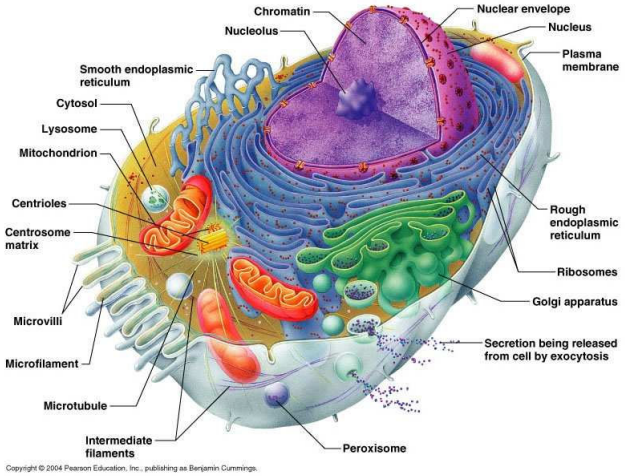

Figure 2.1: *Schematic of a typical animal cell, showing subcellular components [Marieb & Hoehn 2010].*

2.2 The Eucaryotic Cell

In Table 2.2 I give a short decription of the role of each organelle appearing in Figure 2.1. Some of the organelles (including the nucleus and the cytoskeleton) are further described because they play a critical role in cell movement, which is of great importance for this thesis. For further information, the reader may refer to `http://www.nature.com/scitable`.

Organelles	**Role**
Ribosome	The ribosome is a complex molecule made of ribosomal RNA molecules and proteins that form a factory for protein synthesis in cells. It is responsible for translating encoded messages from messenger RNA molecules to synthesize proteins from amino acids.
Endoplasmic Reticulum - ER -	A network of tubules and flattened sacs that serve a variety of functions in the cell. There are two regions of the ER that differ in both structure

	and function: the rough ER and the smooth ER.
rough ER	It manufactures membranes and secretory proteins. In certain leukocytes (white blood cells), the rough ER produces antibodies. In pancreatic cells, the rough ER produces insulin.
smooth ER	It serves as a transitional area for vesicles that transport ER products to various destinations. In liver cells it produces enzymes that help to detoxify certain compounds. In muscles, it assists in the contraction of muscle cells, and in brain cells, it synthesizes male and female hormones.
Golgi apparatus (Golgi complex)	It is responsible for manufacturing, warehousing, and shipping certain cellular products, particularly those from the ER.
Lysosomes	They are active in recycling the cell's organic material and in the intracellular digestion of macromolecules. In addition, in many organisms, lysosomes are involved in apoptosis (programmed cell death).
Peroxisomes	Microbodies bound by a single membrane and containing enzymes that produce hydrogen peroxide as a by-product. Their functions include detoxifying alcohol, bile acid formation, and using oxygen to break down fats.
Mitochondria	The cell's power producers. They convert energy into forms that are usable by the cell. Located in the cytoplasm, they are the sites of cellular respiration which ultimately generates fuel for the cell's activities. They are also involved in other cell processes such as cell division and growth, as well as cell death.
Centrosome	The main microtubule organizing center of the animal cell as well as a regulator of cell-cycle progression. It is composed of two orthogonally arranged centrioles surrounded by an amorphous mass of protein termed the PeriCentriolar Material (PCM).
Centriole	A cylinder shaped cell structure found in most eukaryotic cells. It is usually made up of nine sets of microtubule triplets, arranged in a cylindrical pattern. Its position determines the position of the nucleus and plays a crucial role in the spatial arrangement of the cell.

Table 2.2: *Eukaryotic Cell Organelles*

2.3 Nucleus

The spherical nucleus typically occupies about 10 percent of a eukaryotic cell's volume, making it one of the cell's most prominent features [1]. It is surrounded by a double-layered membrane, the nuclear envelope, which separates the contents of the nucleus from the cellular cytoplasm. Apart from the nuclear envelope, the nucleus consists of the nucleolus, an organelle that manufactures chromatin and ribosomes. The chromosomes are threadlike strands, made of a long DNA molecule whose 3D-conformation is ensured by proteins called histones inside a global proteo-nucleic architecture called chromatin, that carry the genes and functions in the transmission of hereditary information.

The nucleus is the information processing and administrative center of the cell. It is often considered as the "brain" of a cell. Its main function is to control gene expression and mediate the replication of DNA during the cell cycle. It contains the cell's hereditary information and controls the cell's growth and reproduction.

2.4 Actin

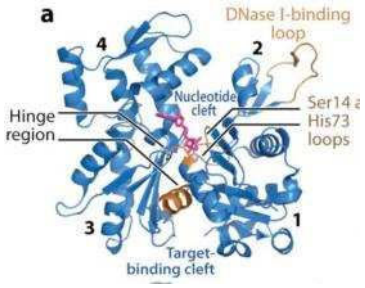

Figure 2.2: *Classical view of the structure of the actin monomer [Dominguez & Holmes 2011]. Subdomains 1-4 are labeled. Together, subdomains 1 and 2 form the outer (or small) domain, whereas subdomains 3 and 4 constitute the inner (or large) domain. Two large clefts are formed between these domains: the nucleotide and target-binding clefts.*

Actin is generally the most abundant protein in most eukaryotic cells, see Figure 2.2. It is highly conserved and participates in more protein-protein interactions than any other type of protein [Dominguez & Holmes 2011]. These properties, along with its ability to transition between monomeric (G-actin) and filamentous (F-actin) states under the control of nucleotide hydrolysis, ions, and a large number of actin-binding proteins, make actin a critical player in many cellular functions, ranging from cell motility and the maintenance of cell shape and polarity to the regulation of transcription. Moreover, the interaction of filamentous actin (see Section 2.6.3) with myosin forms the basis of muscle contraction.

[1] http://micro.magnet.fsu.edu/cells/nucleus/nucleus.html

2.5 Myosin

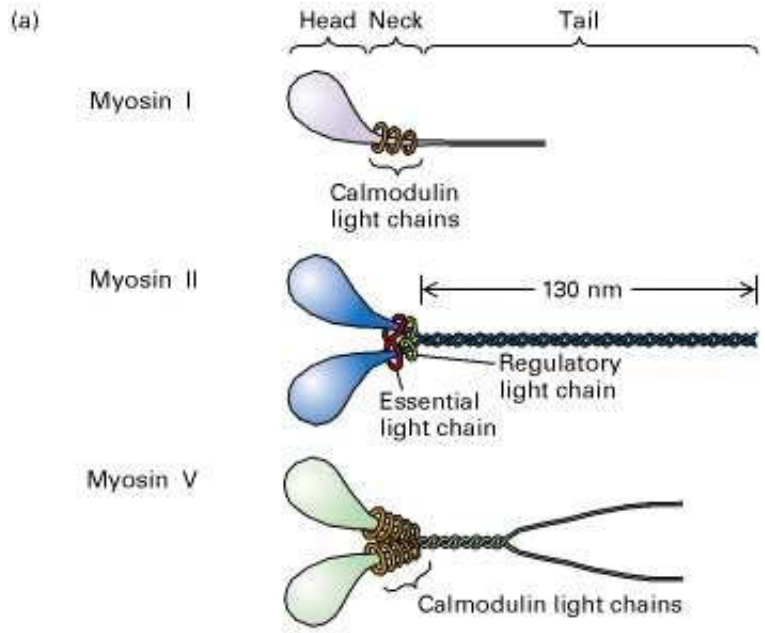

Figure 2.3: *The three major myosin proteins are organized into head, neck, and tail domains, which carry out different functions: the head binds actin and has ATPase activity, the light chains bound to the neck regulate the head domain and the tail dictates the specific role of each myosin in the cell [Lodish et al. 2000].*

Many cellular movements depend on interactions between actin filaments and myosin (often called actin-myosin complex). Myosin is an ATPase that moves along actin filaments by coupling the hydrolysis of ATP to conformational changes [Lodish *et al.* 2000] (Figure 2.3). This type of enzyme, which converts chemical energy into mechanical energy, is called a mechanochemical enzyme or, colloquially, a motor protein. We could say that myosin is the motor, actin filaments are the tracks along which myosin moves, and ATP is the fuel that powers the movement.

Thirteen members of the myosin gene family have been identified by genomic analysis. Myosin I and myosin II, the most abundant and thoroughly studied of the myosin proteins, are present in nearly all eukaryotic cells. Myosin V has also been isolated and characterized. Although the specific activities of these myosins differ, they all function as motor proteins. Myosin II powers muscle contraction and cytokinesis, whereas myosins I and V are involved in cytoskeleton-membrane interactions such as the transport of membrane vesicles. The activities of the remaining proteins encoded by the myosin gene family are now being discovered. We are mostly interested in Myosin II, which is the driving factor of cell contraction during morphogenesis (see Sections 2.8.1 and 2.9.1).

2.6 Cytoskeleton

In this section, we will analytically describe the cytoskeleton of an eucaryotic cell. The way the cytoskeleton functions is very important regarding the point that this thesis is trying to prove.

The cytoskeleton is an organized network of three primary protein filaments: microtubules, actin filaments, and intermediate fibers. As its name implies, the cytoskeleton helps to maintain cell shape and gives support to the cell. In addition to that, the cytoskeleton is also involved in cellular motility and in moving vesicles within a cell. In the following paragraphs, we will analyze the functions of each of the three types of filaments that compose the cytoskeleton. We focus on the function of each category of filaments as it is the target of our modeling.

2.6.1 Microtubules

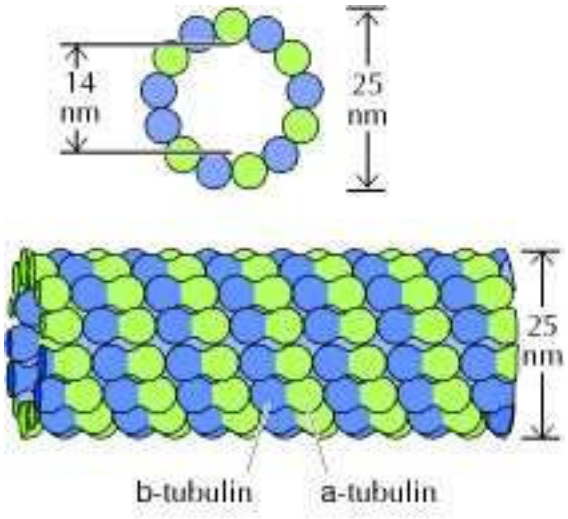

Figure 2.4: *Microtubules are created after the polymerization of a-tubulin and b-tubulin. They are composed of 13 protofilaments assembled around a hollow core.* *http://education-portal.com/academy/lesson/microtubules-definition-functions-structure.html*

Microtubules are fibrous, hollow rods composed of a single type of globular protein, called tubulin with a diameter of about $25nm$, that function primarily to help support and shape the cell (Figure 2.4). They also function as routes along which organelles can move. They are typically found in all eukaryotic cells and are a component of the cytoskeleton, as well as cilia and flagella. Microtubules play a huge role in the movements that occur within a cell. They form the spindle fibers that manipulate and separate chromosomes during mitosis. Examples of microtubule fibers that assist in cell division include polar fibers and kinetochore fibers [Cooper 2000].

2.6.2 Intermediate Filaments

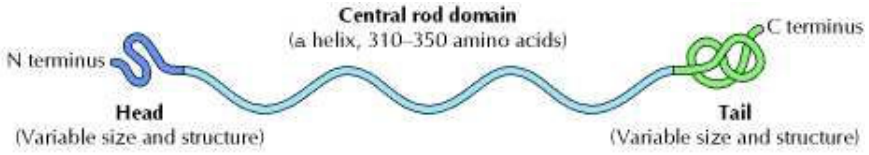

Figure 2.5: *Structure of intermediate filament proteins [Cooper 2000].*

Intermediate filaments have a diameter of about $10nm$. They contain a central α-helical rod domain of approximately 310 amino acids (Figure 2.5). An α-helix is a common structure of proteins, characterized by a single, spiral chain of amino acids stabilized by hydrogen bonds. Their principal function is structural and consists mostly in reinforcing cells and organizing cells into tissues. They provide mechanical support for the plasmic membrane where they come into contact with other cells, but they do not participate in cellular motility.

2.6.3 Actin Filaments

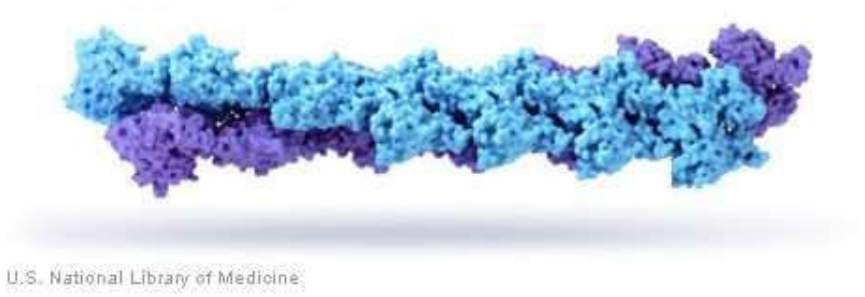

Figure 2.6: *Actin filaments are created by the polymerization of actin monomers (G actin).*

Also known as microfilaments, the actin filaments are the thinnest filaments of the cytoskeleton (diameter of about $7nm$ [Cooper 2000]). They are flexible and relatively strong linear polymers of actin sub-units (see Section 2.4) found in the cytoplasm of all eukaryotic cells. Their functions are to provide mechanical strength to the cell, link transmembrane proteins and generate locomotion in cells such as some leukocytes and the amoeba.

2.7 Drosophila Melanogaster

Drosophila melanogaster is a small, common fly found near unripe and rotted fruit. It has been a favourite organism for biological research, initially in the field of genetics, but in the investigation of other fundamental problems in biology (e.g. in the fields of ecology and neurobiology) as well.

The reasons why it has been so popular an organism for biologists and people who study genetics are:

- They are small, easily handled and it is easy to manipulate individuals with very unsophisticated equipment.
- Drosophila are sexually dimorphic (males and females are different), making it quite easy to differentiate the sexes.
- It is easy to obtain virgin males and females, as virgins are physically distinctive from mature adults.
- Flies have a short generation time (10-12 days) and do well at room temperature.
- The care and culture requires little equipment, is low in cost and uses little space even for large cultures.
- Its ecological versatility makes it a very robust laboratory organism.

2.8 Early Development of the Drosophila Melanogaster embryo

This section is dedicated to the description of the development of the *Drosophila Melanogaster* embryo until cellularization.

A typical drosophila egg hatches after 12-15 hours (at 25 °C). The early drosophila development occurs rapidly in a multinucleate cell called a syncytium, or syncytial blastoderm. Figure 2.7 shows the consecutive stages that undergoes a drosophila embryo during the first 3 hours after fertilization [Watters 2005]. During the first three cell divisions, the nuclei remain clustered close to the anterior pole of the embryo. As the cell cycles continue, the nuclei start to migrate and become evenly distributed along the anteroposterior axis of the embryo, in a process called axial expansion (divisions 4-7). The eighth division signals the beginning of a process called cortical migration. Several nuclei move towards the cortex forming a confined monolayer or a sublayer under the shell of the egg. The rest of the nuclei that stay in the interior are the yolk nuclei. During the tenth nuclear cycle, the nuclei that are positioned close to the posterior end of the embryo (known as germline precursors), start to push through the plasma membrane, to form pole cells. This phase

Figure 2.7: *Nuclear divisions during early drosophila development [Watters 2005]. During divisions 1-3, the nuclei divide but stay close to each other. During divisions 4-7, the nuclei continue to divide and spread out along the anterior-posterior axis of the embryo (axial expansion). During divisions 8-10, the nuclei migrate to the cortex of the embryo (cortical migration). Pole cells form at the posterior end of the embryo (cycle 9), while yolk nuclei remain in the interior. Once most of the cortical nuclei have completed 4 mitotic divisions, they are surrounded by membranes that invaginate from the surface and the cellular blastoderm is formed.*

of early drosophila development finishes with four more nuclear divisions followed by the process of cellularization.

2.8.1 Cellularization

The process that describes the enclosure of individual nuclei in individual cells is known as cellularization. It starts during the interface of the fourteenth cycle and lasts for 65 to 70 minutes [Mazumdar & Mazumdar 2002].

The nuclei that have migrated to the cortex of the embryo, are spherical with a diameter of $5\mu m$ (see Figure 2.8(a)). The sister centrosomes are located apically and microtubules start to appear. Cellularization happens in four distinct phases [Mahowald 1963].

In the first phase which lasts 10 minutes, two things happen simultaneously: the initially spherical nuclei ($5\mu m$ of diameter) that have migrated to the cortex of the embryo start to elongate [Lecuit & Wieschaus 2000] and the furrow canals (FC) are formed. A furrow canal (FC) is the leading edge of the furrow (named

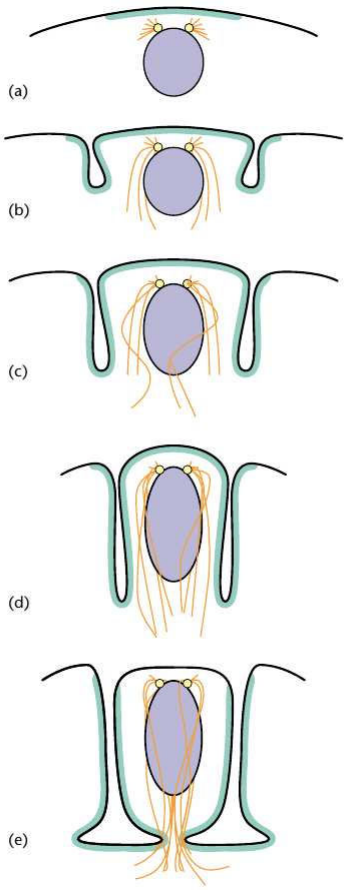

Figure 2.8: *(a) Cellularization of the cortical nuclei begins with the actin (green) concentrated at the cortex above each nucleus [Tram et al. 2001]. The centrosome pair (yellow) is apically positioned and the microtubules (orange) start to elongate. (b and c) The plasma membrane starts to invaginate and the actin is concentrated at the cortex and the leading edge of the invaginating furrow. (d) The furrows have finished their invagination and begin to extend along the cortex in order to complete the formation of the cells (e).*

by [Fullilove & Jacobson 1971]) and it is associated with the concentration of actin and myosin II [Young *et al.* 2009].

Each of the next three stages lasts around 20 minutes. In phase 2 the nuclei complete their elongation and the FCs start to invaginate. This invagination is quite slow and finishes at phase 3, when the FCs reach the basal end of the elongated nuclei (depth of around $35\mu m$ [Kotadia *et al.* 2010]). In phase 4, the actin and myosin II combine to induce contractile forces between the FCs [Miller & Kiehart 1995]. The furrows constrict laterally and finally pinch off to form the blastoderm cells in a process known as basal closure.

2.9 Gastrulation in the Drosophila Melanogaster embryo

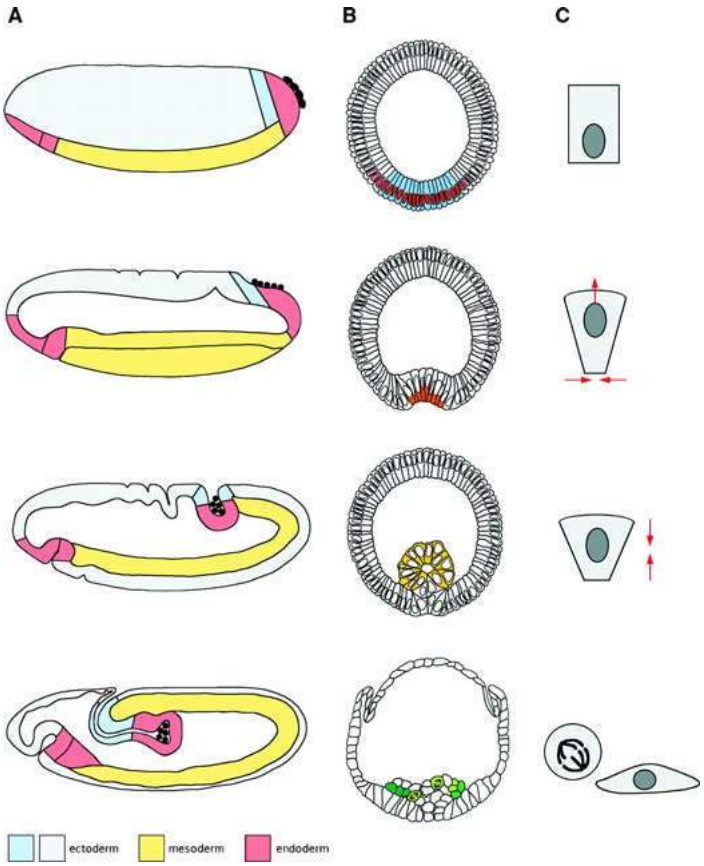

Figure 2.9: *The four stages of gastrulation (A) from a lateral point of view, (B) cross-section on the anteroposterior axis, (C) deformation of an individual mesodermal cell [Leptin 1999]. The 3 cell movements of the mesoderm primordium (marked in yellow) in (A) are presented in time sequence: Formation of the furrow in the ventral side of the embryo (ventral furrow invagination), invagination of the posterior part of the embryo (posterior midgut invagination), the germ band extends onto the dorsal side of the embryo (germ band extension). In the end, the mesoderm is fully internalized and starts to form a single cell layer (B). In (C) the movement of the nucleus of a constricting cell is schematically shown. Notice how at the beginning it is located close to the basal surface of the cell and then eventually moves towards the apical edge.*

Gastrulation is the process describing the segregation of the primordia (organs or tissues in their earliest recognizable stage of development) of the future internal tissues, the mesoderm and the endoderm, into the interior of the developing embryo [Leptin 1999]. During this process, the embryo of the Drosophila Melanogaster transforms from an initial monolayered simple structure called the blastula to a

multilayered embryo with three germ layers (see Figure 2.9).

Right after cellularization, the embryo consists of around 6000 cells at the cortex forming a sublayer under the egg surface. It is ellipsoid or "bean-shaped", around $500\mu m$ long with an average diameter of $180\mu m$ [Grumbling *et al.* 2006].

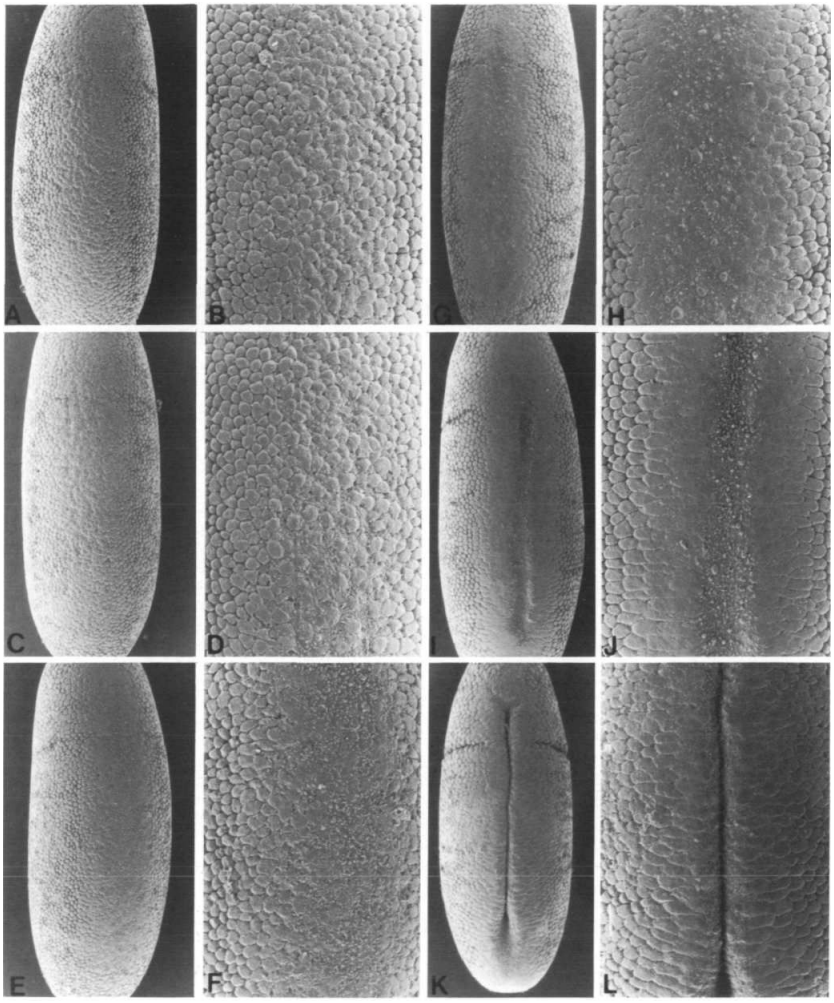

Figure 2.10: *Scanning electron micrographs of ventral furrow formation [Sweeton et al. 1991]. In the early phase of ventral furrow formation, the primordium is identified as a flattened zone (A,B). The midventral cells within this zone begin to constrict (C,D). As the cell apices constrict, membrane is extruded creating blebs on the surface (E,F). The outlines of constricting cells become lost beneath this blebbing (F). As more cells constrict, a shallow groove forms and the more lateral cells are drawn towards the ventral midline (G-J). As the ventral furrow forms, it extends anteriorly to the deepening cephalic furrow. The sides of the furrow are brought together as it invaginates into the interior of the embryo to give rise to mesoderm (K,L).*

2.9.1 Ventral Furrow invagination

Gastrulation starts with the formation of the ventral furrow, a process called ventral furrow invagination. Ventral furrow formation starts right after the most ventrally located cells of the embryo have finished cellularization [Sweeton *et al.* 1991]. The process begins with the flattening of the apical edges of the cells along the ventral side of the embryo (Figure 2.10). Under normal circumstances, it is a zone of 18 cells wide and 60 cells long (from approximately 20% to 80% of the egg length) that lose the rounded shape of their apical edge and adhere to each other closely.

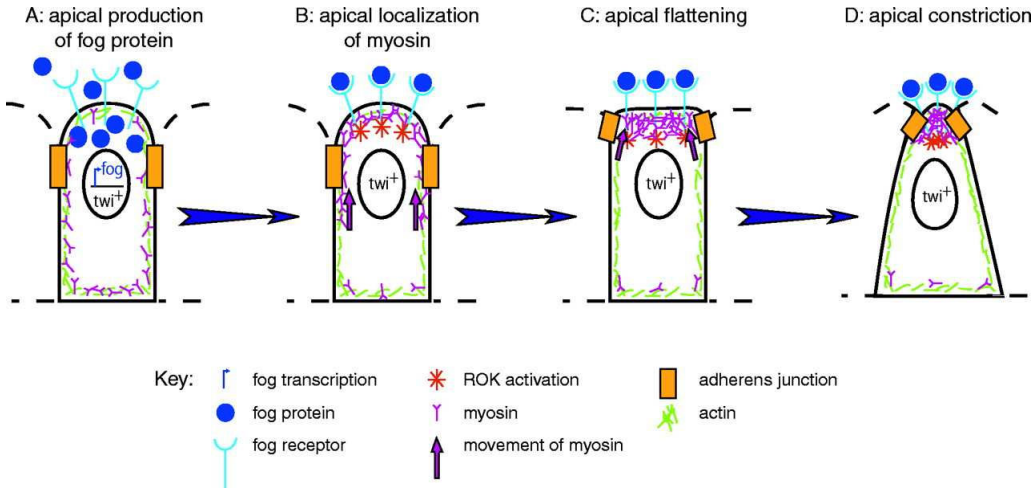

Figure 2.11: *Schematic of fog function controlling cell shape change [Dawes-Hoang et al. 2005]. (A) As a consequence of twist (twi) expression, the ventral cells activate transcription of the fog gene, resulting in the production and secretion of fog protein from the apical side of the cell (blue dots). (B) This local source of actomyosin contractility drives myosin (pink) to the apical side of the cell (arrows). (C) The actin-myosin complex is tethered to the cell surface through adherens junctions called also belt desmosomes (orange). (D) The continued contraction of apical actin-myosin exerts further force on the adherens junctions, pulling them close together, resulting in the apical constriction of the cells.*

Along the dorso-ventral axis, the maternal protein Dorsal is distributed in a gradient in the blastoderm nuclei that reaches its highest point in the most ventral nuclei [Leptin 1999, Johnston & Nusslein-Volhard 1992]. Dorsal activates the expression of two transcription factors, Twist and Snail, in a band of ventral cells that include the mesoderm primordium. Both genes are also expressed in cells outside of the mesoderm primordium [Leptin 1999, Reuter & Leptin 1994], so their existence alone is not enough to define its area. Fog (folded gastrulation gene) and at least two other genes are needed to accelerate and coordinate cell shape changes [Seher *et al.* 2007].

According to [Dawes-Hoang *et al.* 2005], fog is both necessary and sufficient to drive apical myosin localization (see Figure 2.11). Once localized apically, myosin

continues to contract. The force generated by continued myosin contraction is translated into a flattening and constriction of the cell surface through a tethering of the actinomyosin cytoskeleton to the apical adherens junctions. Once the apical flattening is complete, the cells progressively constrict their apical sides and become wedge-shaped (see Figure 2.9(c)). More specifically, apical constriction occurs by means of pulses of rapid constriction interrupted by pauses during which cells must stabilize their constricted state before reinitiating constriction [Martin *et al.* 2008].

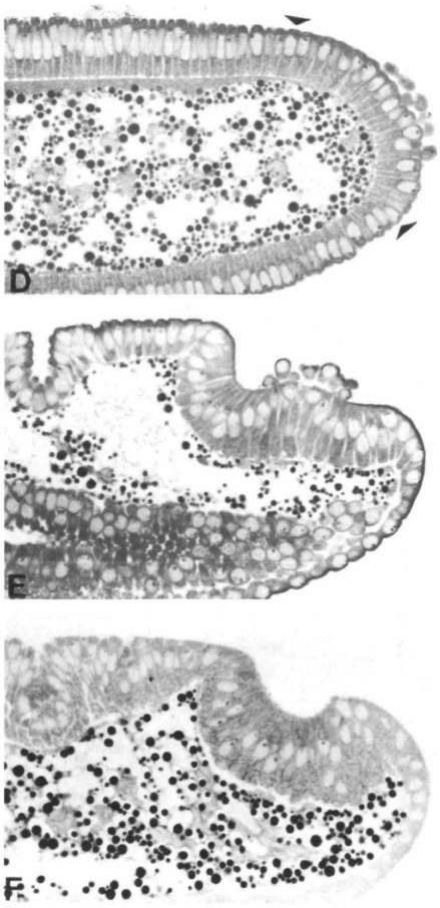

Figure 2.12: *A sagittal section of a midgastrula shows the posterior midgut invagination [Sweeton et al. 1991].*

The processes of apical flattening and apical constriction make the most ventrally located cells become wedge-shaped. This generates a bend in the tissue that causes the cells to invaginate. Finally, an indentation is created, which is then completely internalized to finish the creation of the ventral furrow. Once inside the embryo, the mesoderm primordium loses its epithelial structure and disperses into single cells which divide and migrate out on the ectoderm to form a single cell layer.

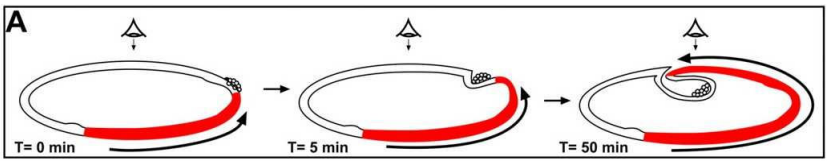

Figure 2.13: *Side-view diagram illustrating the process of germband elongation (GBE) [da Silva & Vincent 2007]. Notice how the posterior tip of the germband (red) moves towards the anterior of the embryo.*

2.9.2 Movement of the nucleus during the Ventral Furrow Invagination

During ventral furrow invagination, the nuclei of the ventral cells, initially positioned directly underneath the apical cell cortex, begin to migrate basally (Figure 2.9(c))[Kam *et al.* 1991]. The base of the cell enlarges and is flattened onto the yolk sac [Sweeton *et al.* 1991]. These observations suggest that flattening exerts a pressure on the underlying nuclei and cytoplasm, pushing the contents of the cell basally. In [Sweeton *et al.* 1991] they propose that the elongation of the cells and the shift in nuclear positions are passive responses to the constriction of the cell apices. The nuclei reach their full depth of about two thirds of the cell length at approximately 6 minutes after the onset of gastrulation.

2.9.3 Posterior Midgut Invagination

A few minutes after the ventral furrow has begun to invaginate, a similar series of cell-shape changes begins to occur in the anterior and the posterior midgut rudiments. The posterior and anterior midguts are formed by disk-shaped primordia located at the posterior and anterior pole of the embryo respectively.

The anterior midgut rudiment loses its epithelial characteristics a short time after gastrulation and becomes a solid cluster of rounded, apolar cells flanked by the anterior mesoderm. In contrast, the posterior midgut remains epithelial until late endoderm primordium (usually known as the posterior midgut or PMG primordium). These cells also constrict at their apical ends and become wedge shaped, and eventually invaginate, while at the same time the posterior end of the embryo is pushed dorsally by independent ectodermal cell movements. The posterior endoderm remains epithelial for a longer period and will only disperse into individual cells much later. These cells then use the mesodermal cell layer as substratum for migration towards the middle of the embryo, where they will meet up with the cells of the anterior endoderm to form the continuous endodermal cell layer that will become the midgut epithelium

2.9.4 Germ Band Extension

During early embryogenesis, the germband [da Silva & Vincent 2007], which gives rise to the segmented trunk of the larva, doubles in length while thinning commensurately. In this case, the elongating tissue is constrained by external membranes and the germband folds over itself as it elongates (Figure 2.13). At the end of elongation, the posterior half of the germband ends up on the dorsal side of the egg, while the anterior half remains on the ventral side throughout. Upon completion of germband extension (GBE), the posterior tip of the germband has travelled over 70% of the egg length towards the head region.

2.10 Conclusion

The first question that gave rise to this thesis is: "What is the role of the apical constriction of ventral cells in the invagination?".

In [Martin *et al.* 2008], they used Spider-GFP, a green fluorescent protein that outlines individual cells, to monitor the process of ventral furrow invagination in wild embryos (Figure 2.14). In their videos [2] we notice that the area where the apical constriction starts, and the area where the invagination starts differ. In fact, the actin-myosin contractions occur first in the ventral medial layer, while the invagination starts from the ventral curved extremities and then propagates to the medial area.

To study the relationship between the apical constriction and the ventral furrow invagination, I created a biomechanical model of the embryo of the Drosophila Melanogaster. I use this model to check if it might be possible to successfully simulate the process of the ventral furrow invagination relying only on active and passive forces applied on the unique geometry of the model.

[2] http://www.nature.com/nature/journal/v457/n7228/extref/nature07522-s2.mov

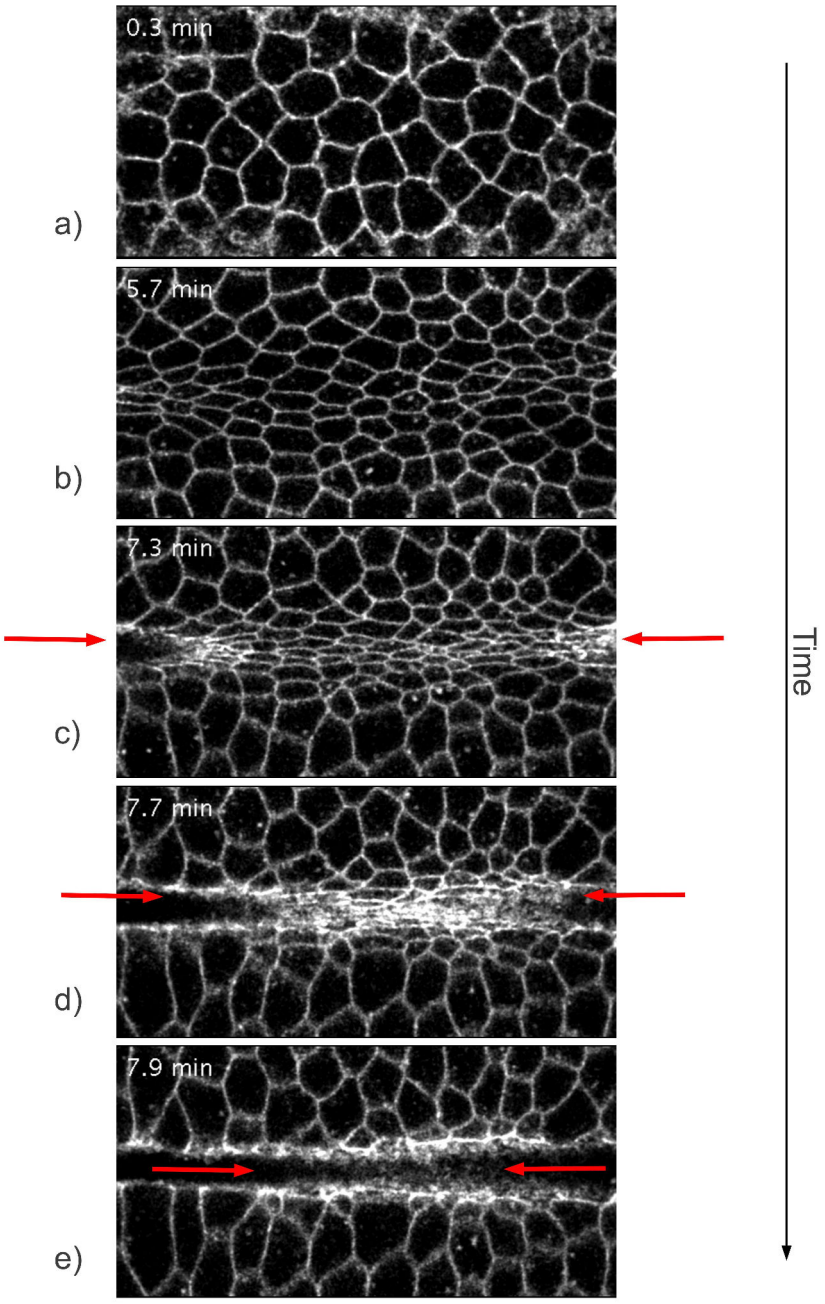

Figure 2.14: *Z-slices of cell membranes revealed with Spider-GFP showing the apical constriction of ventral cells followed by invagination [Martin et al. 2008]. With the red arrows in (c), I aim to point out that the cells located in the extremities of the embryo are the first to invaginate and as they move towards the interior of the embryo, they disappear from the image. In (d) and (e), the cells closer to the center of the embryo move towards the interior as well, showing a propagation of the invagination from the extremities to the ventral medial layer.*

Chapter 3

Biomechanical Cell Modeling

Contents

3.1 Introduction

Living cells in an organism are constantly subjected to mechanical stimulations throughout life. These stresses and strains can arise from both the external environmental conditions and internal factors. Depending on the magnitude, direction and distribution of these mechanical stimuli, cells can respond in a variety of ways.

As mentioned in Chapter 2, many biological processes are influenced by changes in cell shape and structural integrity. Cell growth [Huang & Ingber 1999], differentiation, migration, and even apoptosis (programmed cell death) [Chen *et al.* 1997] are some examples. The bridge that connects genetic and molecular-level events to tissue-level deformations that shape the developing embryo is biomechanical forces [Wyczalkowski *et al.* 2012].

Biomechanics is the application of basic principles of solid and fluid mechanics to study physical functions of organisms. The biomechanical analysis of a phenomenon

or a process requires a constant interplay between theory and empirism, or in other words, between qualitative and quantitative approach. More precisely, the following steps are required (not obligatory to be followed in the order of statement):

- Qualitative description of the process and description of the physical mechanisms behind it.
- Experiments with the components supposed to control the process removed or altered and analysis of the consequences of the removal/alteration of each component.
- Quantitative description of the process including morphometric and kinematic analysis of the structures involved, measurement of the forces exerted and of the mechanical properties of the tissues subjected to the forces.
- Empirical verification of the predictions of the model.

An area of biomechanical modeling that is of particular interest is the modeling of soft tissues. By soft tissue we refer to a primary group of tissues which bind, support and protect our human body and structures (organs) as the organs containing the tissue develop, grow, regenerate, cicatrize and age. The most known soft tissue in the human body is the skin (around 16% of the human adult weight).

When it comes to modeling soft tissues, there are three specific features that need to be met.

- **Physical properties of the tissue.** The tissue may change its shape, size or substance as the organism develops, grows and ages. The tissue undergoes modifications at the cellular level that are reflected in its physical properties.
- **Effect of the environment of the tissue.** The evolution of a tissue or an organ through time may be inhibited or restrained by other organs. Obviously, the development of the subject tissue will be more hindered if it is close to hard tissue like a bone rather than if it was close to another soft tissue.
- **Validation.** There are certain criteria that define the efficiency of a model: precision, robustness, real-time simulation. Depending on the particular case, those criteria do not always bare the same importance. For example, when creating a model to simulate a prostate biopsy, the precision is much more important than real-time simulation.

There are two main approaches for the modeling of soft tissues: continuous approaches (Finite Element Method, Finite Difference Method, Finite Volume Method, Boundary Element Method, Long Element Method, Tensor Mass) and discrete approaches (Mass-Spring Network). The main advantage of continuous approaches is that they offer a strong theoretical background, whereas discrete models are based more on “intuition”, so it is difficult to control their parameters and assess them.

On the other hand, continuous models are time consuming, demand a lot of computational resources, especially when it comes to interaction with different types of tissues. On the contrary, discrete models are usually faster and offer a way to build complex models. Although the implementation depends of the chosen method, the modeling scheme is always organized in four main stages:

- geometry representation;
- properties, parameters or behaviour definitions;
- specifications of the constraints and loads;
- solution representation (in terms of displacements, state changes...);

The main differences between the two methdos are [Chabanas & Promayon 2004]:

1. the transition from the stage of geometry representation to the stage of defining the properties and behaviour of the model;
2. the solution stage

In the next Section, I will attempt to present a brief overview of the discrete and continuous modeling methods along with specific examples created to study morphogenesis. I will mostly focus on the models targeted specifically on the formation of the ventral furrow.

3.2 Biomechanical Discrete Models

As mentioned in Section 3.1, the discrete models contain parameters that are not directly linked to physical properties. Their main advantage is calculation speed and easy implementation, so they are mostly used in early stages of a study in order to test empirical observations.

The most popular discrete models are the Mass-Spring-Networks (MSN). In MSN modeling, an object is usually represented by a polygon (2-Dimensions) or a volume solid (3-Dimensions) mesh. The nodes are considered as focal points assembling the mass of the object while the edges connecting the nodes are considered as springs without mass. The force applied by a spring is a combination of its stiffness and its length. Consequently, the interaction between neighbour nodes is modeled by elastic links.

The calculation of the deformation or movement of the object is done iteratively. At each iteration, the forces applied by all individual springs on the nodes are summed up and the new positions of the nodes are calculated by integrating the new positions in the equations of the dynamical system. Suppose that the mass of the modeled object is discretized in n mass points m_i, linked by springs. At every instant t, each point i has a position x_i. The sum of the forces $\mathbf{F}_i$ applied on a node

is a combination of the forces applied by the corresponding springs and by external parameters. So, the equation controlling the movement of each point is:

$$m_i \ddot{\mathbf{x}}_i = \mathbf{F}_i \tag{3.1}$$

The force $\mathbf{F}_i$ applied on a single node i can be expressed as:

$$\mathbf{F}_i = \mathbf{F}_{int_i} + \mathbf{F}_{ext_i} - d_i \dot{\mathbf{x}}_i \tag{3.2}$$

where $d_i \dot{\mathbf{x}}_i$ is the shock absorption (damping) of the node i depending on its speed, $\mathbf{F}_{ext_i}$ is the sum of the system's external forces and $\mathbf{F}_{int_i}$ is the sum of the forces applied by other nodes on the point i. Let

$$\mathbf{F}_{int_i} = \sum_{j=1}^{n} \mathbf{r}_{ij} \tag{3.3}$$

where $\mathbf{r}_{ij}$ is the force applied on the node i by the spring between nodes i and j. If there is no spring between the two nodes, this term is 0. Usually, the most commonly used springs react according to the displacement of their ends from the rest state, such as:

$$\mathbf{F}_{int_i} = \sum_{j=1}^{n} \mathbf{r}_{ij} = \sum_{j=1}^{n} \frac{\mathbf{x}_j - \mathbf{x}_i}{||\mathbf{x}_j - \mathbf{x}_i||} \left(k_{ij}(||\mathbf{x}_j - \mathbf{x}_i|| - l_{ij})\right) \tag{3.4}$$

where k_{ij} is the stiffness coefficient of a spring et l_{ij} is the rest length of a spring linking nodes i and j. The equation 3.1 corresponds to the movement of a single node. Consequently, the movement of n nodes is a system of n equations that can be expressed by the following:

$$[M]\ddot{\mathbf{x}} + [D]\dot{\mathbf{x}} + [K]\mathbf{x} = \mathbf{F}_{ext} \tag{3.5}$$

where $\mathbf{x}$ is a $3n$ vector collecting the positions of all the nodes and M, D and K are diagonal $3n \times 3n$ matrices collecting the mass, the damping and the stiffness.

Mass-Spring Models have been used quite extensively to study plant morphogenesis. [Fracchia *et al.* 1990] used the mass-spring approach to visualize map L-system models (a method to model cellular arrangements, focused on their topology rather than their geometry [Lindenmayer & Rozenberg 1979]). The shape of cells and the entire tissue is calculated as the equilibrium between the internal pressure within the cells and the tension of cell walls modeled by a MSN. [Rolland-Lagan *et al.* 2003] analyzed the growth parameters observed during Antirrhinum majus petal development. They modeled the tissue as a grid, whose regions are linked by springs with resting lengths corresponding to that of the mature organ. Spring models using beam elements for which values of stiffness and extensibility are defined can be viewed as the simplest models for a cell wall [Prusinkiewicz & Lindenmayer 1990].

Spring models have also been used as a growing template to test morphogenetic rules [Rudge & Haseloff 2005] where the growth of elastic cell walls was represented by springs of varying natural lengths.

3.3 Biomechanical Continuous Models

A very popular method to study the physical properties of materials is the continuum mechanics. The continuous models are based on the equations of continuum mechanics after spatial or nodal discretization:

- spatial discretization: each modeled object is decomposed to existing geometric elements such as triangles, cubes, hexahedra etc.
- nodal discretization: each modeled object is described by a number of nodes with certain degrees of freedom and a physical description of each behaviour.

Before commiting to the analysis of the continuum modeling methods, there are certain introductory concepts that need to be explained. These concepts are:

- displacement of an object,
- deformation,
- boundary conditions and constraints,
- the behaviour law of a material (constitutive equation),
- elasticity,
- linear elasticity,
- hyper-elasticity,
- viscoelasticity,
- plasticity.

I will briefly explain each of these concepts in the following paragraphs.

3.3.1 Displacement of an object

When an object moves, each point changes their position from an initial $\mathbf{x}_0$ to a current $\mathbf{x}$. The displacement of this point is the vector between the initial and the current position such as: $\mathbf{u}(x) = \mathbf{x} - \mathbf{x}_0$ (Figure 3.1).

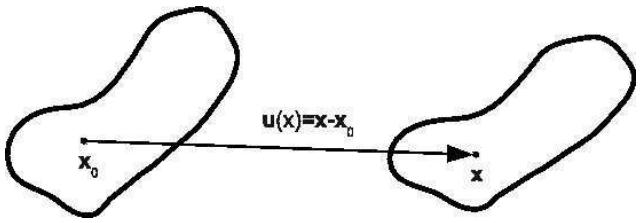

Figure 3.1: *Displacement of a point after the object has been deformed.*

3.3.2 Deformation

In order for an object to be considered deformed, at least two of its points must undergo different displacements. The deformations can be characterized by using the gradient of the displacement field $\nabla \mathbf{u}$. The concept of strain is used to evaluate how much a given displacement differs locally from a rigid body displacement. One of such strains for large deformations is the Lagrangian finite strain tensor (also called Green-Lagrangian strain tensor), defined as:

$$\varepsilon_G = \frac{1}{2}(\nabla \mathbf{u} + [\nabla \mathbf{u}]^T + [\nabla \mathbf{u}]^T \nabla \mathbf{u}) \tag{3.6}$$

For small shape changes, the term $[\nabla \mathbf{u}]^T \nabla \mathbf{u}$ can be omitted, which makes the equation linear and simplifies the calculations by a lot. So, the linear equation, also called infinitesimal strain tensor [Bower 2012], is:

$$\varepsilon_C = \frac{1}{2}(\nabla \mathbf{u} + [\nabla \mathbf{u}]^T) \tag{3.7}$$

3.3.3 Boundary Conditions and Constraints

Boundary conditions are used to specify the loads applied to a solid. There are several ways to apply loads on a mesh:

- Displacement boundary conditions. The displacements at any node on the boundary or within the solid can be specified.
- Symmetry conditions.
- Prescribed forces.
- Distributed loads (aerodynamic loads, hydrostatic fluid pressure...)
- Body forces (gravitational loads, electromagnetic forces...)
- Contact (for example with another solid)
- Load history (the prescribed loads and displacements are applied as a function of time)

More complicated constraints are also possible, such as connecting different types of elements and constraining a boundary to remain flat. At the most basic level, constraints can simply be used to enforce prescribed relationships between the displacements or velocities of individual or group of nodes in the mesh.

3.3.4 The behaviour law of a material

The internal forces in a structure or component are generally called called the "stress". Stress is defined as force per unit area and has the same units as pressure.

The behaviour law of a material (most commonly known as the constitutive equation) approximates the response of that material to external stimuli. In other words, it is a set of equations relating stress to strain:

$$\sigma = f(\varepsilon) \tag{3.8}$$

Elasticity is the tendency of solid materials to return to their original shape after being deformed. Linear elasticity is a linear approximation which reproduces quite well the deformations of an elastic material, as long as they are small (Figure 3.2). A material is considered linearly elastic if it is isotropic (same behaviour in all directions) and satisfies Hooke's law:

$$\sigma = E\varepsilon \tag{3.9}$$

where E is the Young Modulus, a measure of the stiffness of an elastic material. It is defined as the ratio of the stress along an axis over the strain along that axis in the range of stress in which Hooke's law holds. Hooke's law can be also stated as a relationship between force F and displacement x:

$$F = kx \tag{3.10}$$

where k is the stiffness, a constant factor characteristic of a spring.

Materials that don't satisfy Hooke's (linear elasticity) law may be viscoelastic (the time-dependent resistive contributions are large, and cannot be neglected), plastic (the applied force induces non-linear displacements in the material) or hyperelastic (the applied force induces displacements in the material following a Strain energy density function) [Charlton *et al.* 1994].

A **hyperelastic** material's behaviour is described by a constitutive equation relating the strain energy density W of the material to the deformation gradient. There are many types of hyperelastic material models, with the most common of them being the *neo-Hookean*:

$$W = C_{10}(\bar{I}_1 - 3) + D_1(J-1)^2 \tag{3.11}$$

where $C_{10} = \frac{E}{1+\nu}$, $D_1 = \frac{E}{6(1-2\nu)}$, $\bar{I}_1 = 2Tr([\varepsilon]) + 3$ et $J = \sqrt{det(2[\varepsilon] + I)}$. $J = 1$

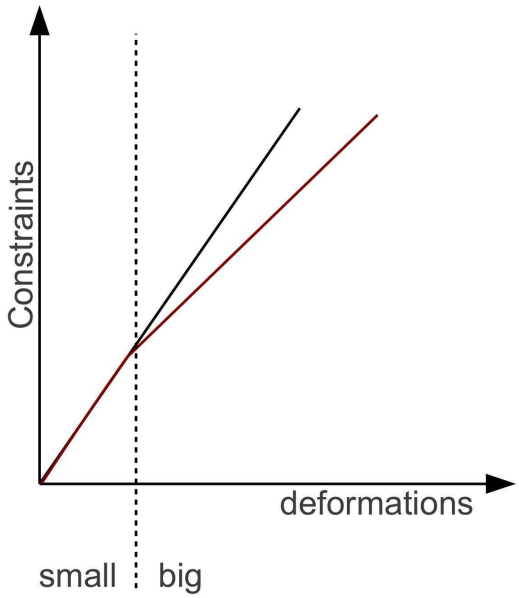

Figure 3.2: *Elastic behaviour of a material. The linear approximation is valid for small deformations. Depending on the application and accuracy required, the limit between small and big requirement in deformation may vary between 5%-20%.*

for an incompressible material. Other hyperelastic constitutive laws may be used as well, like the *Mooney-Rivlin law* [Mooney 1940].

The stress-strain law must then be deduced by differentiating the strain energy density:

$$\sigma = \frac{\partial W}{\partial \varepsilon} \tag{3.12}$$

The calculations involve complex algebra, which can be found in books of applied mechanics like [Charlton *et al.* 1994].

A **viscoelastic** material exhibits both viscous and elastic characteristics when undergoing deformation. Viscous materials, like honey, resist shear flow and strain linearly with time when a stress is applied. Elastic materials deform when stretched and quickly return to their original state once the stress is removed. Viscoelastic materials have elements of both of these properties and, as such, exhibit time-dependent strain. A particular property of viscoelastic materials is that they exhibit hysteresis in their stress-strain curve (Figure 3.3).

Finally, a **plastic** deformation of a material is an irreversible deformation, so the rest state is totally different in the beginning and in the end of the deformation.

3.3.5 Finite Element Method

Probably the most popular continuous modeling method is the Finite Element Method (FEM). In the FEM formulation [Zienkiewicz & Taylor 2000], the para-

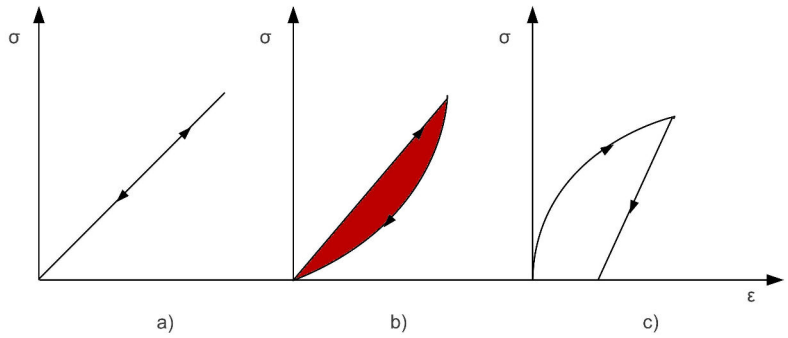

Figure 3.3: *Stress-Strain curves for a purely elastic material (a), a viscoelastic material (b) and a plastic material (c). The red area in (b) is a hysteresis loop and shows the amount of energy lost in a loading and unloading cycle. The material in (c) suffers plastic deformation and fails to return to its rest shape.*

metric domain is partitioned into finite sub-domains. The modeled object is discretized in a number of elements of a relatively simple shape (triangles, quads, tetrahedrons, hexahedrons...), resulting to the creation of a mesh. The vertices of the simple-shaped elements are called nodes of the mesh. The physical properties of the object are described by partial differential equations (PDE) from the scientific domain of continuum mechanics. The deformation of each element is defined by polynomial interpolation functions. Interpolation allows to find the displacement of each point of the element in accordance to the displacement of the nodes. Obviously, the choice of the mesh and the interpolation function have a great influence on the precision of the method.

After creating the mesh and choosing the interpolation function, the finite element method is solved step-by-step. Let an element e for which the displacement of its nodes is $\mathbf{U}^e$. The FEM goes through the following steps:

- Approximation of the displacement of all points of e as a function of $\mathbf{U}^e$ (this step is optional and can be ommitted).
- Calculation of the total deformation as a function of the nodes' properties.
- Calculation of constraints and boundary conditions as forces applied on the nodes of the elements with the aid of the constitutive equation (see Section 3.3.4)
- In the case of linearly elastic materials, for each element, we get an equation of the following type:

$$\mathbf{F}^e = [K^e]\mathbf{U}^e \tag{3.13}$$

  where F^e are the forces applied on the nodes of the element and $[K^e]$ is the stiffness matrix of the element.

- Assembly of the contribution of each element to the total deformation of the object.

The resolution of the system of equations with the FEM can be either **static** or **dynamic**, depending on the assumptions made concerning the physical properties of the material. These assumptions are related to the type of the modeled soft tissue and to the performance criteria of the simulation.

In a **static** resolution, the effect of the inertia and the viscoelasticity is small, thus can be neglected. In the **static** case, the system becomes:

$$\mathbf{F} = [K]\mathbf{U} \tag{3.14}$$

where $\mathbf{U}$ is the unknown vector with all the nodal diplacements, K is the global stiffness matrix of the object (characteristic of the physical properties of the material) and $\mathbf{F}$ is the vector that represents the set of forces applied on the system. The stiffness matrix K is independent of the displacement vector $\mathbf{U}$ if its geometrical relation is linear and vice versa. If the relation is linear, then there are two types of methods that can be used to solve the problem:

- Direct methods that solve the system by inverting the stiffness matrix K (decomposition LU, QR or Cholesky factoring).
- Iterative methods like the relaxation technique (Jacobi or Gauss-Seidel) or projection technique (conjugate gradient).

On the other hand, a **dynamically** solved system is expressed as follows:

$$[M]\ddot{\mathbf{U}} + [D]\dot{\mathbf{U}} + [K]\mathbf{U} = \mathbf{F} \tag{3.15}$$

where M is the mass matrix, D is the damping matrix and $\ddot{\mathbf{U}}$ and $\dot{\mathbf{U}}$ the acceleration and velocity of the displacement vector over time. The system of equations is then solved using an integration method presented in Section 3.3.7.

3.3.6 Other Continuous Methods

The first continuous modeling method developed is the Finite Difference Method (FDM). [Terzopoulos *et al.* 1987] propose to discretize the local physical equations with the finite difference method. Each intersection that cuts up the regular grid representing the model can define the position of a node. The physical properties and the equations of motion are connected to each node. This way, we achieve to discretize the energy linked to each node. Although the FDM is easier to be implemented than the FEM, it has severe draw-backs: the regular mesh makes it more difficult to approximate the boundaries of an object.

The **Finite Volume Method** (FVM) is a well suited method for the numerical simulation of various types of conservation laws [Eymard *et al.* 1999]. It is based on

spatial discretization of the modeled object. The constraint tensor σ is introduced, which helps to calculate the internal force $\mathbf{F}$ on a certain plane:

$$\mathbf{F} = \sigma \mathbf{n} \tag{3.16}$$

with $\mathbf{n}$ the normal of the considered plane. The force applied on a facet of surface A of a finite element is defined as:

$$\mathbf{F}_A = \int_A \sigma \mathrm{d}\mathbf{A} \tag{3.17}$$

The constraint tensor inside an element is constant if the shape functions are linear. To obtain the forces on each node, the force on every facet of all elements is calculated. Then, the obtained forces on the adjacent facets of a node are added up on it.

The advantages of this method is its intuitive geometrical basis and the rather simple calculation of the forces. On the other hand, this method becomes quite ineffective when the geometry of the model is complex or we need to model the interactions with more than one object.

Another alternative continuous method was proposed by [James & Pai 1999] where the calculation of the behaviour of an elastic object is done on its surface instead of its volume. In the **Boundary Element Method** (BEM), the boundaries of the modeled object are cut up in disjoint elements, inside which the displacement field is interpolated as a function of the nodal displacement. The main advantage of the BEM is that it doesn't require a volumetric mesh but just a surface mesh. The number of nodes treated is diminished as well as the number of equations, which improves the calculation time comparing to FEM. Nevertheless, the method can be applied on very specific materials: only linear homogeneous and isotropic materials can be modeled. In addition, the BEM cannot take into account the movement of the nodes in the interior of modeled object.

The **Long Element Method** (LEM) was proposed by [Costa & Balaniuk 2001] in order to model objects filled with fluid. The object is decomposed in parallelepiped long elements and the tissues are considered as elastic, non-linear and incompressible. The deformations have always the same direction: the main axis of the elements (length). The two basic principles that describe this model is the Pascal Principle ("Pressure is transmitted undiminished in an enclosed static fluid.") and the volume conservation. Unlike the other methods, LEM uses bulk variables such as pressure, density and volume in order to model the object. These parameters are relatively easier to be identified compared to the mass of an element. Although no pre-calculation or condensation is required in the implementation of this model, the LEM suffers from the problem that most methods suffer as well: it is only valid for small deformations.

The **Tensor-Mass Method** (TMM) [Delingette *et al.* 1999] was originally pro-

posed as an alternative method in order to solve the problems of the Finite Element Method in a local and iterative way. TMM discretizes the modeled object in a mesh made of tetrahedrons while its mass is concentrated on the nodes of the mesh (lumped mass). For each node of the mesh, the movement equation is:

$$M\ddot{\mathbf{U}}_i + D\dot{\mathbf{U}}_i + K\mathbf{U}_i = \mathbf{F}_i \tag{3.18}$$

where M is the inertia matrix, D the viscoelasticity matrix, K the stiffness matrix and F the elastic force applied on the node. The elastic force applied on each node can be defined as:

$$\mathbf{F}_{int_i} = [K_{ii}]\mathbf{u}_i + \sum_{j\ neighbour\ of\ i} [K_{ij}]\mathbf{u}_j \tag{3.19}$$

where $[K_{ii}]$ is the contribution of the i-th node on all the elements it participates and $[K_{ij}]$ is the contribution of its j neighbour nodes. The elastic force of each node is then added to the dynamic local equation in order to calculate the displacement field in the next step.

In the first version of the TMM proposed by [Delingette *et al.* 1999], the Tensor-Mass model was viable only for small displacements. [Picinbono *et al.* 2000] enhanced the method in order to include large displacements by using a non-linear displacement tensor and non-linear elasticity.

In Table 3.1 the MSN, the performance of Tensor Mass and FEM methods is compared in modeling "brain shift" [Deram 2012]. "Brain shift" is the induced deformation of the brain after a neurosurgical operation. In Table 3.2 the same three methods are compared in terms of precision or Relative Error Normal (REN) [Deram 2012]. As a general conclusion, the Mass-Spring method is the fastest among the 3 methods, but for this specific example, the precision of the method is the most important characteristic. Thus, the Finite Element Method seems to be the most suited for modeling the brain shift.

Concerning the understanding of embryogenesis, the calculation speed is less important than the precision and the robust scientific background of the study. Consequently, the Finite Element Method (and in general the methods based on the continuum mechanics) seems to have the edge over the Discrete Methods. I will address this topic more in detail in Section 3.5.

3.3.7 Integration Methods

Knowing the position of each point of a tissue at each time-step is essential for the simulation of its behaviour. The models presented in the previous sections allow the calculation of the positions of the points using the equation:

$$\ddot{\mathbf{x}} = f(\dot{\mathbf{x}}, \mathbf{x}, t) \tag{3.20}$$

Models	FPS	Calculation Time (s)
Mass-Spring SOFA	101	6
Tensor Mass SOFA	35	16
FEM SOFA	14	40

Table 3.1: *Comparison of the calculation time for the three compared models: a Mass-Spring Network, a Tensor-Mass and a Finite Element model. The simulations were performed in the SOFA framework*

Models	REN (%)			Distance (mm)		Volume	
	min.	max.	avr.	min.	max.		(%)
Mass-spring SOFA	3,63	90,58	40,59	0,23	4,52	1,81	96,74
Tensor-Mass SOFA	2,98	50,26	16,56	0,9	3,32	0,86	97,80
MEF SOFA	4,16	46,41	15,31	0,10	2,96	0,77	98,11

Table 3.2: *Precision metrics for the three compared models: Mass-Spring Network, a Tensor-Mass and a Finite Element model.*

where $\mathbf{x}(t)$ is the vector containing the positions of all the points at time t and f is a model-dependent function. In most of the occasions, this equation cannot be solved analytically, this is why we use a numerical integration.

After choosing a certain time-step dt, we have to find an approximate value for $x(0)$, $x(dt)$, $x(2dt)$... Thus, the second order differential equation (3.20) can be written as a system of first order equations.

$$\begin{cases} \dot{\mathbf{x}} &= \mathbf{v} \\ \dot{\mathbf{v}} &= f(\mathbf{v}, \mathbf{x}, t) \end{cases} \tag{3.21}$$

The value of $x(t + dt)$ can be found using two types of integration methods:

- **explicit** integration method. $x(t+dt)$ depends only on the position and speed of the points at time t.
- **implicit** integration method. $x(t + dt)$ depends on the position and speed of the points at time $t + dt$.

In the next sections we briefly present the most simple and elementary explicit and implicit methods. For a generic overview on the integration methods, the existent bibliography is very rich (the reader may refer to [Hauth *et al.* 2003] for example).

3.3.7.1 Explicit integration method

The most simple integration method is the **Euler Method**. It is based on a Taylor expansion as follows:

$$\begin{cases} \mathbf{x}(t+dt) & = \mathbf{x}(t) + dt\ \mathbf{v}(t) \\ \mathbf{v}(t+dt) & = \mathbf{v}(t) + dt\ f(\mathbf{v}(t), \mathbf{x}(t), t) \end{cases} \tag{3.22}$$

The explicit methods have the advantage of being easy to implement and fast but they can be unstable if the time-step is big or if f is too "stiff" [1].

3.3.7.2 Implicit Integration Methods

The **Implicit Euler Method** is given by the following system:

$$\begin{cases} \mathbf{x}(t+dt) & = \mathbf{x}(t) + dt\ \mathbf{v}(t+dt) \\ \mathbf{v}(t+dt) & = \mathbf{v}(t) + dt\ f(\mathbf{v}(t+dt), \mathbf{x}(t+dt), t) \end{cases} \tag{3.23}$$

The advantage of implicit over explicit methods is that they normally don't have instability problems. On the other hand, they are more demanding in terms of calculations.

3.4 Mathematical Models

Mathematical models present a usually robust way to quantitavely test a biological process. The development of mathematical models can serve many purposes in quantitave biology [Koehl 1990]:

- To simplify complex problems by abstracting the essential elements of a system. A quantitative formulation of a problem allows to define which parameters of a system need to be studied and can suggest new experiments to test the theory.
- Models allow to conduct experiments to explore the consequences of manipulating a system that could not be performed empirically.
- Mathematical models are required to understand the non-intuitive physical behaviour of small organisms, where internal forces are negligible whereas viscosity is very important.

However, it is important to recognize that mathematical models can never include all of the complexities inherent to biological systems. They are rather utilitarian constructions designed to help understand some aspect of the system or study specific parameters. Thus said, they were the first models to be created and proposing a formalism concerning morphogenesis, so I consider them worth mentioning.

[1] a stiff equation is a differential equation for which certain numerical methods for solving the equation are numerically unstable, unless the dt extremely small

The first attempts to present a mathematical formalism for morphogenesis dates back to 1952. [Turing 1952] addressed the following problem: "How can a tissue be patterned?" His theory suggested that cells actually respond to a chemical pre-pattern. Turing proposed that if an underlying pattern of growth hormone went through a symmetry-breaking transition (bifurcation) then there would be more hormone in one place than in the others, and this would initiate a bud. He extended this notion to that of a morphogen, namely a chemical to which cells respond by differentiating in a concentration-dependent way.

A system of morphogens was considered, reacting and diffusing in such a way that, in the absence of diffusion, they exhibited a spatially uniform steady state. The introduction of diffusion could lead to an instability (currently the well-known diffusion-driven instability) resulting in a spatially heterogeneous pattern of chemical concentrations. This was the first example of an emergent phenomenon (the behaviour of the system, in this case a patterning instability, emerges from the components and is not part of the components). In his system, the reaction kinetics are stabilising and we know that diffusion is stabilising in the sense that it homogenises spatial patterns. Therefore, two stabilising systems interacted to produce an instability.

At the end of the 1960s, under the advices of Waddington [Waddington 1952] (who defined after J. Needham [Needham 1936] the notion of chreod (or morphogenetic surface)), René Thom was the first scientist to develop a general mathematical theory of morphogenetic processes. Broadly, the general concept of his model is: A phenomenon can be described by a system S which, at any given moment, can occupy a specific internal state. The internal states are finite and mutually exclusive. An internal process X controls the system by defining the state that will be occupied by the system at any given point. The junction between physical models and morphological schemes is made by considering that the control space is the spatio-temporal extension of a material substrate. The models proposed by Thom for embryogenesis describe the qualitative variation of perceptible qualities that can be observed in the substrate [Petitot 2011].

Turing and Thom were the "pioneers" on the subject of the development of spatial pattern and form. Since then, many models of how different processes can conspire to produce pattern have been proposed and analysed. They range from gradient-type models involving a simple source-sink mechanism [Wolpert 1969] to reaction-diffusion models based on the Turing theory. [Gierer & Meinhardt 1972] presented a phenomenological model with an activator-inhibitor system, a hypothetical model with series of trimolecular autocatalytic reactions involving two chemicals was probosed be [Schnakenberg 1979] and [Kernevez *et al.* 1979] proposed the empirical model with an immobilized-enzyme substrate-inhibition mechanism involving the reaction of uric acid with oxygen. Cellular automata models have also been proposed in which the tissue is discretised and rules are introduced as to how different elements interact with each other [Bard 1981].

In 1993, [Spirov 1993] proposed a model studying the response of a morphogen reaction-diffusion system to changes of geometry in the developing sea urchin embryo. Their simulations suggest three modes of model dynamics: invagination with following elongation and then metamerization of a "gut"; invagination followed by formation of bilaterally symmetrical "pockets" of the initial invagination; "gut" invagination followed by determination of the "oral field" and the beginning phase of "mouth" formation. Very recently, [Wang *et al.* 2013] evoked the significance of reaction-diffusion equations for gastrulation. They constructed a model for cell proliferation with differentiation into different cell types. They described the cell population densities by coupled reaction-diffusion partial differential equations, which allows steady wavefront propagation solutions.

The problem with the mathematical models trying to explain a biological procedure is that the geometry of the objects cannot be taken into account. Thus, recently scientists have turned to biomechanics in order to find the connection between genetic and molecular-level events and tissue-level deformations that shape the developing embryo.

3.5 Biomechanicals Models of Morphogenesis

In this section, I present an overview of the models proposed to simulate morphogenetic processes. I separate them into two categories: discrete biomechanical models and continuous biomechanical models.

3.5.1 Discrete Biomechanical Models

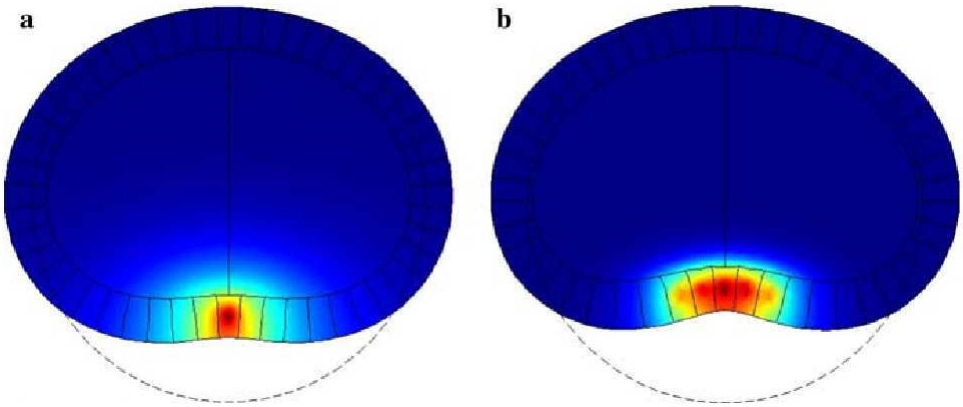

Figure 3.4: *Two configurations of the model of the 2D embryo proposed by [Forest & Demongeot 2008] after shape changes depending on the number of producing cells: (a) only the most ventral cell, (b) the five most ventral cells. Color represents the level of morphogen concentration (red = high level, blue = low level) and the dash line marks the initial exterior delimitation of the epithelium.*

Discrete Biomechanical Models, as mentioned in Section 3.2, are easy to implement and don't require a lot of calculation power. Therefore, they are mostly used to study the molecular mechanisms that affect morphogenetic processes, which are rarely taken into account by Continuous Models.

In 2008, [Forest & Demongeot 2008] used the reaction-diffusion theory to try to create a general formalism for tissue morphogenesis (Figure 3.4). Tissue is considered to be a multi-cellular system whose behaviour is the result of all constitutive cells' dynamics. Morphogenesis is then considered as a spatiotemporal organization of cells' activities. The behaviour of a tissue is the result of the coupling of the cellular system (a tissue is defined as the collection of its constitutive cells) with the control system. In this case, the cellular system is defined by a specific number of partial differential equations to express the linear elasticity of the tissue and another partial differential equation to express the effect of the control system. The control system is the diffusion of the morphogen that determines the effect of the cellular active forces.

Recently, [Sherrard *et al.* 2010] proposed a two-step process for invagination during ascidian gastrulation. The Ascidiacea (commonly known as the ascidians or sea squirts) is a class of sac-like marine invertebrate filter feeders. [Sherrard *et al.* 2010] created a 2D model for the embryo consisting of coupled layers of endoderm and ectoderm, and an explicit dependence on Rho, a cellular regulatory signal. During the first step, the endodermal cells become wedge-shaped due to Rho-dependent apical contraction and the ectoderm is subsequently pulled around them. The second step consists of a Rho-independent basolateral contraction that shortens and spreads the endodermal cells, while their apical sides remain contracted and relatively stiff. According to the authors, this second step drives invagination.

Extending the study of the effect of molecular mechanisms on morphogenetic movements, [Driquez *et al.* 2011] proposed a model based on the stress-activation mechanism suggested by [Odell *et al.* 1981] mentioned earlier in the paragraph. The model examines how the recently identified contractile oscillations in an epithelium [Martin *et al.* 2008, Martin *et al.* 2010] can lead to a sustained contractile force. In the simulation, a region containing a specified stochastic distribution of relatively small oscillating contractions eventually coordinates in phase to stretch a single cell beyond its critical length. This triggers a sustained contraction of that cell, which leads to a collective constriction. In the 2D model this mechanism produces a wave of contraction similar to that observed in vivo.

Conclusion on the Discrete Biomechanical Models

Although the discrete biomechanical models are rather simple to implement and do not demand a lot of computation power, they have certain draw-backs that right now hamper their use. The results that they produce are not always realistic, especially from a mechanical point of view. In addition, the relation between the physical

parameters of the modeled objects and the stiffness of the elements is difficult to define and is always computed approximately. As computers are becoming stronger and stronger and computation power is becoming less of an issue, researchers turn to continuous methods (mostly to the Finite Element Method) in order to create more robust models with a strong physical background. Continuous biomechanical models simulating morphogenetic processes are the subject of the next section.

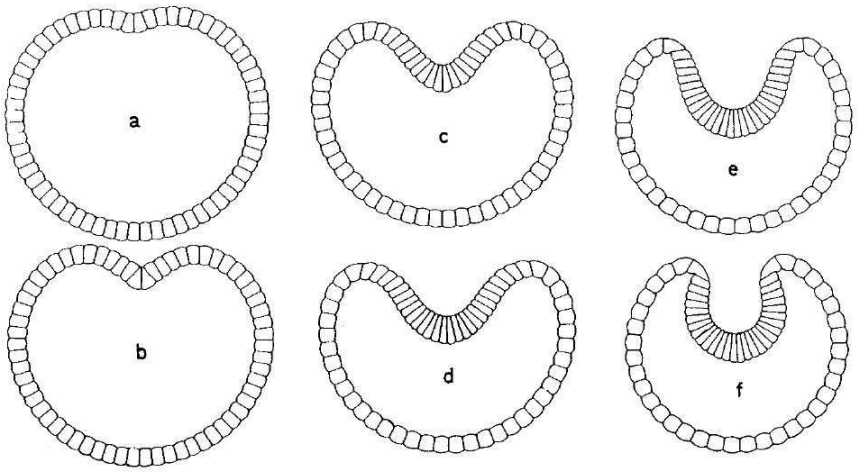

Figure 3.5: *Successive instances of the 2D model of the ventral furrow formation in the blastula of Amphioxus proposed by [Odell et al. 1980].*

3.5.2 Continuous Biomechanical Models

The investigations of the mechanics that drive morphogenesis started in the early 1980s. [Odell *et al.* 1980, Odell *et al.* 1981] presented a 2-Dimensional model of an epithelium of the Amphioxus (a small marine animal). Each cell is treated as a viscoelastic truss-like element with a contractile apex (Figure 3.5). In a circular ring of cells, a specified contraction of the apical surface of one cell of the apex (simulated by a shortening of the stress-free length) stretches neighbouring cells. If stretched beyond a critical amount, the neighbouring cells start to contract as well. Depending on the value of certain parameters, this approach shows how a propagating contraction wave may cause a local invagination, similar to the ventral furrow formation.

Regional variations in mechanical properties can strongly affect morphogenetic shape change. However, the lack of knowledge concerning the mechanical properties in embryos, makes it difficult to distinguish between multiple mechanisms that produce similar shapes. To illustrate this point, [Davidson *et al.* 1995] used spherical finite element models to test five possible mechanisms for sea urchin invagination (Figure 3.6):

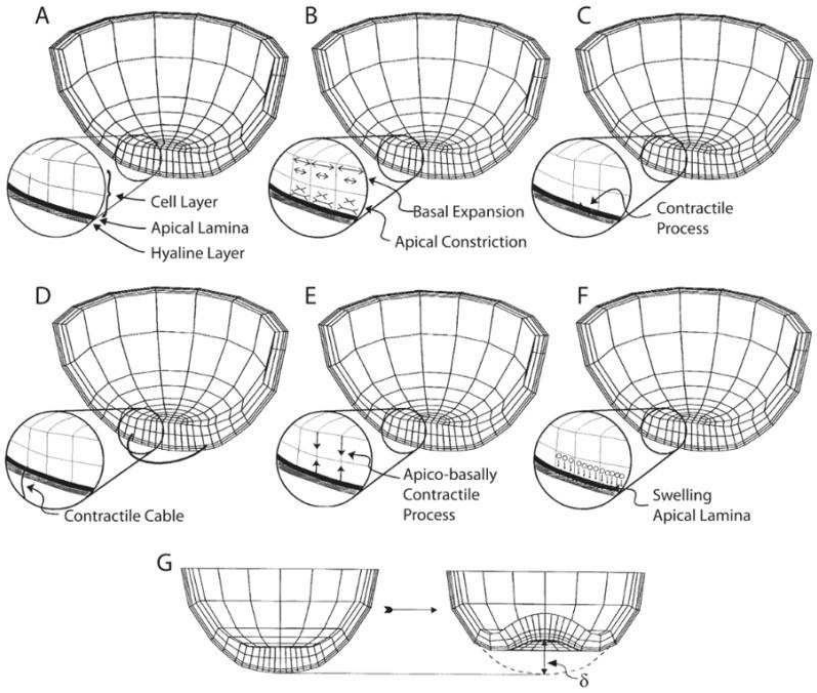

Figure 3.6: *Proposed mechanisms using the finite element method for sea urchin invagination [Davidson et al. 1995]. (A) General features of the models. (B) Apical constriction. (C) Cell tractor. (D) Multicellular contractile ring surrounding the invaginating region. (E) Apico-basal contraction (F) Bending caused by gel swelling (G) Representative deformation*

- apical constriction/basal expansion within a circular region;
- cell tractoring, as cells in a ring at the outer edge of the invaginating region emit protrusions (rods) that contract and pull the ring radially inward, buckling the cells inside the ring;
- circumferential contraction of an actomyosin ring surrounding the invaginating region buckles cells inside the ring;
- apico-basal contraction causing cells in the invaginating region to spread and buckle due to constraints from surrounding tissue;
- regional swelling in the apical lamina with constrained expansion causing the invaginating region to bend inward.

However, in a more recent study, the mechanisms of apical constriction and contractile ring appeared to be ruled out [Davidson *et al.* 1999].

A more recent 2D biomechanical model of the ventral furrow invagination based on deformation gradient decomposition was proposed by [Munoz *et al.* 2007]. They used the continuum growth theory proposed by [Rodriguez *et al.* 1994] to simulate

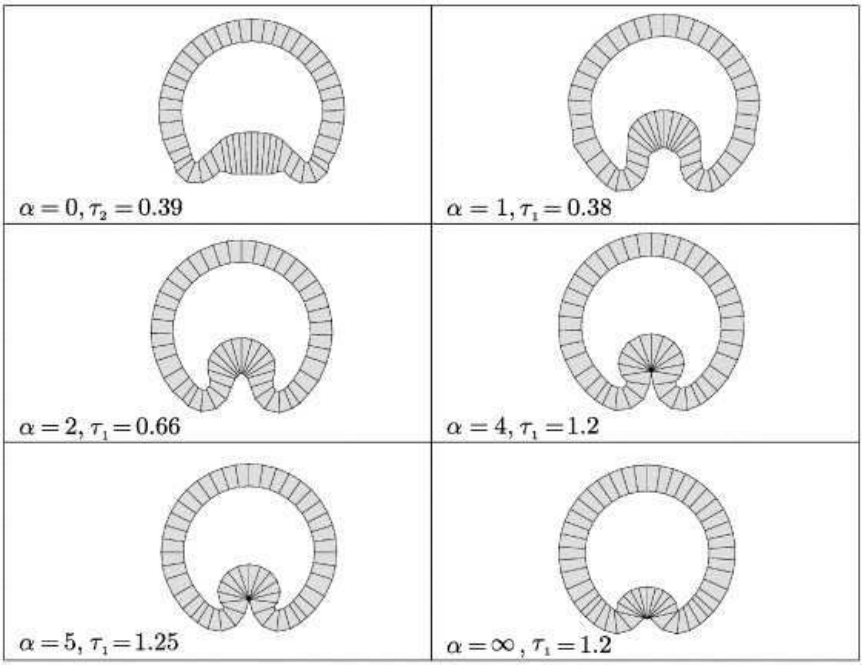

Figure 3.7: *Deformed configurations of the 2D model proposed by [Munoz et al. 2007] with the results obtained with different values of* α*, where* $\alpha = \tau_1/\tau_2 = constant$.

active changes in cell shape in a series of models for ventral furrow formation. A deformation gradient decomposition method was used to model the permanent active deformations and the passive hyperelastic deformations as a local quantity applied to the continuum that models the epithelial layer. Apical constriction and basal elongation of the mesodermal invaginating cells are combined with apico-basal shortening causing a transverse extension in the ectoderm outside this region (Figure 3.7.).

A variation of the 2-dimension model of [Munoz *et al.* 2007] was proposed by [Conte *et al.* 2008]. The new 3-dimension model is used to investigate multiple combinations of invagination mechanisms and to analyse the effect of the surrounding vitelline membrane and internal fluid as factors prohibiting or affecting the cell movement (Figure 3.8). Ectodermal spreading and correlated cell shape changes are combined with regional data on gene expression to understand the principles behind a morphogenetic event.

The same growth theory proposed in [Munoz *et al.* 2007, Conte *et al.* 2008] was used by [Allena *et al.* 2010] to create a more generic model of the Drosophila embryo to study morphogenesis. The authors simulate three early morphogenetic movements: ventral furrow formation, cephalic furrow formation and germ band extension. The main novelty of this model is that it reproduces the three previously mentioned developmental events in one common framework.

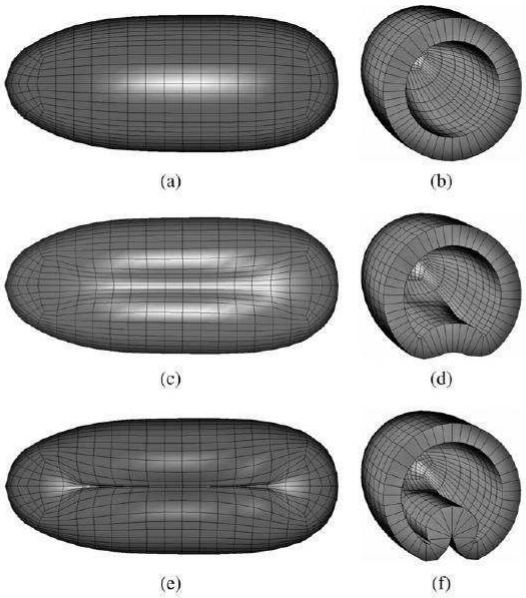

Figure 3.8: *3D ellipsoid model of the ventral furrow formation presented by [Conte et al. 2008]. (a) and (b) show respectively a ventral view and a cut-away view of the undeformed finite element model of the embryo in its initial configuration. (c) and (d) show a later stage of the simulation in which the embryo model is deformed. (e) and (f) show the final stage of the simulation of ventral furrow invagination.*

Conclusion on the Continuous Biomechanical Models

Although the continuous biomechanical methods require a very big amount of calculations, which translates into time and expensive hardware, they still have the advantage over the discrete models. First of all and more importantly, the main benefit from using continuous methods is the fact that we can attribute physical properties to the modeled soft tissues. This way, we can profit of the physical laws in order to precisely describe the behaviour of the elements in our model. In addition, changing the input parameters is easy, in case the result is more accurate enough or, in the opposite case, when the accuracy is not the most important part of the simulation. Depending on the desired *precision/cost* ratio (whether cost translates to time, computing power or money...), we can parametrize the model so that it suits best our purpose. Finally, continuous methods also allow the simulation of interactions between different tissues or materials.

3.6 Conclusion

In this chapter, I presented the mathematical, the discrete and the continuous biomechanical methods to model soft tissues. In order to answer the question that gave birth to the biggest part of this thesis: “How does apical constriction affect

the ventral furrow invagination?" (see Section 2.10 in page 20), I considered that a mathematical model does not suffice. We hypothesized that the specific "bean-shaped" geometry of the embryo plays an important role and mathematical models cannot take it into account.

To understand the role of the geometry of the embryo, a biomechanical model is necessary. In the next chapter I will describe the first attempt made to simulate the ventral furrow invagination with a discrete model. I will insist both on the positive feedback and on the negative aspects of the discrete model and explain why and how, after a certain point, it became clear that we needed a continuous model based on the Finite Element Method in order to efficiently validate and support our hypothesis.

Chapter 4

Modeling the Drosophila Ventral Furrow Invagination

Contents

4.1 Introduction

In this chapter I will present the work done in the course of this thesis attempting to answer the questions raised in the two introductory chapters:

- **What is the role of the apical constriction of ventral cells in the invagination?**
- **Is a discrete model sufficient to explain the mechanism that drives ventral furrow invagination? Is the Finite Element Method more adequate to simulate embryogenetic processes?**

Section 4.2 presents the discrete model of the ventral furrow invagination. Sections 4.2.2 and 4.2.3 shows an example of how the discrete model is used in order to study important factors during morphogenesis. In Section 4.2.2, the speed of the invagination in different parts of the embryo is measured in the model to test the first hypothesis. In Section 4.2.3, the model is coupled with a Reaction-Diffusion

Partial Differential Equation (RD-PDE) for myosin dispatching, to study the relation between myosin dispatching and cell contractions. Finally, the model of the ventral furrow invagination based on the Finite Element Method is presented in Section 4.3. Each section presents the articles respectively published in "ECAL'11, Advances in Artificial Life" and in the "Proc. IEEE Workshops of Int. Conf. on Advanced Information Networking and Applications (WAINA) Conf 2011" and the article that is going to be submited to the Journal of BMC Bioinformatics.

4.2 Discrete Model of the Ventral Furrow Invagination

In this section, the physically based discrete model of the embryo of the Drosophila Melanogaster is presented. The principles controling the behaviour of the model are explained and then I present the scientific articles in which this model has contributed.

4.2.1 Behaviour control of the physically based discrete model

In this section, I explain the general principles followed to create the discrete biomechanical model of the ventral furrow invagination. This model (presented in Section 4.2.2) is the original idea behind this thesis. The model is based on an object oriented library developed in [Promayon *et al.* 2003] and [Marchal *et al.* 2006]. More details about this library can be found in Annex A.

The behaviour of cells, defined as cellular objects in the simulation is controlled, by three general principles: elasticity, contractility and incompressibility. Elasticity and contractility are considered as forces applied on each particle. They are denoted ${F_e}^*$ and ${F_c}^*$ respectively. Incompressibility is considered as a constraint that acts directly on the particles' positions. In the following paragraphs, we describe how these physical principles were implemented.

Elasticity

The general principle is that elasticity is based on a shape memory force and on the so called rest shape attractor.

Each particle is defined by a position, a mass, a list of connected particles (neighbors) and elastic properties. Let P be the position of a given particle and N_i, $i \in \{1, ..., n\}$ the positions of the n neighbors of this particle. The idea is to express the position P^* of the rest shape attractor of the particle as a function f of the position of his n neighbors. f computes the position of the rest shape attractor of the particle P based on the configuration of the neighboring particles at time t and some scalars defined at rest shape, i.e. when the cell is not deformed. In addition, f is expressed as a generalized discrete formulation of barycentric coordinates. If a deformation occurs, P^* corresponds to the position that minimizes the distance

between the current and the rest shape. A single spring is then used to generate an elastic force that brings the particle towards its attractor.

Consequently, a "memory" force ${F_e}^*$ is generated between the current position of the particle and the position of its attractor, given by the following statement:

$$ {F_e}^* = k_e(P^* - P) $$

where k_e is the elasticity coefficient (which in our work is defined as a simple scalar uniformly distributed along the particles).

Contractility

The characteristics of contractility are its application particles, its mechanical and electrical properties and, mainly, the fibers which it incorporates. In our model, contractility is generated by creating fibers between given particles. The principle used here is again a force created by an attractor. Each neighboring particle located in the direction of the fiber is considered as an attractor. An internal force ${F_c}^*$ is generated between the current position P of a particle and the position ${P_i}^*$ of each of its attractors:

$$ {F_c}^* = k_c(P_i^* - P) $$

where k_c is the contractility coefficient. This coefficient models the activation, contraction and relaxation phases. It can vary during the simulation. A positive coefficient yields to an active contraction. When k_c has decreased to zero, the contractile force is nullified and the cell returns to its original configuration, due to the elasticity property.

Incompressibility

In this section, we present the principle of the method implemented to control the volume of the cells. Consider the surface of an object in 3D represented by a triangular mesh with n vertices. Let P_1,...,P_n be the positions of these vertices and F_1,..., F_m the m triangular facets. Let X be the vector of size $3n$ composed by the positions of all the vertices: X=(P_1,...,P_n) is the vector describing the state of the polyhedron. Let $V(X)$ be the volume function of the mesh with V_0 the initial volume. The technique implemented is as follows: suppose a deformation of the triangular mesh represented by the vector X'. The method implemented allows us to find a vector X'' similar to X', whose volume is equal to V_0 (the initial volume). Consequently, what we need to do is determine the displacement of each vertex, solving the following system:

$$ \begin{cases} X'' = X' + \lambda \nabla V(X') \\ V(X'') = V_0 \end{cases} $$

where ∇V is the gradient of the volume V and λ is a scalar.

The solution can be written as the following system of equations:

$$\begin{cases} P_i'' = P_i' + \lambda \nabla_i, \forall i \in \{1, ..., n\} \\ \sum_i V_i'' = V_0 \end{cases}$$

with

$$\nabla_i = \frac{1}{3N} A_i$$

where P_i'' is a vector denoting the new position of each particle, ∇_i is the i-th component of the gradient of the volume function and A_i is the area vector of the i-th facet.

It can be proven that the solution of the previous system can be given by a third degree equation where λ is the only unknown scalar. Then, the displacements $\lambda \nabla_i$ of the vertices of the mesh are applied according to the value of λ.

In our model, a cell surface is made of 12 triangles linking the particles.

4.2.2 General architecture of a genetic regulatory network. Applications to embryologic control

This section includes the published paper that presents the use of the physically based discrete model of the embryo of the Drosophila Melanogaster is presented [Demongeot *et al.* 2011]. In section "Physical Model of Ventral Furrow" and Figures 6 and 7 of the article, we focus on the extremities of the embryo. The simulation in Figure 8 shows that, although there is an equal initial distribution of elasticity and contractility along the model, the process of invagination starts from the extremities of the geometry and propagates to the ventral medial area. This is more obvious in Figure 9, where the whole model of the embryo after invagination is compared with an instance of the *in vivo* study of [Martin *et al.* 2008].

General architecture of a genetic regulatory network. Applications to embryologic control

Jacques Demongeot[1], Alexandra Henrion-Caude[2], Athanase Lontos[3], Emmanuel Promayon[3]

[1]Université J. Fourier Grenoble 1, AGIM, CNRS FRE 3405, 38706 La Tronche, France
[2]Université Paris Descartes, INSERM U 781, Hôpital Necker – Enfants Malades, 149 rue de Sèvres, 75015 Paris, France
[3]Université J. Fourier Grenoble 1, TIMC-IMAG, CNRS UMR 5525, 38706 La Tronche, France
Jacques.Demongeot@agim.eu

Abstract

The general architecture of a genetic regulatory network consists of strong connected components of its interaction graph, to which are attached three kinds of sub-structures:
- a set of up-trees, rooted in the sources of the interaction graph, represented either by small RNAs like microRNAs: nuclear miRs or mitochondrial mitomiRs, i.e., translational inhibitors respectively of the messenger mRNAs and of the transfer tRNAs, or by gene repressors and/or inductors,
- a set of circuits in the core (in graph sense) of the strong connected components of the interaction graph,
- a set of down-trees going to the sinks of the interaction graph, i.e., to genes controlled, but not controlling any other gene.

The various state configurations it is possible to observe in the above sub-structures correspond to different dynamical asymptotic behaviors. The network dynamics have in general a small number of attractors, corresponding in the Delbrück's paradigm to the functions of the tissue they represent. Examples of such dynamics will be given in embryology: cell proliferation control network in mammals and gastrulation control network in Drosophila *melanogaster*.

Introduction

Genetic networks can be considered as the analogues of neural networks for controlling the expression of genes. Their time constants are different (e.g., the rhythms of protein expression are of the order of magnitude of some minutes and those of neural firing are of some milliseconds) but their connectivity is about the same (in-degree between 1.5 and 3, i.e., the mean number of the genes or neutrons influencing positively or negatively other ones is between 1.5 and 3) as well as the number of their strong connected components (rarely more than 2 for the control of a dedicated function). For these reasons, many common mathematical features have been adopted by the modelers in charge of designing the interaction graph of such networks: i) Boolean representation of the state space (1 if the gene is expressed, 0 if not), ii) Hopfield-like transition function (Demongeot and Sené, 2008d; Demongeot et al., 2008c, 2009b, 2011b, in press) and iii) extraction of the same features, like entropy and motifs (Demongeot et al., 2010). We will use in this paper this common theoretical framework in order to interpret examples of the genetic network dynamics.

Generalities about the architecture of the interaction graph of a genetic network

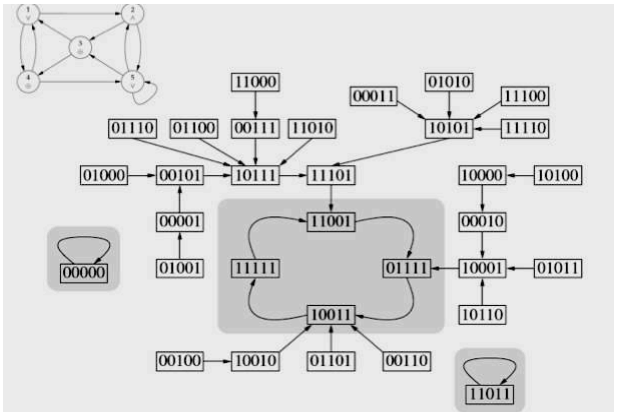

Figure 1: The interaction graph (top left) and the trajectory graph of a Boolean genetic regulatory network

The architecture of a genetic network can be decomposed into 3 directed graphs: i) the interaction graph with positive (resp. negative) arrows for induction (resp. repression), ii) the trajectory graph made of the consecutive states from an initial state until an asymptotic behavior (fixed state or limit-cycle of periodic states) and iii) the updating graph with an arrow between two genes if the target gene is updated after the source one. The knowledge about the first graph is given by DNA-protein interactions, about the second by DNA array devices recording gene expression and about the third by the chromatin clock. This architecture shows in Figures 2 and 3 some common features: i) a set of up-trees, issued from the sources of the interaction graph of the network, made either of small RNAs like siRNAs or microRNAs (nuclear miRs or mitochondrial mitomiRs, respectively translational inhibitors of the messenger mRNAs and of the transfer tRNAs), or of gene repressors and/or inductors, self-expressed without any

other gene controlling them, ii) a set of circuits in the core (in the graph sense) of the strong connected components of the interaction graph. These circuits are unique or multiple, disjoint or intersected, reduced to one gene or made of several ones, negative (having an odd number of negative interactions) or positive, and iii) a set of down-trees going to the sinks of the interaction graph.

By identifying each function of a regulatory network to one of the attractor of its dynamics as suggested by Delbrück (Demongeot, 1998), it is possible to count the number of the attractors provided by isolated circuits, and the number – largely reduced – brought by tangential or intersected circuits (Demongeot et al., 2009b, 2011a, 2011b, in press), depending on the updating mode fixed by the chromatin dynamics.

The control of the genetic networks by microRNAs (miRs). Example of mitomiRs

Since a decade, numerous small RNAs issued from the non coding part of plant and animal genomes (like silencing siRNAs and microRNAs or miRs) have been found as inhibiting the translation by hydridizing the mRNAs with the help of RNA-binding oligo-peptides. This inhibition is partly aspecific because of the large number of possible mRNA targets for each small RNA. On Figure 2, the dynamics of a circuit of size 3 (3-circuit) is analyzed, when one gene of the 3-circuit is inhibited by a miR. If the inhibition is associated to another inhibition of this gene or if it is sufficiently strong, it is able to transform a limit-cycle behavior in a fixed configuration, the circuit being either negative or positive (Figure 2 top left and top middle). When the miR inhibition is less than the activation on the target gene, then the periodic behavior is conserved (Figure 2 top right). We can say that the inhibitory influence by the small RNAs is exerted only on sufficiently "weak" circuits, like on the carved (weak) zones of an etching on which only the nitric acid can carve.

Recently some nuclear miRs like miR-1977 (Figure 3) have been discovered whose targets are mitochondrial mRNAs coding for enzymes of the oxidative phosphorylation (Bandiera et al., 2011). Such miRs have been called mitomiRs (Dass et al., 2010). This discovery invited to examine if there exist parts of the non-coding mitochondrial DNA (called the d-loop, cf. Figure 3) susceptible to code for hybridizing RNAs blocking the free parts (the loops) of the mitochondrial tRNAs: the corresponding inhibition would be totally aspecific and exerted in situ without nuclear control in order to slow oxidative phosphorylation in absence of a strong energetic need. This effect could be useful for ruling the balance Pasteur/Warburg effect versus OxPhos effect, allowing to avoid both cancers in case of Pasteur/Warburg dominance and degenerative diseases in case of oxidative phosphorylation dominance (Demetrius et al., 2010; Israel and Schwartz, 2011).

Several sequences corresponding to the tRNA loops – essentially the tRNA D-loop, but also Anticodon-loop and TψC-loop have been found both in nuclear and in mitochondrial miRs. We will take in the following as reference the Lewin's tRNA given in (Krebs et al., 2009): it has been proved that the loops sequence in this reference tRNA was the closest among all known tRNAs to an Archetypal Basic RNA sequence of 22 bases (called RNA AB) verifying the following variational min-max principle:

- to be as short as possible,
- to present one and only one triplet corresponding to each amino-acid, in order to serve as "matrimonial agency" favouring the vicinity of any couple of amino-acids, close to RNA AB, and able to form strong peptide bonds (i.e., covalent chemical bonds formed by two amino-acids, when the carboxyl group of one reacts with the amine group of the other) between them, in order to initiate the peptide building as an ancestral tRNA, well conserved for example in the present Gly-tRNA of Œnothera *lamarckiana*.

For satisfying the constraints above, the RNA AB must be circular and contain at least 20 triplets. The minimal solution is given in (Demongeot and Besson, 1983; Demongeot and Moreira 2007; Demongeot et al. 2006, 2008a, 2009a, 2009c). The corresponding RNA AB sequence can be given in circular or hair-pin form and could be considered as the ancestor of the present tRNA loops. We will indicate in the following in blue the possible hybridization sites, by using the complementary pairing A-U, C-G and G-U:

1) for the nuclear mitomiRs, we have a pairing with:
- the D-loop and TψC-loop (13/22) (Bandiera et al., 2011)
5' UAAAUGGUACUGCCAUUCAAGA 3' AB
3' AAUUGUCGAUUCGUGGGAUUAG 5' miR 1977
- the Anticodon-loop (12/22) (Bandiera et al., 2011)
5' UUCAAGAUAAAUGGUACUGCCA 3' AB
3' AUAAGAGCGUGCCUGAUGUUGGU 5' miR 1974
- the TψC-loop (12/22) (Bandiera et al., 2011)
5' GAUAAAUGGUACUGCCAUUCAA 3' AB
3' AUCUUUCCGAUCCUGGUUUGG 5' miR 1978

2) for the mitochondrial mitomiRs, we have a pairing with:
- the D-loop (Cui et al., 2007)
the sequence **AAUGGUA** is found in many species in the CSB part of the mitochondrial d-loop (Figure 3)
- the TψC-loop (Sbisa et al., 1997)
the sequence **GUACAUU** is found in many species in the ETAS part of the mitochondrial d-loop (Figure 3)

Each pairing described above corresponds to a probability less than 10^{-4} to occur (Demongeot and Moreira, 2007) and could correspond to the relics of an ancient protein building mechanism without ribosomes, in which the amino-acids were directly linked to RNA chains or cycles playing the role of matrimonial agency, i.e., facilitating the grouping of amino-acids, hence favoring the constitution of peptidic bonds between them (for other hypotheses concerning the catalysis of peptidic synthesis, see (Huber and Wächtershäuser, 1998; Hsiao et al., 2009)). When tRNA loops are hybridized by nuclear or mitochondrial mitomiRs, efficacy and specificity of the complex made of amino-acid, tRNA and amino-acyl-synthetase (enzyme esterifying an amino-acid for complexing it to a specific tRNA) can be affected, causing an inhibition of the translation mechanism.

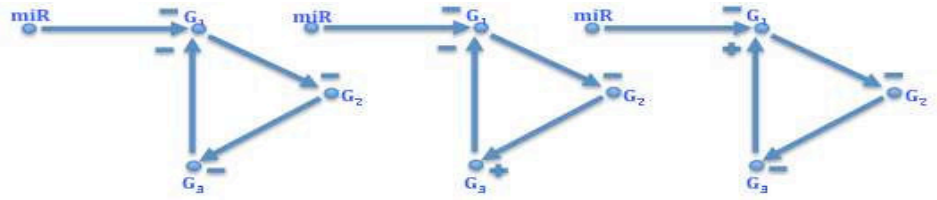

miR	G1	G2	G3	miR	G1	G2	G3	miR	G1	G2	G3
0	1	1	1	0	1	1	1	0	1	1	1
0	0	0	0	0	0	0	1	0	1	0	0
0	1	1	1	0	0	1	0	0	0	0	1
0	0	0	0	0	1	1	1	0	1	1	1

miR	G1	G2	G3	miR	G1	G2	G3	miR	G1	G2	G3
1	1	1	1	1	1	1	1	1	1	1	1
1	0	0	0	1	0	0	1	1	0 (1)	0	0
1	0	1	1	1	0	1	1	1	0 (0)	1 (0)	0 (1)
1	0	1	0	1	0	1	1	1	0 (1)	1	0 (1)

Figure 2: Top) Architecture of 3-circuits controlled by a miR, with negative (left) and positive (middle and right) circuits. Middle) Periodic dynamics when the miR is not expressed (miR=0). Bottom) Fixed configuration if the miR is expressed (miR=1), except if the miR inhibition is less than the gene activation (in parentheses), case in which the periodic behavior is conserved.

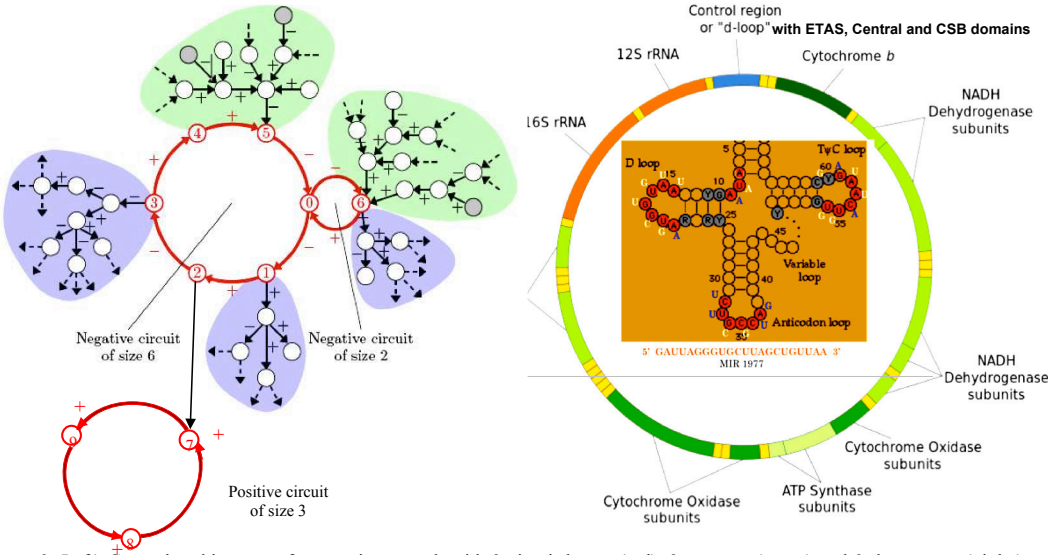

Figure 3: Left) General architecture of a genetic network with 2 circuit layers (red), 2 up-trees (green) and 3 down-trees (violet). Right) the circular mitochondrial DNA with its non-coding part (d-loop blue) and inside a tRNA structure hybridized by miR 1977.

Genetic network ruling the cell-cycle

The genetic network ruling the cell-cycle in mammals, centered on the gene E2F, is crucial for cells because of its links with Engrailed network controlling: i) through gene Elk the potassium channels in hippocampus neurons ruling the memory (Top of the Figure 4) and ii) through genes Engrailed/GATA-6, c-Myc and RAS, in a double incoherent control pathway (with both positive and negative arrows, respectively in red and green in Figure 4), the apoptosis and proliferation processes. This last control must be very precise if the tissue controlled has to keep constant its cell number. A way to obtain this acute control is to intersect in the Engrailed network several circuits (cf. Figure 4 Bottom right and (Demongeot et al., 2009b, 2011a, 2011b, in press)) and to exert an inhibitory control through miRs and/or mitomiRs, themselves possibly controlled by p53 (Figure 4 Middle).

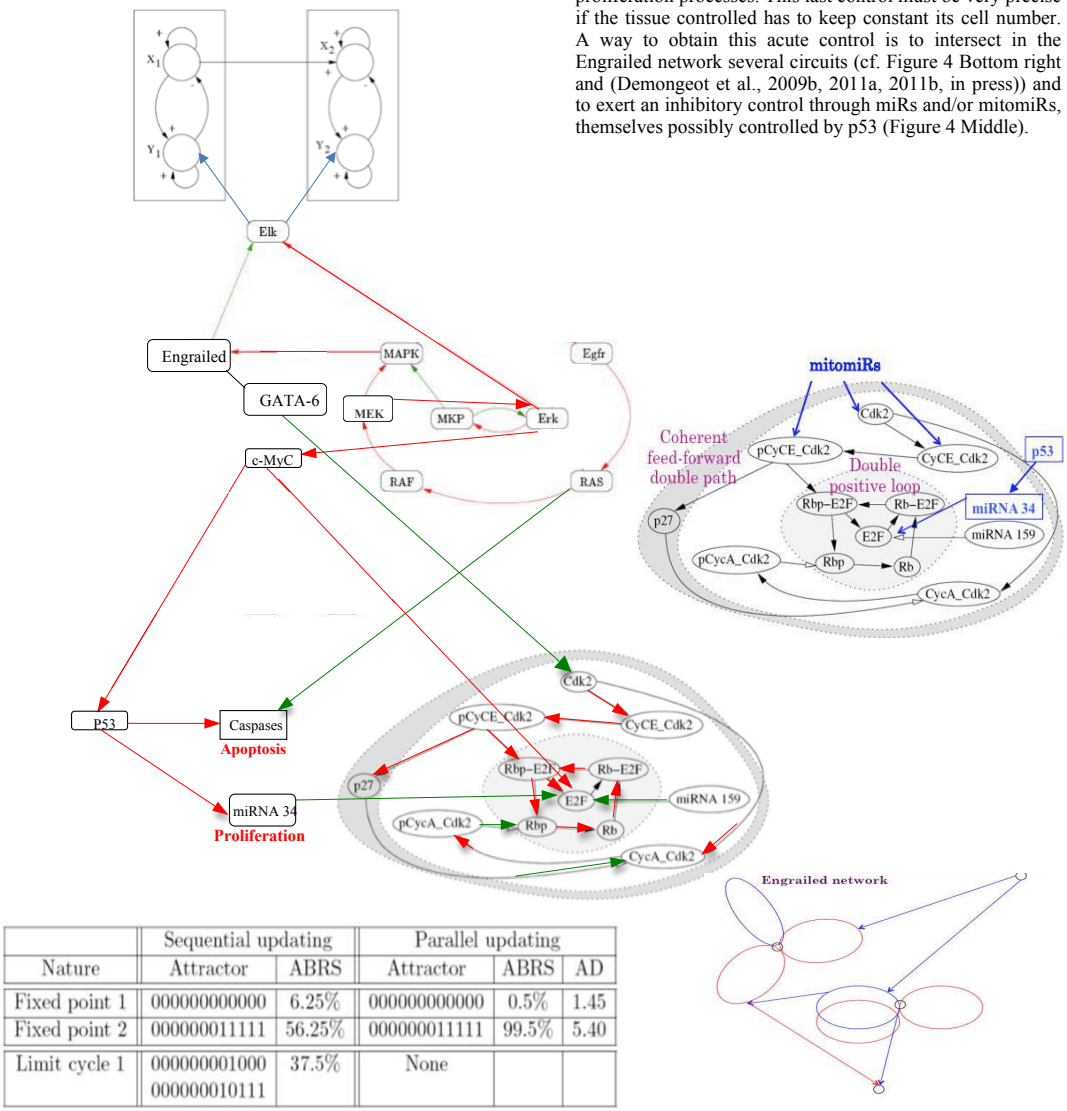

	Sequential updating		Parallel updating		
Nature	Attractor	ABRS	Attractor	ABRS	AD
Fixed point 1	000000000000	6.25%	000000000000	0.5%	1.45
Fixed point 2	000000011111	56.25%	000000011111	99.5%	5.40
Limit cycle 1	000000001000 000000010111	37.5%	None		

Figure 4: Middle right) Cell cycle controlling genetic network centered in mammals on the E2F box inhibited by small RNAs (miRs or nuclear and/or mitochondrial mitomiRs). Top left) Engrailed network controlling the potassium channels of hippocampus neural networks. Middle left) Engrailed network controlling both apoptosis and proliferation processes. Bottom left) Attractors of the dynamics specific to the E2F box. Bottom right) General structure of the Engrailed network.

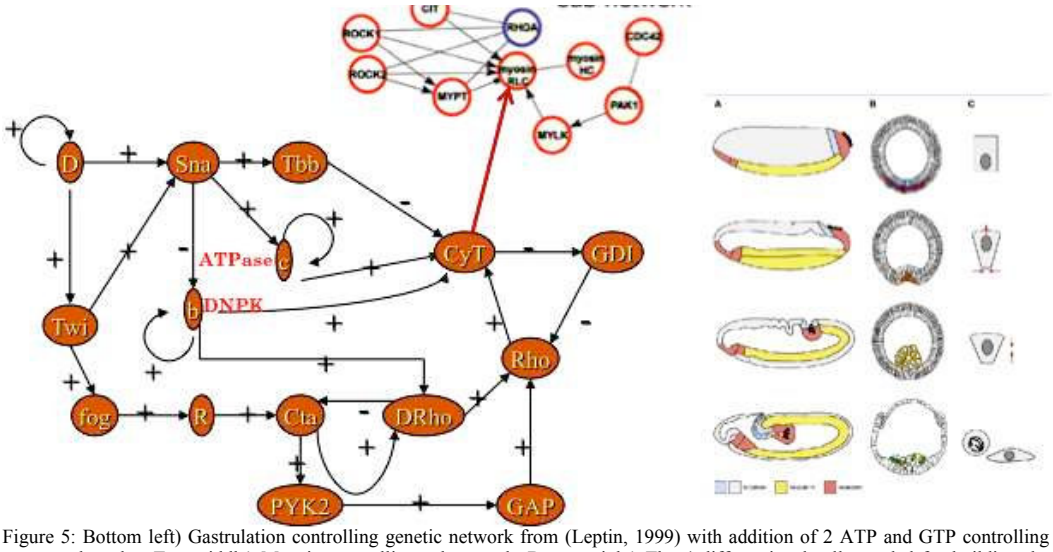

Figure 5: Bottom left) Gastrulation controlling genetic network from (Leptin, 1999) with addition of 2 ATP and GTP controlling enzymes b and c. Top middle) Myosin controlling subnetwork. Bottom right) The 4 differentiated cells needed for building the future digestive tube.

A triple action (accelerate, stop and slow down the cell cycle) on proliferation process is exerted negatively by the gene GATA-6 which is inhibited 1 time out of 2 by MAPK, and successively positively and negatively by the gene c-MyC which is activated 1 time out of 2 by Erk. The limit cycle of order 4 brought by the negative circuit of size 2 (MKP/Erk) leads genes MKP, Erk, MAPK, Engrailed, GATA-6, c-MyC, p53, miRNA34, Cdk2, E2F and caspases to the limit-cycle: 01100001001, 11110100001, 10011110000, 00000011011. Then the second fixed point of the E2F box is reached 1 time out of 4 and the caspases/apoptose box is activated 1 time out of 2: this result allows the exponential growth of the cell number to be compensated in a tissue by the linear growth of the apoptosis, 2 daughter cells replacing 2 dead cells during one period of the limit cycle, hence ensuring the conservation of the tissue volume and tissue function, any disequilibrium of the balance giving either a tumor growth or tissue rarefaction.

Genetic network ruling the gastrulation

The gastrulation is a dynamical process occurring at the end of the blastula phase. It is an early embryonic stage, including mass movement of cells to form complex structures from a simple starting form. Experiments in vivo have shown that there are many types of mass cell movement taking place during gastrulation: ingression, invagination, involution, epiboly, intercalation and convergent extension. In the next Section, we will focus on the simulation of the phenomenon of invagination of cells, which leads to the creation of the ventral furrow. In order to control the gastrulation process, a genetic regulatory network has been proposed in (Leptin, 1999). This network has been improved by adding 2 genes (Figure 5 Bottom left): ATPase (enzyme located inside the inner mitochondrial membrane ensuring the resourcing of ATP from ADP) and DiNucleotide Phosphate Kinase (enzyme resourcing GTP from GDP and ATP). This addition of genes allows the network to pass from 2 to 4 attractors, providing the 4 types of differentiated cells (from bottle cell to intestinal epithelial cell) needed to achieve and finish the digestive tube (Figure 5 Bottom right). The CyT node correspond to the genes involved in the CyToskeleton formation, i.e., essentially the genes of Actin, Tubulin and Myosin, the latter being controlled by a specific subnetwork (Figure 5 Top middle). When the genes coding for the two types of Myosin (RLC, with Regulatory Light Chain and HC, with Heavy Chain) are expressed, then the ventral furrow invagination can start. We will model this process in the next Section showing with a simple mechanical model that it begins by a cell contraction followed by an invagination at the two extremities of the Drosophila embryo, extended after to central embryo region.

Physical Model of Ventral Furrow

Several successful models have already been created in order to simulate the process of ventral furrow invagination in Drosophila *melanogaster*. Although they have been extensively monitored, the parameters driving the movement and deformation of cells are not fully explained. We shall describe the structure of our physical model, the parameters we used to create it, the assumptions we made and the new possibilities and questions raised by this approach. This work focuses on the area of the structure where the phenomenon begins. As a result, we have modelled the upper part of one side of blastula (Figure 6) as described in (Abbas et al., 2009).

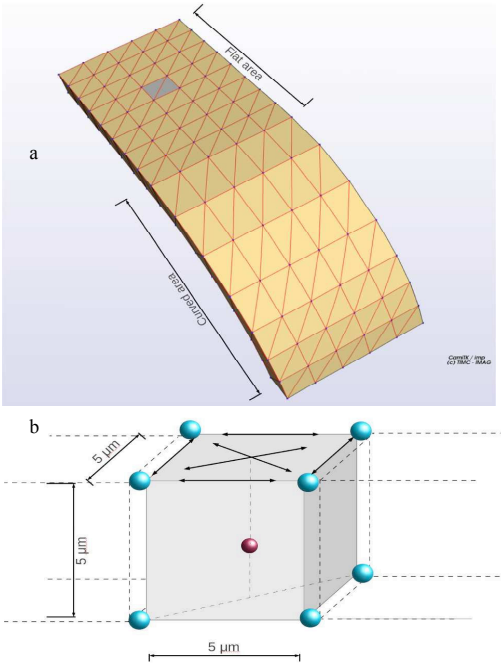

Figure 6: a) Representation of the simulated embryo structure at its initial shape and b) of an individual cell located at area of the centre row of the structure with its centrosome in red.

In our approach, the structure consists of 75 cells arranged in 15 columns of 5 cells each. The first 8 columns form the central part of the structure. The curvature of the structure starts at column 9 and ends at column 15, for a total curvature of 90° (Figure 6a). Each cell is modelled as a hexahedral object, composed of 9 particles. 8 particles are used as the vertices of the hexahedron and one particle is located in the middle, denoting the centrosome of each cell. The cells, with the aid of a biomechanical library, are defined as individual physical objects, with three distinct characteristics: incompressibility, elasticity and contractility. The structure is represented on Figure 6 at its initial shape and an individual cell is located at the central row of the structure. The grey cell corresponds to the cell presented in Figure 6b. The cells of the central area are modelled by cubes with edges of 5µm2, resulting to 6 facets of initial surface equal to 25µm2. The initial volume is 125µm3. Muscular forces (black arrows) connect the particles of the top facet of the cell. The red sphere represents the centrosome, initially located at the centre of the cell. The particles are modelled as nodes with the ability to interact with their environment. They are defined by their position and their mass. Elastic and muscular forces are applied on them and they can also be submitted to boundary conditions. Their combined displacement is the crucial factor that affects the cell deformation and movement. The incompressibility algorithm, uses the facets geometry and a displacement constraint, to keep the volume of cells constant. Elasticity forces are defined between neighbouring particles in order to model the tissue reaction against deformation (Henon et al., 1999; Promayon et al., 2003). The elasticity parameters have a small value, so that the cell shape can be modified quite easily by other forces. As a result, we have deformable cells, with nearly unchangeable volumes (which imitates the behaviour of cells in vivo). In addition, using muscular forces, we can induce the contraction of cellular objects similar to those due to the Myosin excess (Patwari and Lee, 2008). Using a higher value of the elasticity parameter for the centre particle (centrosome), we ensured that this particle stays close to the centre of the cell, even when the cell is deformed. This allows us to model the rigidifying effect of the cytoskeleton. In vivo experiments have shown that neighbouring cells form Adherens Junctions (AJs), which contain complexes of the transmembrane adhesion molecule E-cadherin and the adaptors α-catenin and ß-catenin (Gumbiner, 2005; Martin et al., 2010). In addition, these AJs are formed in the apical areas of the lateral surfaces of the cells (Tepass and Hartenstein, 1994; Oda and Tsukita, 2000). In our model, we have considered AJs to offer very strong linking between cells. Therefore, the vertices of the hexahedron are merged, summing up the forces and constraints of all concurrently surrounding cells. This allows a faster propagation of the forces during the simulation.

Simulation

Particles at the top of each cell in the central row are linked by muscular forces, which are used to model the forces applied by the orthogonal perpendicular Myosin fibres (Figure 6b). The norm of these forces for each particle is the same, resulting from a uniform distribution of forces along the structure, as suggested in (Brodland et al., 2010). More, boundary conditions are applied to the movement of some particles to verify the symmetry of the simulation (Figure 7):

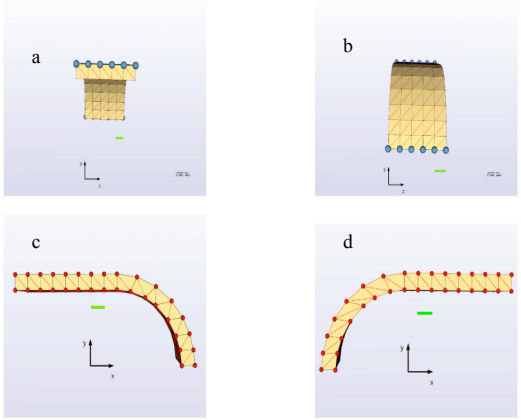

Figure 7: Representation of the boundary conditions imposed on the simulated embryo structure.

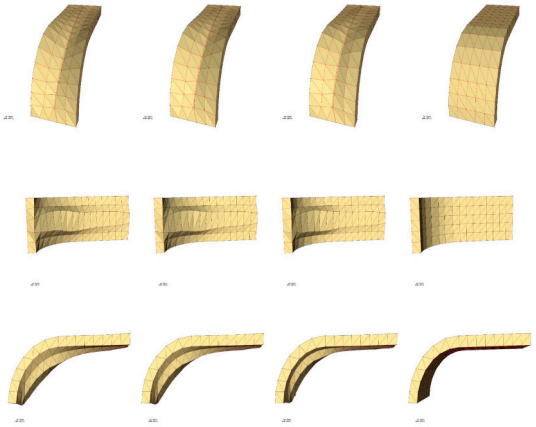

Figure 8: Simulation of the ventral furrow invagination process in Drosophila *melanogaster*.

i) the first boundary condition implies that structure edges cannot move in any direction (Figures 7a,b), ii) the second is applied on the side parts of the structure (Figures 7c,d).

The particles can "slide" on the x and y axis but they cannot move on the z axis. These boundary conditions allow the simulation to consider that this model is a part (Figure 8) of a bigger structure, with cells expanding from all sides, in order to form a tubular shape, as presented in Figure 9. At the beginning of the simulation, all the particles are submitted to forces of equal value. This is achieved by applying uniform elasticity and contractility coefficients along the structure. The simulation is divided in time-steps. Each time-step corresponds approximately to 0.05 seconds. At each time-step, the following processing takes place:
- the forces are summed up on all the particles and integrated along the structure using a classical integration scheme,
- the velocity and position of each particle are calculated and integrated also along the structure,
- the constraints are applied (incompressibility and boundary conditions).

In Figure 8, we present the geometry obtained for four different instances of the simulation, from three different angles. In the first row, the geometry is shown from the top, in the second row, it is shown from the bottom and in the third row it is shown from the side of the structure. In next papers to appear, we will provide videos of the entire simulation from all three points of view. At the beginning the cells in the centre row are contracting due to the activation of the Myosin fibres (after entering in the Bottle cells attractor of the previous Section). This contraction pulls all the cells of the model towards the centre. Due to the initial geometry of the structure, as shown in Figure 8, the vertical component of the force applied on the particles of the curved area causes the particles to move downward. As the cells located on the centre row of the curved part move downward, they concurrently pull the other cells of the structure as well, due to the cell-cell bonds. As a result, all the cells start to move downwards (see Figure 8).

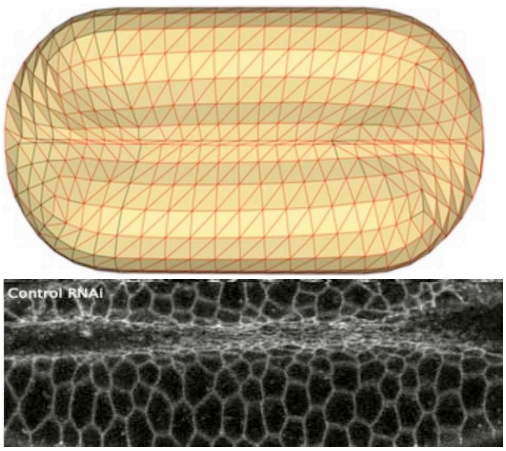

Figure 9: Simulation of invagination starting at the Drosophila embryo extremities (Bottom from (Martin et al., 2010)).

An important factor concerning the invagination process is the surface/volume ratio. In vivo experiments have shown that, as the phenomenon proceeds, the area of the cell in contact with the nourishment fluid decreases (Leptin, 1999). On the other hand, cell volume increases. As a result, the surface/volume ratio decreases with time. It has been noted that it can decrease up to a certain threshold, after which the cell tends to divide (Figure 9) as observed in (Cui et al., 2005).

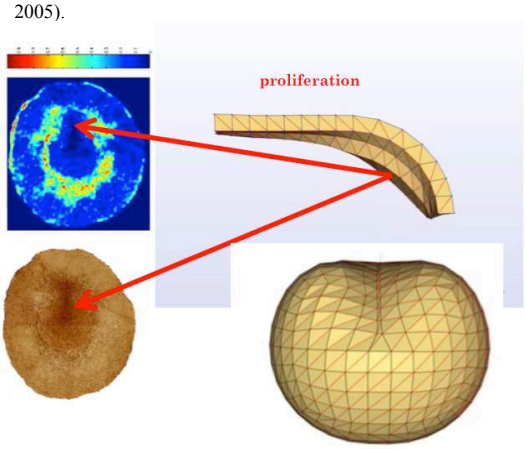

Figure 9: Proliferation occurring at the most invaginated part of the Drosophila embryo extremities, the Top left showing a BrDU pre-mitotic S-phase activity from (Cui et al., 2005)).

Conclusion

We have shown in this paper that the general architecture of a genetic regulatory network involves several genetic circuits, which are crucial for imposing a dynamics having only few attractors, corresponding to few functions to fulfil. This small number of attractors is well controlled by the existence of circuit intersections as well as by the presence of an aspecific inhibitory "noise" from small RNAs, like miRs and mitomiRs.

References

Abbas, L., Demongeot, J. and Glade, N. (2009). Synchrony in Reaction-diffusion models of morphogenesis: applications to curvature-dependent proliferation and zero-diffusion front waves. *Phil. Trans. Royal Soc. A*, 367:4829-4862.

Bandiera S, Rüberg S, Girard M, Cagnard N, Hanein S, Chrétien, D., Munnich, A., Lyonnet, S. and Henrion-Caude, A. (2011) Nuclear Outsourcing of RNA Interference Components to Human Mitochondria. *PLoS ONE* 6:e20746.

Ben Amor, H., Demongeot, J., Elena, A. and Sené, S. (2008). Structural Sensitivity of Neural and Genetic Networks. *Lecture Notes in Computer Science*, 5317:973-986.

Brodland, G., Conte , V., Cranston, P., Veldhuis, J., Narasimhan, S., Hutson, M. S., Jacinto, A., Ulrich, F., Baum, B. and Miodownik, M. (2010). Video force microscopy reveals the mechanics of ventral furrow invagination in drosophila. *Proceedings of the National Academy of Sciences USA* 107:22111-22116.

Cui, C., Yang, X., Chuai, M., Glazier, J. A. and Weijer, C. J. (2005). Analysis of tissue flow patterns during primitive streak formation in the chick embryo. *Developmental Biology* 284 :37-47.

Cui, C., Ji, R., Ding, F., Qi, D., Gao, H., Meng, H., Yu, J., Hu, S. and Zhang, H. (2007). A complete mitochondrial genome sequence of the wild two-humped camel (*Camelus bactrianus ferus*): an evolutionary history of camelidae *BMC Genomics* 8:241

Das, S., Ferlito, M., Wang, R.,, Liu, D., Raghavachari, N., Munson, P., Murphy, E. and Steenbergen, C. (2010). Existence of microRNA, "mito-miR-181c", in Heart-Derived Mitochondria: Role in regulation of mitochondrial function by targeting mt-COX1. *Circulation* 122:A20624.

Demetrius, L., Coy, J. F. and Tuszynscki, J. A. (2010). Cancer prokifeartion and therapy: the Warburg effect and quantum metabolism. *J. R. Soc. Interface* 7:2.

Demongeot, J. and Besson, J. (1983). Code génétique et codes à enchaînement I. *C.R. Acad. Sc. Série III* 296:807-810.

Demongeot, J. (1998). Multi-stationarity and cell differentiation. *J. Biol. Systems.*, 6:1-2.

Demongeot, J., Bezy-Wendling, J., Mattes, J., Haigron, P., Glade, N. and Coatrieux, J.L. (2003). Multiscale modeling and imaging: the challenges of biocomplexity. *Proceedings of the IEEE Soc.*, 91:1723 – 1737.

Demongeot, J., Glade, N., Hansen, O. and Moreira, A. (2007). An open issue: the inner mitochondrial membrane (IMM) as a free boundary problem. *Biochimie*, 89:1049-1057.

Demongeot, J. and Moreira, A. (2007). A circular RNA at the origin of life. *J. Theor. Biol.*, 249:314-324.

Demongeot, J., Glade, N. and Moreira, A. (2008a). Evolution and RNA relics. A Systems Biology view. *Acta Biotheoretica*, 56:5-25.

Demongeot, J., Elena, A. and Sené, S. (2008b). Robustness in neural and genetic networks. *Acta Biotheoretica*, 56:27-49.

Demongeot, J., Glade, N., Moreira, A. and Vial, L. (2009a). RNA relics and origin of life. *Int. J. Molecular Sciences*, 10:3420-3441.

Demongeot, J., Ben Amor, H., Gillois, P., Noual, M. and Sené, S. (2009b). Robustness of regulatory networks. A Generic Approach with Applications at Different Levels: Physiologic, Metabolic and Genetic. *Int. J. Molecular Sciences*, 10:4437-4473.

Demongeot, J., Drouet, E., Moreira, A., Rechoum, Y. and Sené, S. (2009c). Micro-RNAs: viral genome and robustness of the genes expression in host. *Phil. Trans. Royal Soc. A*, 367:4941-4965.

Demongeot, J., Elena A., Noual, M., Sené, S. and Thuderoz, F. (2011a). "Immunetworks", attractors and intersecting circuits. *J. Theor. Biology*, 280:19-33.

Demongeot, J., Elena A., Noual, M. and Sené, S. (2011b). Random Boolean Networks and Attractors of their Intersecting Circuits. In Barolli, L. et al., editors, *IEEE AINA' 11 & BLSMC' 11*, pages 483-487. IEEE Press, Piscataway.

Demongeot, J., Noual, M. and Sené, S. (in press). Combinatorics of Boolean automata circuits dynamics. To appear in *Discrete Applied Mathematics*.

Forest, L., Glade, N. and J. Demongeot, J. (2007). Liénard systems and potential-Hamiltonian decomposition. Applications. *C. R. Acad. Sci. Biologies*, 330:97-106.

Forest, L. and Demongeot, J. (2008). A general formalism for tissue morphogenesis based on cellular dynamics and control system interactions. *Acta Biotheoretica*, 56:51-74.

Gumbiner, B (2005). Regulation of cadherin-mediated adhesion in morphogenesis. *Nat. Rev. Mol. Cell Biol.* 6:622-634.

Henon, S., Lenormand, G., Richert, A. and Gallet, F. (1999). A new determination of the shear modulus of the human erythrocyte membrane using optical tweezers. *Biophys. J.* 76:1145-1151.

Hsiao, C. L., Mohan, S., Kalahar, B. K. and Williams, L. D. (2009). Peeling the Onion: Ribosomes are ancient molecular fossils. *Molecular Biology and Evolution* 26:2415-2425.

Huber, C. and Wächtershäuser, G (1998) Peptides by activation of amino-acids with CO on (Ni,Fe)S surfaces: Implications for the origin of life. *Science* 281:670-672.

Israel, M. and Schwartz, L. (2011). On the metabolic origin of cancer : substances that target tumor metabolism. *Biomedical Research* 22, 22 :132-166.

Krebs, J. E., Kilpatrick, S. T. and Goldstein, E. S. (2009) *Lewin's Genes X*. Jones & Bartlett Learning, Sudbury, MA.

Leptin, M. (1999). Gastrulation in drosophila: the logic and the cellular mechanisms. *EMBO J.* 18:3187-3192.

Martin, A., Gelbart, M., Fernandez-Gonzalez, R., Kaschube, M., Wieschaus, E. (2010) Integration of contractile forces during tissue invagination. *J. Cell Biol.* 188:735-749.

Michon, F., Forest, L., Collomb, E., Demongeot, J. and Dhouailly, D. (2008). BMP-2 and BMP-7 play antagonistic roles in feather induction. *Development*, 135:2797-2805.

Oda, H. and Tsukita, S. (2000). Real-time imaging of cell-cell adherens junctions reveals that drosophila mesoderm invagination begins with two phases of apical constriction of cells. *Journal of Cell Science* 114:493-501.

Patwari, P. and Lee, R. (2008) Mechanical control of tissue morphogenesis. *Circ. Res.* 103:234-243.

Pratt, A. J. (2010). Evolution, Selection and the Metabolic Foundations of the RNA World. In Fellermann, H. et al., editors, *Artificial Life XII Proceedings of the Twelfth International Conference on the Synthesis and Simulation of Living Systems*, pages 49-56. MIT Press, Cambridge, MA.

Promayon, E., Martiel, J. L. and Tracqui, P. (2003). Physically-based 3D simulations of cell deformations and migrations. In Alt, W., Chaplain, M., Griebel, M. and Lenz, J., editors, *Polymer and Cell Dynamics -Multiscale Modeling and Numerical Simulations*, pages 125-138, Birkhauser, Berlin.

Sbisà, E., Tanzariello, F., Reyes, A., Pesole, G. and Saccone, C. (1997). Mammalian mitochondrial d-loop region structural analysis: identification of new conserved sequences and their functional and evolutionary implications. *Gene* 205:125-140.

Tayyab, M., Lontos, A., Promayon, E. and Demongeot, J. (2011c). Modelling and image processing of constriction and proliferation in the gastrulation process of *Drosophila melanogaster*. In Barolli, L. et al., editors, *IEEE AINA' 11 & BLSMC' 11*, pages 473-477. IEEE Press, Piscataway.

Tepass, U. and Hartenstein, V. (1994). The development of cellular junctions in the drosophila embryo. *Developmental Biology* 161:563-596.

4.2.3 Modelling and image processing of constriction and proliferation in the gastrulation process of Drosophila melanogaster

The velocity of invaginating cells is an important factor that helps understanding the interplay of forces during the invagination process. This section includes the article [Tayyab *et al.* 2011], where the same discrete biomechanical model of ventral furrow invagination is used to compare the velocity of the invagination at the extremities of the embryo with the velocity at the ventral medial area. This is achieved by monitoring the displacement of a virtual particle located at the geometrical barycenter of each cell. The velocities of two particles are monitored in Figure 5: one located at the extremity of the geometry and one located at the medial area. The result is coherent with the conclusion of [Demongeot *et al.* 2011] presented in Section 4.2.2.

Modelling and image processing of constriction and proliferation in the gastrulation process of *Drosophila melanogaster*

M. Tayyab[1,2], A. Lontos[2], E. Promayon[2], J. Demongeot[1,2]*

Abstract — **The initial stage of gastrulation, an early stage of embryogenesis, is called invagination, or primitive streak formation. In the first part of the paper, we analyse by using image processing techniques the cell deformation and motion in he *Drosophila melanogaster* embryo searching to delimit the first period of invagination without proliferation. Then, in a second part, we propose a biomechanical model, based only on the consideration of elastic and contractile forces exerted on cell walls and on the centrosome through the combination of myosin contraction and cytoskeleton rigidity. Numerical simulations of this model made during the period of gastrulation without proliferation suggest that the model adequately simulates in-vivo cell behaviour, showing the start of the streak formation at the two extremities of the embryo cylinder, followed by a propagation of the invagination to its central part.**

Keywords: cell contouring, cell counting, gastrulation, biomechanical model, streak formation, invagination simulation

The living organisms are very complex – part digital and part analogy mechanisms. J. von Neumann [1].

I. Introduction

During the morphogenesis of the gastrula, the second step of the embryogenesis after the blastula stage, we observe in the majority of the animal development dynamics, the following phenomena: i) the cell motion is partly guided by chemotaxis, in order to supply their substrate demand, and also to respect the epigenetic architecture ruled by morphogens, ii) the cell shape is due to a constriction controlled by cell differentiation and iii) the final gastric tube is obtained from cell proliferation relaxing the forces exerted on the cell plasmic membrane and optimizing the cellular "nutritive Area / inner Volume" (A/V) ratio. Concerning the differentiation process, some cells of the embryo start to take the shape of a bottle (bottle or flask cells), decreasing the surface at the interface with their nourishment fluid. At the end of the gastrulation, these bottle cells start to divide and grow, increasing their A/V ratio. In this paper, we are attempting firstly to follow by using image processing techniques the first phase of the gastrulation made of pure cell motion causing the invagination without any proliferation, and secondly to show that the cell constriction results in a streak starting on the two extremities of the embryo and propagating secondly to its central part. In order to simulate the initiation of this phenomenon, we use exclusively laws of physics and mechanics. For this purpose, we have created a three-dimensional biomechanical model consisting of a group of cells, forming a structure with two areas: a cylindrical rigid area representing the main embryo body and two curved hemispheric areas constituting the embryo extremities. Each cell is modelled by a set of Newtonian contour particles defining the surface mesh and an inner particle, located at the geometric centre of the cell, mimicking the centrosome. Elastic forces are used to model the rigidifying effect of the tubulin and actin cytoskeleton, and contractile forces to model the action of the myosin fibers. In addition, we have modelled the role of the cadherins by connecting contour particles of adjacent cells. Finally, in order to ensure the symmetry from a partial mesh representing only a part of the embryo, we have applied boundary conditions to the particles located at the lateral extremity edges of the simulated structure. This biomechanical model shows that the inner folding starts at the curved area and then propagates to the rigid one, in accordance with the in vivo process. To compare these results with in vivo experiments, we have monitored the displacement of the centrosome and the cell A/V ratio. Our numerical experiments made during the time lag observed through the microscopic imaging without proliferation suggest that our model adequately simulates thge in-vivo cell behaviour. In a first part, we present image processing techniques and results obtained by applying them on gastrulation microscopic recording of *Drosophila melanogaster* embryo from [2-6]. In a second part, we describe the biomechanical model of streak formation and the third Section will be devoted to the presentation of numerical simulations confronted to real images of the first invagination stage of the gastrulation.

Manuscript received 15th November 2010.
[1]Laboratory AGIM, FRE CNRS University J. Fourier of Grenoble, Faculty of Medicine, 38700 La Tronche, France
[2]Laboratory TIMC-IMAG, UMR 5525 CNRS University J. Fourier of Grenoble, Faculty of Medicine, 38700 La Tronche, France
*corresponding author: Jacques.Demongeot@imag.fr,
e-mails: tayyab.elite@gmail.com, Athanasios.Lontos@imag.fr, Emmanuel.Promayon@imag.fr

II. Image processing

2.1. Image processing techniques: cell countouring and counting

Many cell-based research studies require the counting of cells prior to beginning an experiment. Estimation of cell density in various regions of embryo is thus an integral part of such studies. Profile counts or stereological techniques could be used to have an estimate of the cell density in a particular region. The regions where cell density increases enormously

978-0-7695-4338-3/11 $26.00 © 2011 IEEE
DOI 10.1109/WAINA.2011.152

care, if they occur, our regions of interest. Image enhancement techniques need to be applied on the images to get well-defined cell contours. The available images depict actin-myosin networks in colour. Here, we are focussing more on cell boundaries in a particular region, in order to have an idea of cell density; and to observe cells whether they divide in those regions. After evaluating the colour histogram of the image, we filter out the noise by selecting an appropriate colour threshold value. In absence of noise, cell boundaries are easily visualized and hence cells could be tracked. Cell boundaries are further enhanced by applying contrast algorithms on the colour-filtered image again by using simple threshold values after studying the gray-histogram. Cell proliferation results in increase in volume, thereby causing cells to recurrently contract then stabilize. Older cells are more vulnerable to shrink themselves as a result of forces from the neighbouring cells, due to proliferation at the other end. Cell density, as expected, would increase enormously in such regions with respect to other regions (Figure 1), pushing them due to proliferation. Cell density increasing enormously in such regions with respect to other regions which could lead to invagination, close to the point of maximum cell density.

2.2. Results obtained from cell contouring and counting

Available series of images were processed to have an idea of change of cell density in the region where a constriction appeared at a later stage. After following the image processing steps explained in 2.1., we were able to have an exact visual idea of how the cells move and how changes the cell density in the region where invagination occurs experimentally, and also to observe if there is any division of cell in that region before the development of constriction. This included removal of noise from the images and then applying contrast and contour algorithms, to have an exact visual idea of the number of cells in that region. All cells could be individually tracked, and change of their forms are clearly observed. However, no division of cells was observed in the region where in the later stage, constriction appeared. Instead, cells get squeezed and cell density increased in that particular region before we could see two points in-line, across which this phenomenon occurred, leading finally to the development of a constriction.

I. The Biomechanical Model

3.1. The embryo architecture

The embryo cylindric cephalo-caudal structure (Figure 2) has two zones of cylindricity breaking, the two hemispheric extremities and the cells at the boundary between the two geometries presents a curvature due to a relaxation of the internal rigid properties of their cytoskeleton. Tha appearnce of the gastrulation streak occurs at their level and after propagates to the central cylindric part of the embryo. Taking into account the differential contractility of these boundary cells constitutes the model core and will be implemented over a 3D mesh representing the external embryo surface.

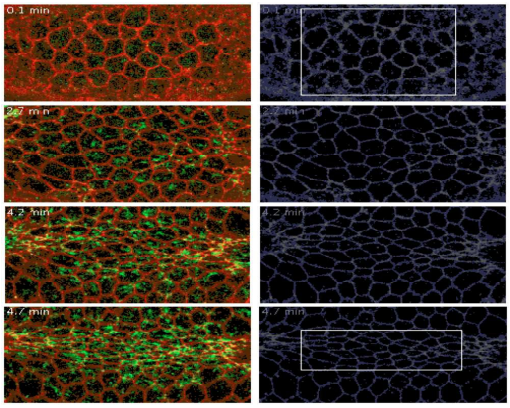

Figure1. Invagination process between initial and final stage from available data, [2-6] just before invagination, rectangle showing area of interest

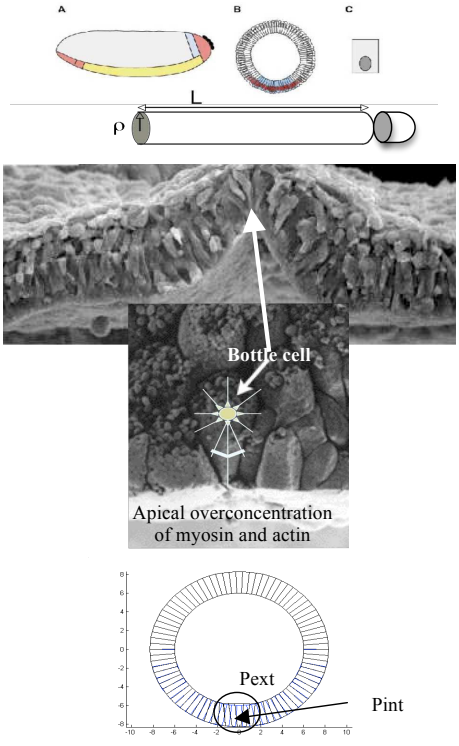

Figure 2. Top: Cylindric structure of *Drosophila melanogaster* embryo of length L and hemispheric left extremityies. Middle: differentiation of the first bottle (or flask) cell. Bottom: equilibrium between external and internal forces

3.2 The model
Each cell evolves following the mechanical laws:
1) the sum of the orthogonal forces exerted on the cell walls is equal to its mass (proportional to its inner area) times its orthogonal (to the wall) acceleration. The external forces are the resultant of the extracellular (Pext) and intracellular (Pint) pressure, the contact forces being exerted by the neighbouring cells (sharing a part or the whole of the wall) exerted by other cells and the internal force is due to the cell pressure exerted via the cyto-skeleton and the plasmic membrane [7]. Each force is equal to a coefficient (e.g. the physical pressure) times the length of the wall on which it is exerted
2) If we suppose that the initial cell configuration is in an equilibrium state, we calculate an admissible set of parameters values respecting this equilibrium
3) Then, we leave the cell system evolve depending on the energetic balance ruling the cytoskeleton apical polymerization [4-6] controlled by a specific genetic regulatory network comprizing essentially concertina (cta), actin, myosin, Rho and RhoGEF genes [7-10], by choosing a small time step, by updating sequentially each cell and by calculating their displacements respecting the no-overlapping rule. At each step we update the cell common walls by supposing that cell contacts are close, ensured between cells by cadherins and gap junctions [11,12], and with the extra-cellular matrix by integrins and adhesins. Cell motion involves a change in its inner area: we suppose that growth occurs where internal forces Fint are larger than external ones Fext (cell has to be stretched), as for constrained growth in continuous media mechanics. When the external forces dominate, the cell is supposed compressible and can be constricted. The cells divide longitudinally or laterally when their ratio perimeter over area is too small [13-17].

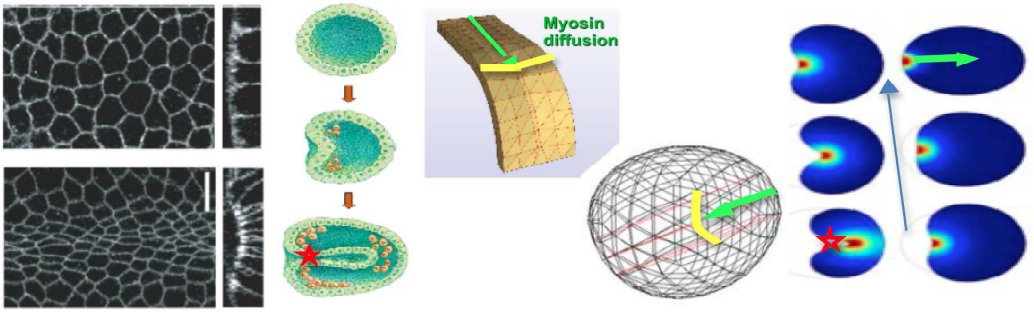

Figure 3: Left: cell contraction due to myosin (experiments [36]). Centre: progressive invagination and streak formation. Right: myosin diffusion along a directrix of the cylindric part of the embryo (green arrow) provoking the invagination before the tube closure (red star). The zero-diffusion domain for myosin is indicated in yellow.

The revolution symmetry breaking consists in making two cylinders inside the embryo cylinder, one coming from the ventral furrow and giving the digestive tube (this phase is called gastrulation) and the other coming from the dorsal furrow and giving the neural tube (this phase is called neurulation). The first gastrulation step consist in an apical concentration overfluctuation of one of the cytoskeleton components (myosin, actin, tubulin,...) or one of the enzymes (ADenylate Kinase - ADK - or Nucleoside Diphosphate Kinase - NDK) or one of the energy molecules (ATP, GTP) involved [18-23]. This apical overconcentration diffuses and reaches the extremities [11,12] of the cylindric portion of the embryo at which gap junctions are less important with the cells of the "hemispheric" terminations. Then two first bottle cells can appear at the two extremities of the diffusion line, then this first contraction can propagate until the center of the cylindric part as noticed in [11,12] during the 6 first hours of the gastrulation in *Drosophila melanogaster*. After this first phase of the ventral furrow formation, for regularizing the tensegrity forces, based on a synergy between balanced tension and compression components of cells, first divisions occur from extremities to center by applying the first Thom's cell law. We can simulate such a process on a transversal slice of the embryo and reproduce the invagination of the gastrulation from both the contraction and consecutively the proliferation phases.

The end of the cell and tissue growth stops correspond to the end of the morphogenesis process: this can be observed when the second Thom's tissue law is applicable (the surface to volume ratio of an organ becoming adverse) or when the organ is completely covered by an anatomic boundary like an aponeurosis made of fibrous cells or an autoassemblage of extracellular ingredients.

In both these cases, a couple of morphogens acting often simultaneously in opposite (e.g. a couple of activator and inhibitor like BMP-7 and BMP-2 in feather morphogenesis in the chicken [24-27] can induce the chemotactic motion of fibroblats or the biosynthesis of the elements constituting the auto-assemblage (like proteins and phospholipids). The fact that for a certain value of their viscosity ratio, the morphogens can coexist for a relatively long time in a precise location can greatly favor the birth of anatomic organ boundaries.

II. Numerical Simulations

The myosin is supposed to diffuse in all directions from a cell in which an excess of myosin is synthesized caused by random fluctuations over-expressing its gene, notably along a directrix

of the cylinder constituting the body of the embryo of *Drosophila melanogaster*. This directrix represents the shortest path until the hemispheric extremities of the embryo on the boundary of which cells change of curvature (yellow on Figure 3). The whole model mixes a Multi-Agents Model (MAM) responsible for cell growth, migration and proliferation with a Reaction-Diffusion Partial Differential Equation (RD-PDE) for myosin dispatching, mainly in charge of cell contraction.

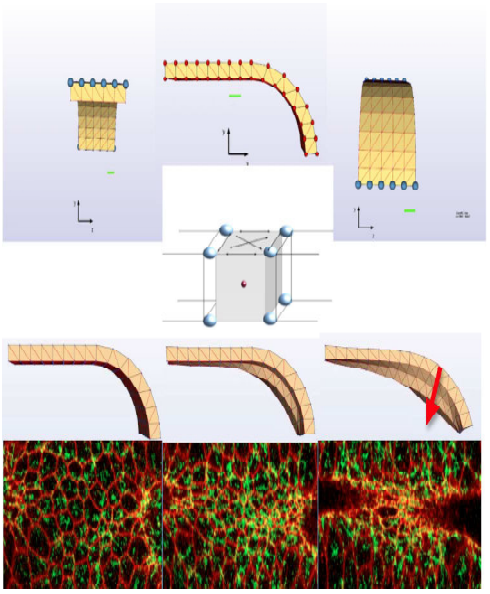

Figure 4: Top: part of the embryo made of cells considered as polyhedra with 8 vertices common with neighbouring cells and a center (the centrosome) related to the vertices by actin filaments and micro-tubules (constituting the elastic and rigid cytoskeleton) on which myosin using ATP exerts contraction forces. Dark blue points are fixed points of the whole structure. Middle: profile of the structure under the contractile action of the myosin showing the start of the streak at the boundary of the hemispheric extremity of the embryo (red arrow). Bottom: experimental observation of the activity of myosin (fluorescent) with distal invagination

The results of simulation of the hybrid model are given on Figures 3 and 4 showing the same phenomena as those observed in experiments: the progressive invagination starts at the extremities of the embryo and after propagates to the central cylindric part of the embryo. The final step of the gastrulation needs proliferation in order to close the internal of the cell differentiation in bottle (or flask) cells contracted at their apical extremity, provoking during the first minutes of gastrulation a reorganization of the superficial cell layer of the embryo without division, leading to the formation of a streak. Resulting invagination starts experimentally at the 2 extremities of the embryo and propagates to its central part.cylinder which will give birth to the intestinal tube of the adult animal. By following the progressive migration in embryo depth of the centrosomes it appears that the run is faster and deeper for curved cells at the extremities of the embryo than for central cells (Figure 5). The saturation curves representing this displacement behave like the curves representing the evolution of the cell diameter under progressively increasing forces applied externally to the cell, which is a way to induce cell contractions (possibly periodic [30]) similar to those due to myosin (Figure 6) [31, 32]. Some divisions of the observed bottle (or flask) cells whose differentiation is due to myosin gene over-expression, suffice to end the gastrulation process if they occur at critical locations as streak lips (red star on Figure 3), located at the boundary of the zero-diffusion domain both observed and simulated for myosin (in yellow on Figure 3).

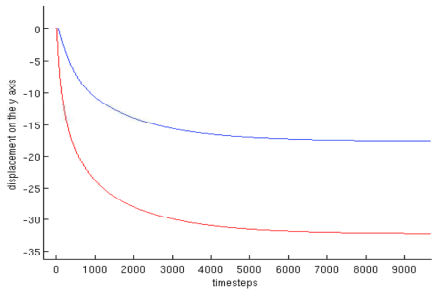

Figure 5: Displacement of centre particle (virtual centrosome) of a cell located on the cylindrical part of the embryo (blue), substantially smaller and slower than displacement of centrosome of cell located at the curved area (red).

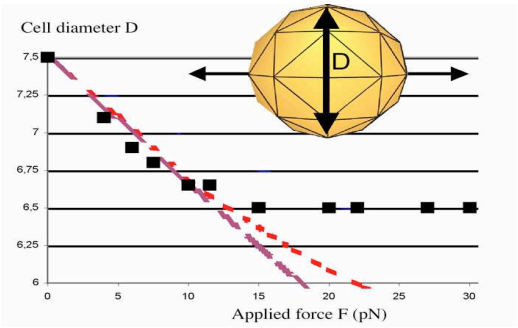

Figure 6: Simulated virtual spherical red blood cell (RBC) suspended in an hypotonic solution. Optical tweezers double trap is simulated by exerting locally a force *Fs* on two opposite nodes of the cell object contour (upper insert). The variation with load of the cell object diameter D(F) (in µm) in a plane perpendicular to the loading direction is simulated and compared to experimental data published by [31] (black squares). With appropriate scaling of the force, it is possible to adjust the elasticity modulus such that experimental mechanical response of RBC is nicely fitted in the linear elastic regime (red). Increasing the elasticity modulus induces a stiffer response which qualitatively reproduces the departure from the linear regime at larger traction forces (violet).

V. Conclusion

We given in this paper some examples (centred around the gastrulation process) concerning different steps of morphogenesis modelling from experimental acquisition of pertinent data until the interpretation in a mathematical framework of the dynamic or the geometric features of observed forms and functions.

We will in the future increase the spatial and temporal resolution of the data by sampling in 3D with a good precision in space (e.g. by using confocal or biphotonic microscopic information), in time (e.g. by using the cine-microscopy) and in function (e.g. by using the Raman vibrational, infrared,..., spectro-microscopy), in order to detect precisely the frontiers between the successive phases of the morphogenetic process of revolution symmetry breaking in the embryo, *i.e.*, i) the morphogen diffusion, ii) the cell migration, iii) the bottle cell differentiation, iv) the streak contraction and v) cell the proliferation ensuring vi) the tube closure.

References

[1] J. von Neumann, "The general and logical theory of automata," Collected Works V, Pergamon Press, Oxford, pp. 288-326, 1951.

[2] http:www.ibioseminars.org

[3] http:www.molbio1.princeton. edu/wieschaus/

[4] A.C. Martin, M. Kaschube, E. Wieschaus, "Pulsed contractions of an actin-myosin network drive apical constriction," Nature, Vol. 457, pp. 495-499, 2009.

[5] A.M. Sokac, E. Wieschaus, "Zygotically controlled F-actin establishes cortical compartments to stabilize furrows during Drosophila cellularization," J Cell Sci., Vol. 121, pp. 1815-1824, 2008.

[6] A.M. Sokac, E. Wieschaus, "Local actin-dependent endocytosis is zygotically controlled to initiate Drosophila cellularization, " Dev Cell., Vol. 14, pp. 775-786, 2008.

[7] M. Leptin, "Gastrulation in Drosophila: the logic and the cellular mechanisms," The EMBO Journal, Vol.18, pp.3187–3192, 1999.

[8] J. Demongeot, J. Aracena, F. Thuderoz, T.P. Baum, O. Cohen, "Genetic regulation networks: circuits, regulons and attractors," Comptes Rendus Biologies, Vol. 326, pp. 171-188, 2003.

[9] J. Aracena, M. González, A. Zuñiga, M. Méndez, V. Cambiazo, "Regulatory network for cell shape changes during Drosophila ventral furrow formation," J. Theor. Biol., Vol. 239, pp. 49-62, 2006.

[10] F. Caraguel, M. Tayyab, F. Giroud & J. Demongeot, "Evolution of the genetic regulatory networks: the example of the cell cycle control network. From gastrulation modelling to apocatagenesis," in: *IEEE AINA' 10 & BLSMC' 10*, IEEE Press, Piscataway, pp. 767-774, 2010.

[11] H. Oda, S. Tsukita, "Real-time imaging of cell-cell adherens junctions reveals that Drosophila mesoderm invagination begins with two phases of apical constriction of cells," Journal of Cell Science, Vol. 114, pp. 493-501, 2000.

[12] R.E. Dawes-Hoang, K.M. Parmar, A.E. Christiansen, C.B. Phelps, A.H. Brand, E.F.Wieschaus, "Folded gastrulation, cell shape change and the control of myosin localization," Development, Vol. 132, pp. 4165-4178, 2006.

[13] R. Thom, "Stabilité structurelle et Morphogenèse," Benjamin, New York, 1972.

[14] L. Forest, J. Demongeot, "Cellular modelling of secondary radial growth in conifer trees: application to Pinus radiata," Bull. Math. Biol., Vol. 68, pp. 753-784, 2006.

[15] L. Forest, S. Martinez, F. Padilla, J. Demongeot, J. San Martin, "Modelling of auxin transport affected by gravity and differential radial growth," J. Theor. Biol., Vol. 241, pp. 241-251, 2006.

[16] L. Forest, J. San Martin, F. Padilla, F. Chassat, F. Giroud, J. Demongeot, "Morphogenetic processes: application to cambial growth dynamics. Acta Biotheoretica," Vol. 52, pp. 415-438, 2004.

[17] L. Forest, J. Demongeot, "A general formalism for tissue morphogenesis based on cellular dynamics and control system interactions," Acta Biotheoretica, Vol. 56, pp. 51-74, 2008.

[18] N. Glade, J. Demongeot, J. Tabony, "Numerical Simulations of microtubule self-organisation by reaction and diffusion," Acta Biotheoretica, Vol. 50, pp. 232-248, 2002.

[19] J. Tabony, N. Glade, J. Demongeot, C. Papaseit, "Biological self-organisation by way of microtubule reaction-diffusion processes," Langmuir, Vol. 18, pp. 7196-7207, 2002.

[20] J. Tabony, N. Glade, C. Papaseit, J. Demongeot, "Microtubule self-organisation as an example of the development of order in living systems," J. Biol. Phys. Chem., Vol. 4, pp. 50-63, 2004.

[21] N. Glade, J. Demongeot, J. Tabony, " µ tubule self-organisation by reaction-diffusion processes causes collective transport and organisation of cellular particles," BMC Cell Biol., Vol. 5:23, 2004.

[22] N. Glade, J. Demongeot, J. Tabony, "Numerical Simulations of microtubule self-organisation by reaction and diffusion," Acta Biotheoretica, Vol. 50, pp. 232-248, 2002.

[23] J. Tabony, N. Glade, J. Demongeot, C. Papaseit, "Biological self-organisation by way of microtubule reaction-diffusion processes," Langmuir, Vol. 18, pp. 7196-7207, 2002.

[24] L. Abbas, J. Demongeot, N. Glade, "Synchrony in Reaction-diffusion models of morphogenesis: applications to curvature-dependent proliferation and zero-diffusion front waves, Phil. Trans. Royal Soc. A, Vol. 367, pp. 4829-4862, 2009.

[25] F. Michon, L. Forest, E. Collomb, J. Demongeot, D. Dhouailly, "BMP-2 and BMP-7 play antagonistic roles in feather induction," Development, Vol. 135, pp. 2797-2805, 2008.

[26] L. Forest, F. Michon, S. Cadau, J. Demongeot, D. Dhouailly, "What is the biological basis of pattern formation of skin lesions? Viewpoint 4. Skin Patterns belong to three main types, determined at three steps of development," Exp. Dermatology, Vol. 12, pp. 559-564, 2006.

[27] J. Demongeot, "Biological boundaries and biological age," Acta Biotheoretica, Vol. 57, pp. 397-419, 2009.

[28] B. Baum, N. Perrimon, "Spatial control of the actin cytoskeleton in *Drosophila* epithelial cells," Nat. Cell Biol., Vol. 3, pp. 883-890, 2001.

[29] J. Gates, J.P. Mahaffey, S.L. Rogers, M. Emerson, E.M. Rogers, S.L. Sottile, D. Van Vactor, F.B. Gertler, M. Peifer, "Enabled plays key roles in embryonic epithelial morphogenesis in *Drosophila*," Development, Vol. 134, pp. 2027-2039, 2007.

[30] A.C. Martin, M. Kaschube, E.F. Wieschaus, "Pulsed contractions of an actin-myosin network drive apical constriction," Nature, Vol. 457, pp. 495-499, 2009.

[31] S. Hénon, G. Lenormand, A. Richert, and F. Gallet, "A new determination of the shear modulus of the human erythrocyte membrane using optical tweezers," Biophys J., Vol. 76, pp. 1145-51, 1999.

[32] P. Tracqui, E. Promayon, P. Amar, N. Huc, V. Norris, and J.L. Martiel, "Emergent features of cell structural dynamics: a review of models based on tensegrity and nonlinear oscillations," in: *Modelling and simulation of biological processes in the context of genomics*, P. Amar, F. Képès, V. Norris and P. Tracqui (eds.), Genopole, Evry, 2003, pp. 160-189.

The model was also used in [Demongeot *et al.* 2012] to study the forces developed on the facets of ventral cells, as well as the effect of actomyosin coalescence to the $surface/volume$ ratio of an invaginating cell. This ratio is important because it is considered to be highly connected to the time and conditions at which a cell undergoes mitosis. According to this model, the cells at the extremities have their $surface/volume$ ratio reduced faster than the cells at the ventral medial area, thus they are inclined to undergo mitosis faster than them.

4.2.4 Conclusion on the Biomechanical Discrete Model of Ventral Furrow Invagination

Although the results obtained by the biomechanical discrete model are consistent with the *in-vivo* process of the ventral furrow invagination, it suffers from the lack of a robust physical background (for more details see Chapter 3 on page 23). It is unclear how the parameters that control the elasticity and contractility work, thus making it very difficult to assess.

The positive part of this work is that our initial hypothesis concerning the crucial role of the geometry regarding apical constriction and invagination had a valid basis, as it was reproduced by an "a minima" biomechanical model. The negative part is that the physical laws on which the model is based are simplified, thus making it difficult to validate the results of the simulations. To overcome the negative part while keeping the positive feedback from the discrete model, we kept the same geometry (with some minor adjustments to emphasize on the shape of a "bean") but used the Finite Element Method to model the elasticity of the cells. In the next section, I explain the basic principles of the Finite Element Model of the Ventral Furrow Invagination for the embryo of the Drosophila Melanogaster.

4.3 Finite Element Model of the Ventral Furrow Invagination

In this section, I present the model of the ventral furrow invagination of the embryo of the Drosophila Melanogaster based on the Finite Element Method. The principles controlling the dynamics of the model are explained in Annex A. Contrary to the articles previously mentioned, this is the core of my PhD thesis and is based entirely on my work. The article is nearly ready for submission to the Journal of BMC Bioinformatics.

Biomechanical 3D Simulation of the Gastrulation/Invagination Process of the Drosophila Melanogaster

Athanasios Lontos*[1,2], Emmanuel Promayon*[2] and Jacques Demongeot[3]

[1]UJF-Grenoble 1 / CNRS / TIMC-IMAG UMR 5525, Grenoble, F-38041, France
[2]UJF-Grenoble 1 / CNRS / TIMC-IMAG UMR 5525, Grenoble, F-38041, France
[3]UJF-Grenoble 1 / CNRS / AGIM FRE 3405, Grenoble, F-38041, France

Email: Athanasios Lontos*- athanasios.lontos@imag.fr; Emmanuel Promayon*- emmanuel.promayon@imag.fr; Jacques Demongeot - jacques.demongeot@agim.eu;

*Corresponding author

Abstract

Background: The embryo of the *Drosophila Melanogaster* undergoes a series of cell movements during its development. Invagination is the initial step of gastrulation, early stage of embryogenesis, which initiates the creation of the ventral furrow.

Results: We suggest that this particular cell movement can be explained exlusively by studying the mechanics of the embryo. For this purpose, we have created an "a minima" biomechanical model based on the Finite Element Method. Cells are modeled by an elastic hexahedron contour. A uniform initial distribution of elasticity is applied to the cells along the model and springs are used to model the contraction of the ventral area. The results of the simulations of the "bean-shaped" geometry of the *Drosophila Melanogaster* model are compared with a spherical geometry where we apply exactly the same principles.

Conclusions: The numerical simulations show that, despite the equal initial distribution of contractility along the contraction area of the model, the invagination starts at the ventral curved extremities of the embryo and then propagates to the ventral medial layer, which corroborates microscopic observations. This phenomenon may therefore be attributed uniquely to the specific shape of the embryo. This cannot be observed in the simulations of a spherical geometry.

Background

Morphogenesis is a general concept in biology including all the processes which generate shapes and cellular organizations in a living organism. It originates from the combination of two greek words, "$\mu o \varrho \varphi \eta$" ("morphe", which stands for form, shape) and "$\gamma \epsilon \nu \epsilon \sigma \iota \varsigma$" ("genesis" which stands for principle, origin, birth). Consequently, morphogenesis refers to the "Birth of forms". The looseness of this definition has allowed this term to be enthusiastically embraced by researchers examining the factors and parameters controlling the creation of tissues, organs and ultimately life.

A very important stage of morphogenesis in animals is gastrulation. The early embryo performs rapid nuclei divisions followed by cellularization until the formation of the blastula, a geometrically simple closed elongated sphere or "bean-shaped" structure that consists of a single cell layer enclosing the hollow blastocoel [1]. Gastrulation includes mass movements of cells to form complex structures (e.g. tissues) from a simple initial shape (blastula). At this point, a typical blastula consists of around 5000-6000 cells enclosing the yolk (material stored in an egg that supplies food to the developing embryo), with around 100 cells from the anterior to the posterior pole [2].

There are a number of inner cell structures that affect the cell movement and spatial behaviour:

- The **cytoskeleton** plays an important part in cellular motion and shape. It consists of three kinds of protein filaments: actin filaments, intermediate filaments and microtubules [3, 4].
- The **adherens junctions** (AJs) contain complexes of the transmembrane adhesion molecule E-cadherin and the adaptors β-catenin and α-catenin [5, 6]. They are formed in the lateral surfaces of the cells and they offer strong links between neighboring cells [7, 8].
- The **myosin fibers** are thin filaments found in the cytoplasm of the cytoskeleton of cells. They are flexible, versatile and relatively strong and they serve as tensile platforms for muscle contraction [9].

One of the most important cell movements during gastrulation is the invagination of the ventral cells, which initiates the creation of the ventral furrow. The process starts after the flattening of the cells on the ventral midline [2]. The myosin of the most ventrally located cells becomes concentrated at their apical sides [10, 11]. This excess of myosin causes the constriction of their apical surface and a simultaneous apico-basal elongation. At this point, these cells move inwards and initiate the invagination.

A lot of research and bibliography have been dedicated to modeling the ventral furrow invagination. A very popular organism which has served as reference for these models is the *Drosophila Melanogaster*. One

contribution of this work focuses on the study of the relationship between the apical constriction of the ventral cells and the invagination. In [7], the *in vivo* monitoring of the invagination in the *Drosophila Melanogaster*, shows that the area where the apical constriction starts, and the area where the invagination starts differ. In fact, the actin-myosin contractions occur first in the ventral medial layer (VML), while the invagination starts from the ventral curved extremities (VCE) and then propagates to the VML. So the question remains: 'What makes the invagination start from the curved extremities?' In this work, we attempt to answer this question from a mechanical point of view only.
We analyze the effect of a factor that, to our knowledge, has not yet been extensively studied: the geometry of the embryo. For this purpose, we have created an "a minima" 3D biomechanical model of the embryo of the *Drosophila Melanogaster*, which incorporates the previous mentioned factors:

- **elasticity** of the cells due to the cytoskeleton,
- **strong bonds** between cells due to AJs,
- **contraction** of the apical face due to the myosin fibers.

The *in vivo* phenomenon and the dynamic numerical simulations are compared to analyze the impact of the embryo's geometry on the invagination process. Furthermore, we apply the same principles on a spherical geometry and compare the results of the two simulations. The comparison between the results of the simulations on the "bean-shaped" and the spherical geometry provides a better understanding of this impact.

Related Work

The mechanical theories proposed for ventral furrow formation rely on specific assumptions concerning the behaviour of the epithelial cells, the mechanisms that drive invagination and the effect of the environment. In some models, the epithelium is considered to be subdivided into two regions with distinct characteristics, the prospective mesoderm and the prospective ectoderm [12, 13]. In [14] only the mesoderm is modeled, whereas in [15] the epithelium is modeled as a homogeneous area whose cells have the same mechanical properties but differ in size.
Probably the most important difference of the models for ventral furrow formation, from a biomechanical point of view, is the definition of the invagination-inducing mechanisms. [12, 14, 16] use pre-defined active deformations to model the apical constriction and apico-basal elongation of the ventral cells. In [13] the

active deformations follow experimental observations obtained by the method of Video Force Microscopy [17]. Passive deformations are the result of applied forces (usually contractile forces corresponding to the effect of the myosin excess) and force balance [12–16, 18].
The effect of the environment of the embryo is taken into account by almost all models. The shell that surrounds the embryo known as vitelline membrane, is most commonly represented by a rigid shell enclosing the epithelium [12–14, 16]. When the vitelline membrane is neglecteded [12, 16], the invagination is predicted but the round shape of the embryo is not reproduced. The methods modeling the effect of the yolk are various: [12, 13, 16] model it as internal pressure on the basal areas of the cells, [19] as a compressible fluid at rest and [20] as an incompressible viscous fluid. Most consider it as incompressible [12, 15, 16, 20], although some models consider it as compressible [13, 19], but without a significant variation in the result of the simulations. In [18] the effect of the yolk is not taken into account. All the mechanical theories proposed for ventral furrow invagination are extensively discussed in [21].

Methods

We used the Finite Element Method (FEM) to model the elasticity of the embryo of the *Drosophila Melanogaster*. Explicit forces where superimposed using discrete springs to model specific filament behaviors.

Geometry

To ensure the specific shape of the *Drosophila Melanogaster*'s embryo [22, 23], the 3D biomechanical model is composed by an elongated sphere (or "bean-shaped" mesh, symmetric along the dorsoventral axis (Figure 1(a)(b)(c)), consisting of 1516 nodes forming 756 monolayered hexahedra modeling the cells. The total length of the mesh is $460\mu m$ and the diameter of its cross-section is $250\mu m$. We consider the instant when the apical flattening of the most ventrally located cells has been finished and the invagination is imminent. The spherical mesh consists of 904 nodes forming 450 monolayered hexahedra (Figure 1(d)). The diameter of its cross-section is $250\mu m$, as in the *Drosophila Melanogaster*'s model.
Each hexahedron is approximately $20\mu m \times 20\mu m \times 40\mu m$, resulting to an average volume of around $160\mu m^3$. For reasons of calculation efficiency, the size of one hexahedron is approximately equal to the size of four cells of the embryo. Cells on the ventral midline area of the embryo (see outlined cells in Figure 1(a)) are of particular interest in the invagination process. We distinguish two sub-areas of the ventral midline: the Ventral Medial Layer (VML) and the Ventral Curved Extremities (VCE), as described in

Figure 2(b).

The environment of the embryo is mainly composed by the vitelline, the chorion and the yolk, that impact the cell movements. We model the vitelline as a rigid external shell that surrounds the embryo and blocks outwards trajectories of the elements. In other work [12], the yolk is modeled as a fluid which hinders the invagination, but, to our knowledge, there is not sufficient scientific data concerning its effect on the process. Thus, the yolk is not taken into account in our model and the area inside is empty.

Likewise geometry, the simulating time was scaled to reflect real time. The equivalence between the biological and in-silico cells is presented in Table .

Cell Elasticity

The nodes are modeling the focal points of the forces produced by the cells, whose combined displacements produces the cell deformations and movements. Each hexahedron defines an elastic element in the FEM. We choose a simple linear elasticity constitutive law with a rather small Young modulus $E = 1000Pa$ [24]. Concerning the Poisson ratio, we have chosen for ν a popular value in the bibliography of cell and soft tissue modeling of $\nu = 0.3$ [12, 25–27].

All the cells have the same properties and comparably equal initial volumes, regardless of their position in the structure.

Apical Constriction

The domain of the flattened ventral zone where the invagination occurs is from approximately 20% to 80% of the egg length [2]. In order to simulate the apical constriction of the cells, contraction forces are generated between the nodes of the apical surface of each cell using discrete springs (Figure 2). It should be noted that, to our knowledge, there is little experimental data regarding the value of the active forces that cells can generate at this stage of the morphogenesis. [17] aims to provide such data but the directions of the forces in 3D are not specified. Consequently, the intensity of the contraction forces was optimized in order to conform to observed changes in shape [8]: it was chosen so that it can induce a 70% decrease of the apical surface of the cell located at the VML. The same value is applied to all the cells of the ventral area of the embryo (outlined row of cells in Figure 2(b)) in order to ensure an equal initial distribution of forces along the anteroposterior axis of the structure. The number of the contractile hexahedra can be modified in the model to study the effect of the area of contraction.

Cell-to-cell bonds

Adherens junctions (AJs) are binding neighboring cells. They are formed in the lateral surfaces of the cells [8, 28, 29]. In our model, we have considered AJs to be located on the vertices of the cells (hexahedra) and to offer an unbreakable binding [7, 8]. This is naturally achieved by the mesh connectivity, which also allows a direct propagation of the forces during the simulation.

Implementation and Resolution

The simulation of the 3D biomechanical model of the embryo is performed by SOFA[1] (an open-source Simulation Open Framework Architecture) [30, 31] using CamiTK/MML[2], an open-source framework to compare and evaluate biomechanical simulations [32]. The hexahedral elements are implemented following the method described in [33]: the deformation of each element is decomposed into a rigid motion and a pure deformation, and a fast implicit dynamic integration without assembling a global stiffness matrix. The contractile forces are generated by an explicit 3D mass-spring network linking the nodes of the apical surface of each cell of the ventral area. Each spring uses a Kelvin-Voigt material, where a spring and a damper are acting in parallel. The linear system is solved *dynamically* using a conjugate gradient iterative algorithm. We define a state of equilibrium for our model when all nodal displacements are lower than $0.04\mu m/sec$ (at that point the simulation stops automatically). The resulting behavior of combined soft elasticity and apical constriction is illustrated in Figure 2. Thanks to MML, a set of values are monitored during the dynamic simulation that includes displacements and surfaces, in order to extract details concerning cell behavior and motion.

Results and Discussion

Invagination of the Drosophila Melanogaster embryo

An embryo takes about 15 minutes to invaginate [2, 22]. The simulations were done on a quad-core 3.2 GHz. The invagination process needs 55 time-steps to complete. Consequently, a computation time-step corresponds to 18 seconds of real time. We use this time scaling in order to have a direct comparison between the simulations and the *invivo* process.

The nodes of the apical face of the ventral hexahedra (Figure 2(b)) are submitted to attractive forces of equal intensity (red arrows in Figure 2). Figure 4 shows four instances of the phenomenon from an antero-ventral and a ventral point of view. The entire simulation can be viewed in Videos 1, 2 and 3. The

[1] http://www.sofa-framework.org
[2] http://camitk.imag.fr

invagination of the ventral hexahedra starts right after the initiation of their apical constriction. In addition, as they start to move inwards, they also pull the neighboring hexahedra, thus increasing the invagination. When the model reaches a state of equilibrium and the simulation's stopping criterion has been reached (see **Implementation and Resolution**), the observed total depth of the invagination is $50.7\mu m$ (consistent with the two-photon excited fruorescence (2PEF) study of mesoderm spreading presented in [34]).

Figure 3(a) demonstrates the comparison of the velocities of two hexahedra located at the VML and the VCE of the geometry respectively. The velocity of a hexahedron is measured by computing the displacement of its barycenter at each time-step of the simulation. Let v_m be the velocity of the hexahedron in the VML and v_c be the velocity of the hexahedron in the VCE. We notice that for the first 1.5 minutes the hexahedron in the VCE moves faster than the one in the VML ($v_c > v_m$). After 6 seconds, the difference between the velocities of the two hexahedra reaches its maximum value (approximately $v_c = 1.6 * v_m$).

Invagination of the spherical geometry

Figure 5 demonstrates four instances of the simulation from an antero-ventral and a ventral point of view. The observed total depth of the streak is $52.4\mu m$.

Figure 3(b) demonstrates the comparison of the velocities of two cells, one located at the middle of the ventral midline (corresponding to the VML) and one located at the curved part (corresponding to the VCE). The velocities of the two barycenters are almost equal throughout the simulation, which means that the formation of the inner streak happens simultaneously along the spherical geometry. After 6 seconds, the difference of the velocities of the two hexahedra reaches its maximum value (approximately $v_c = 1.1 * v_m$).

Effect of the geometry of the embryo

Although we assume that the diffusion of myosin along the ventral area is so fast that all the cells start to constrict simultaneously, we have shown that a center node in the VCE displaces faster than a center node in the VML (Figure 3(a)). The node displacements of the embryo after $t = 18$ seconds are representd by a color scale in Figure 6. The difference between the VCE and the VML is clearly visible: the displacement of the nodes in the VCE are in the $[9.45 - 10.8]\mu m$ range while the displacements of the nodes in the VML are in the $[4.11 - 6.78]\mu m$ range. Video 4 in the Supporting Information Section shows a colored simulation, which provides more detailed information on the propagation of the invagination from the VCE

to the VML.

We can conclude that despite the uniform initial distribution of forces along the ventral area of the model, the invagination is non-uniform following the process suggested in [7]. In order to explain this observation, we need to take into consideration the geometry of the embryo. The assymetry of the geometry in the VCE creates an imbalance of forces directed inwards that generates an inward displacement of the node. The contracting forces applied on a node located at the VML do not generate neither imbalance nor displacement. The first nodes to move inwards are the nodes in the VCE. Their inward displacement later pulls the neighboring cell nodes, causing the invagination to propagate towards the VML.

Contrary to [13], where the authors claim that the mesodermal radial shortening forces are the primary cause of the internalisation of the future mesoderm, we claim that the invagination can be attibuted uniquely to the specific shape of the *Drosophila Melanogaster* and the forces generated by the apical constriction of the ventral cells. This is confirmed by the simulation of the spherical geometry, where the invagination occurs almost simultaneously along the spherical geometry (Figure 3(b)). In [21], the authors state that no major differences between the results of 2D and 3D models have been reported so far. However, the asynchronous invagination reported in our simulations, cannot be observed in a 2D model.

Effect of the width of the contraction area

Another aspect we studied in this work is the effect of the width of the contraction area. We have compared the depth of the invagination using 3-rows contraction area or 168 contractile cells (Figure 7 (a)) with the depth obtained with an one-row contraction area or 56 contractile cells (Figure 7 (b)). Our numerical simulations show that, the width of the contraction area has a direct influence on the depth of the furrow. In the first case (area of $168\mu m^2$), the depth of the furrow is $50.7\mu m$ while in the second case (area of $56\mu m^2$) the depth is $20.3\mu m$. This substantial difference is totally expected as the contraction is more intense on the ventral area of the model in the first case.

Perspectives

The FEM model presented in this paper effectively simulates the internalisation of the future mesoderm. On the other hand, we haven't achieved to reproduce the closure of the furrow. Other scientific works [2, 12, 13] suggest that the ventral closure can be attributed to the apico-basal shortening of the invaginated ventral cells.

According to [35], the most ventrally located cells go into mitosis after the internalisation is completed. We

assume that the mechanism that induces the ventral closure which signifies the end of invagination is the proliferation of the ventral cells once they are internalised. This model has to be extended to include cell division in order to verify this hypothesis.

Conclusions

The ventral furrow invagination propagates from the Ventral Curved Extremities to the Ventral Medial Layer [7]. The comparison of the simulations of the invagination process in the "bean-shaped" geometry of the *Drosophila Melanogaster* embryo and the spherical geometry shows that the geometry of the embryo plays an important role. We suggest that the "bean-shaped" geometry of the embryo in conjunction with the apical constriction of the ventral cells are responsible for the invagination.

Acknowledgements

The authors wish to acknowledge the support of the French ministry of research (PhD grant). In additions, this work was supported by French state funds managed by the ANR within the Investissements d'Avenir programme (Labex CAMI) under reference ANR-11-LABX-0004.

References

1. Forgacs G, Newman S: *Biological Physics of the Developing Embryo*. Cambridge University Press 2005.
2. Sweeton D, Parks S, Costa M, Wieschaus E: **Gastrulation in Drosophila: the formation of the ventral furrow and posterior midgut invaginations**. *Development* 1991, **112**:775–789.
3. Karr T, Alberts B: **Organization of the cytoskeleton in early Drosophila embryos.** *J Cell Biol* 1986, **102**:1494–1509.
4. Schejter E, Wieschaus E: **Functional Elements of the Cytoskeleton in the Early Drosophila Embryo**. *Annual Review of Cell Biology* 1993, **9**:67–99.
5. Gumbiner B: **Regulation of cadherin-mediated adhesion in morphogenesis**. *Nat Rev Mol Cell Biol.* 2005, **6**:622–634.
6. Martin A, Gelbart M, Fernandez-Gonzalez R, Kaschube M, Wieschaus E: **Integration of contractile forces during tissue invagination**. *J Cell Biol* 2010, **188**:735–749.
7. Martin A, Kaschube M, Wieschaus E: **Pulsed contractions of an actin-myosin network drive apical constriction**. *Nature* 2008, **457**:495–499.
8. Oda H, Tsukita S: **Real-time imaging of cell-cell adherens junctions reveals that Drosophila mesoderm invagination begins with two phases of apical constriction of cells**. *Journal of Cell Science* 2000, **114**:493–501.
9. Cooper G: *The Cell: A Molecular Approach. 2nd edition.* Sinauer Associates 2000.
10. Leptin M: **Gastrulation in Drosophila: the logic and the cellular mechanisms**. *EMBO J* 1999, **18**(12):3187–3192.
11. Dawes-Hoang R, Parmar K, Christiansen A, Phelps C, Brand A, Wieschaus E: **Folded gastrulation, cell shape change and the control of myosin localization**. *Development* 2005, **132**:4165–4178.

12. Conte V, Munoz J, Miodownik M: **A 3D finite element model of ventral furrow invagination in the Drosophila melanogaster embryo**. *Journal of the Mechanical Behavior of Biomedical Materials* 2008, **1**:188–198.
13. Conte V, Ulrich F, Baum B, Munoz J, Veldhuis J, Brodland W, Miodownik M: **A Biomechanical Analysis of Ventral Furrow Formation in the Drosophila Melanogaster Embryo**. *PLoS ONE* 2012, **7**(4).
14. Allena R, Mouronval A, Aubry D: **Simulation of multiple morphogenetic movements in the Drosophila embryo by a single 3D finite element model**. *Journal of the Mechanical Behavior of Biomedical Materials* 2010, **3**(4):313 – 323, [http://www.sciencedirect.com/science/article/pii/S1751616110000032].
15. Brezavšček AH, Rauzi M, Leptin M, Primo PZ: **A Model of Epithelial Invagination Driven by Collective Mechanics of Identical Cells**. *Biophys J* 2012, **103**(5):1069–1077, [http://linkinghub.elsevier.com/retrieve/pii/S000634951200793X].
16. Munoz J, Barrett K, Miodownik M: **A deformation gradient decomposition method for the analysis of the mechanics of morphogenesis**. *Journal of biomechanics* 2007, **40**:1372–1380.
17. Brodland G, Conte V, Cranston P, Veldhuis J, Narasimhan S, Hutson M, Jacinto A, Ulrich F, Baum B, Miodownik M: **Video force microscopy reveals the mechanics of ventral furrow invagination in Drosophila**. *Proceedings of the National Academy of Sciences* 2010.
18. Spahn P, Reuter R: **A Vertex Model of Drosophila Ventral Furrow Formation**. *PLoS ONE* 2013, **8**(9).
19. Allena R, Aubry D: **A novel technique to parametrize shell-like deformations inside biological membranes**. *Computational Mechanics* 2010, :1–15.
20. Pouille PA, Farge E: **Hydrodynamic simulation of multicellular embryo invagination**. *Physical Biology* 2008, **5**:015005, [http://stacks.iop.org/1478-3975/5/i=1/a=015005].
21. Rauzi M, Brezavšček AH, Ziherl P, Leptin M: **Physical Models of Mesoderm Invagination in Drosophila Embryo**. *Biophysical Journal* 2013, **105**:3 – 10, [http://www.sciencedirect.com/science/article/pii/S0006349513006267].
22. Leptin M, Grunewald B: **Cell shape changes during gastrulation in Drosophila**. *Development* 1990, **110**:73–84.
23. Bownes M: **A photographic study of development in the living embryo of Drosophila melanogaster**. *Journal of embryology and experimental morphology* 1975, **33**:789–801.
24. Davidson L, Oster G, Keller R, Koehl M: **Measurements of Mechanical Properties of the Blastula Wall Reveal Which Hypothesized Mechanisms of Primary Invagination Are Physically Plausible in the Sea UrchinStrongylocentrotus purpuratus**. *Developmental Biology* 1999, **209**(2):221 – 238, [http://www.sciencedirect.com/science/article/pii/S0012160699992497].
25. Maniotis A, Chen C, Ingber D: **Demonstration of mechanical connections between integrins, cytoskeletal filaments, and nucleoplasm that stabilize nuclear structure**. *Proceedings of the National Academy of Sciences* 1997, **94**(3):849–854.
26. Galle J, Loeffler M, Drasdo D: **Modeling the Effect of Deregulated Proliferation and Apoptosis on the Growth Dynamics of Epithelial Cell Populations In Vitro**. *Biophysical Journal* 2005, **88**:62–75.
27. Bidhendi A, Korhonen R: **A Finite Element Study of Micropipette Aspiration of Single Cells: Effect of Compressibility**. *Computational and Mathematical Methods in Medicine* 2012, **2012**:1–15.
28. Tepass U, Hartenstein V: **The Development of Cellular Junctions in the Drosophila Embryo**. *Developmental Biology* 1994, **161**:563–596.
29. Miyoshi J, Takai Y: **Structural and functional associations of apical junctions with cytoskeleton**. *Biochimica et Biophysica Acta (BBA) - Biomembranes* 2008, **1778**(3):670–691.
30. Allard J, Cotin S, Faure F, Bensoussan P, Poyer F, Duriez C, Delingette H, Grisoni L: **SOFA - an Open Source Framework for Medical Simulation**. In *Medicine Meets Virtual Reality, MMVR 15* 2007.
31. Faure F, Allard J, Cotin S, Neumann P, Bensoussan P, Duriez C, Delingette H, Grisoni L: **SOFA: A modular yet efficient simulation framework**. In *Surgetica 2007: Computer-Aided Medical Interventions: tools and applications* 2007.

32. Fouard C, Deram A, Keraval Y, Promayon E: *CamiTK: a Modular Framework Integrating Visualization, Image Processing and Biomechanical Modeling*, Springer Berlin Heidelberg 2012 :323–354.

33. Nesme M, Marchal M, Promayon E, Chabanas M, Payan Y, Faure F: **Physically realistic interactive simulation for biological soft tissues**. *Recent Research Developments in Biomechanics* 2005, **2**:1–22.

34. McMahon A, Supatto W, Fraser S, Stathopoulos A: **Dynamic Analyses of Drosophila Gastrulation Provide Insights into Collective Cell Migration**. *Science* 2008, **322**(5907):1546–1550, [http://www.sciencemag.org/content/322/5907/1546.abstract].

35. Grosshans J, Wieschaus E: **A genetic link between morphogenesis and cell division during formation of the ventral furrow in Drosophila**. *Cell* 2000, **101**:523–531.

Figures

Figure 1: The model of the *Drosophila Melanogaster* embryo as seen from an antero-ventral point of view (a). In (b) a cross-section of the model is presented showing the apical and basal faces of the cells. The dashed area highlights the ventral hexahedra, i.e., the hexahedra of the ventral area of the embryo submitted to the apical constriction. We distinguish two important areas in the model (c): the Ventral Medial Layer (VML) and the Ventral Curved Extremities (VCE). In (d), the spherical model with the respective highlighted area of the ventral cells.

Figure 2: (a) All the cells are modeled as very soft deformable hexahedra. They are defined by 8 nodes located at the vertices of the hexahedra. For VML hexahedra, contraction forces are applied on the apical nodes (red arrows) to induce the apical constriction. The shape of the hexahedron changes, from an initial regular hexahedral shape (left) to a convex shape (right). The most ventrally located cells of the model, on the apical faces of which, contraction forces are applied, are highlighted in (b). The number of rows of hexahedra receiving this force can vary (in this case three rows are contractile representing a total area of $4 * 14 * 3 = 168 \mu m^2$.

Figure 3: Simulation of the ventral furrow invagination process on the "bean-shaped" embryo of *Drosophila Melanogaster*. The velocities of the barycenters of two cells located at the two areas of interest in the model of the *Drosophila Melanogaster* (a) and in the spherical model (b). Notice in (a) the faster movement of the barycenter in the VCE (blue) at the beginning ($v_c > v_m$) and the equalization of the velocities after approximately $t = 2$ minutes ($v_c = v_m$) . In (b), the two barycenters have almost equal velocities throughout the simulation.

Figure 4: Instances of the geometry from an antero-ventral (top) and a ventral point of view (bottom). Notice the apical constriction of the ventral hexahedra which triggers the invagination.

Figure 5: Simulation of the invagination process on the spherical geometry. Instances of the geometry from an antero-ventral (top) and a ventral point of view (bottom).

Figure 6: Colored instance of the *Drosophila Melanogaster* model after $t = 18$ seconds from an ventral point of view. The color scale corresponds to the intensity of the node displacement.

Figure 7: The depth of the invagination is larger for a 3-rows contraction area (a) than the depth for a 1-row contraction area (b).

Tables

Table 1 - Cell Modeling

This table presents the biological aspects included in our model and the corresponding modeling concepts used for the simulation.

in vivo	**in silico**
Embryo of the *Drosophila Melanogaster*	"bean-shaped" hexahedral mesh (756 hexahedra, 1516 nodes)
Cell	Hexahedral cellular element composed of 8 nodes on the contour
Cytoskeleton	Elasticity of the hexahedra
Myosin fibers	Discrete springs offering contraction forces connecting the 4 nodes of the apical surface of the hexahedron
Adherens junctions	Mesh connectivity (nodes are shared between neighboring hexahedra)
External environment of the embryo (vitelline)	Rigid external shell surrounding the embryo

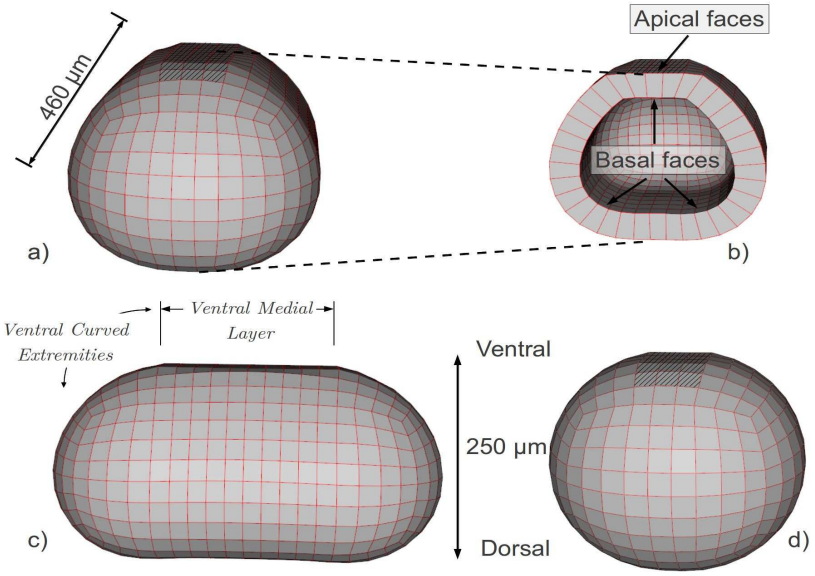

Figure 4.1: *The model of the Drosophila Melanogaster embryo as seen from an antero-ventral point of view (a). In (b) a cross-section of the model is presented showing the apical and basal faces of the cells. The dashed area highlights the ventral hexahedra, i.e., the hexahedra of the ventral area of the embryo submitted to the apical constriction. We distinguish two important areas in the model (c): the Ventral Medial Layer (VML) and the Ventral Curved Extremities (VCE). In (d), the spherical model with the respective highlighted area of the ventral cells.*

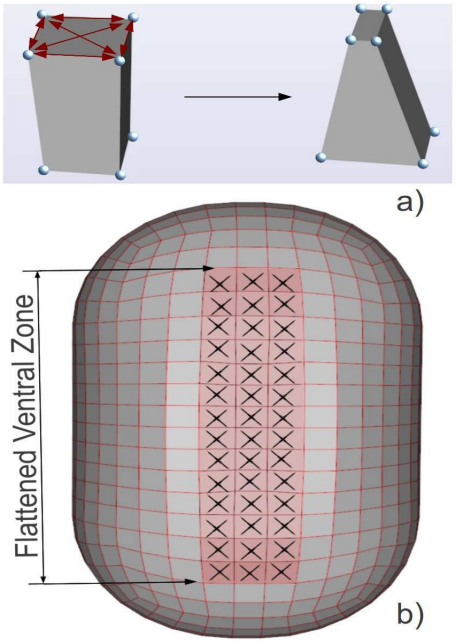

Figure 4.2: *(a) All the cells are modeled as very soft deformable hexahedra. They are defined by 8 nodes located at the vertices of the hexahedra. For VML hexahedra, contraction forces are applied on the apical nodes (red arrows) to induce the apical constriction. The shape of the hexahedron changes, from an initial regular hexahedral shape (left) to a convex shape (right). The most ventrally located cells of the model, on the apical faces of which, contraction forces are applied, are highlighted in (b). The number of rows of hexahedra receiving this force can vary (in this case three rows are contractile representing a total area of* $4 * 14 * 3 = 168 \mu m^2$.

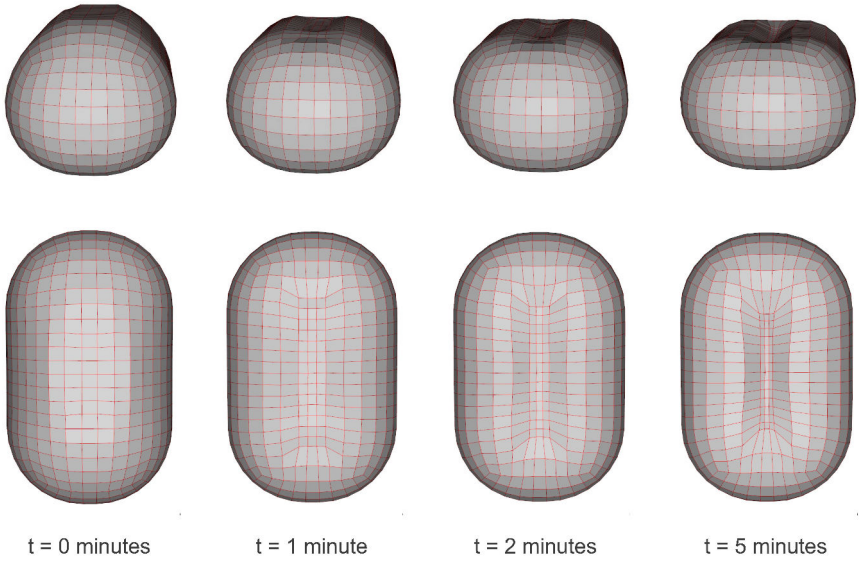

Figure 4.3: *Simulation of the ventral furrow invagination process on the "bean-shaped" embryo of Drosophila Melanogaster. The velocities of the barycenters of two cells located at the two areas of interest in the model of the Drosophila Melanogaster (a) and in the spherical model (b). Notice in (a) the faster movement of the barycenter in the VCE (blue) at the beginning ($v_c > v_m$) and the equalization of the velocities after approximately $t = 2$ minutes ($v_c = v_m$) . In (b), the two barycenters have almost equal velocities throughout the simulation.*

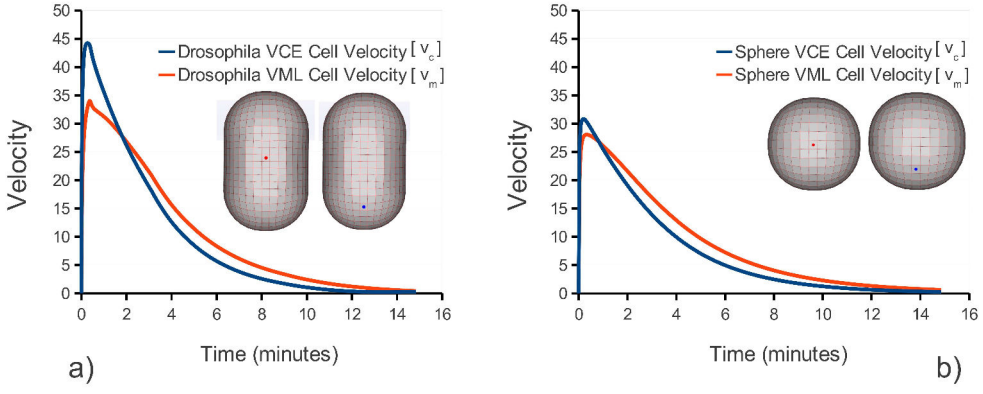

Figure 4.4: *Instances of the geometry from an antero-ventral (top) and a ventral point of view (bottom). Notice the apical constriction of the ventral hexahedra which triggers the invagination.*

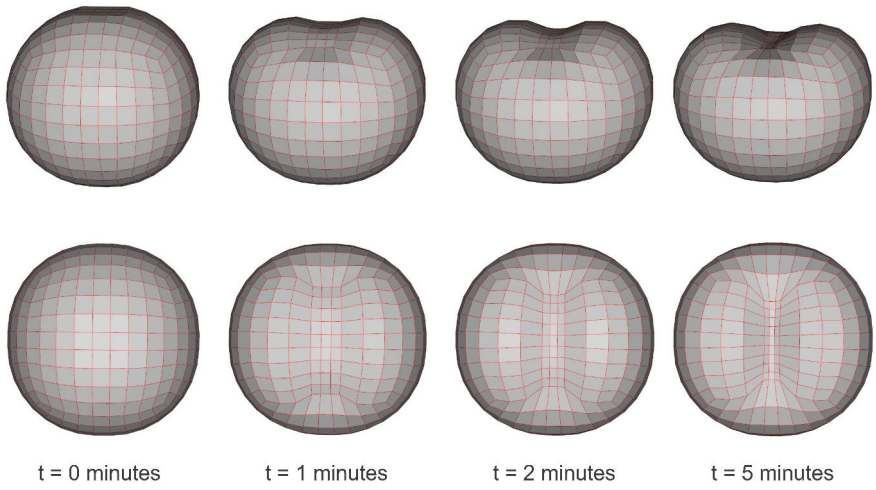

Figure 4.5: *Simulation of the invagination process on the spherical geometry. Instances of the geometry from an antero-ventral (top) and a ventral point of view (bottom).*

Figure 4.6: *Colored instance of the Drosophila Melanogaster model after* $t = 18$ *seconds from an ventral point of view. The color scale corresponds to the intensity of the node displacement.*

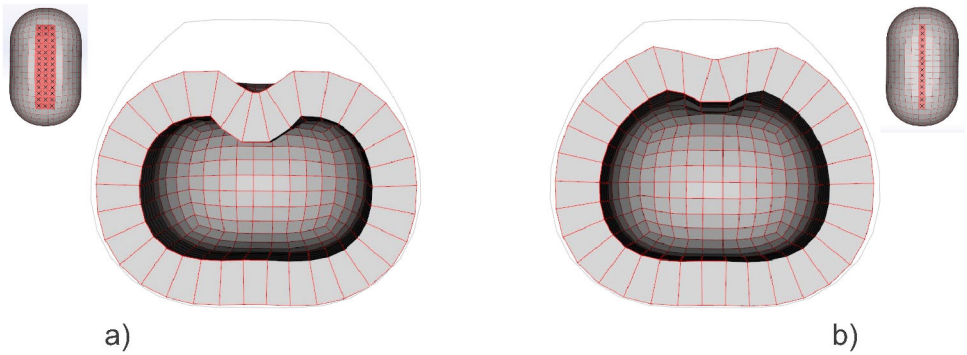

Figure 4.7: *The depth of the invagination is larger for a 3-rows contraction area (a) than the depth for a 1-row contraction area (b).*

4.4 Conclusion

As presented here, both the discrete and the FEM model effectively simulate the internalization of the future mesoderm. The FEM model has the big advantage of being based on the laws of continuum mechanics, thus the cell elasticity parameters (Young Modulus, Poisson ratio...) can be easily manipulated to simulate the cell behaviour as best as possible. On the other hand, both methods prove to be insufficient as far as modeling the closure of the furrow is concerned. Other publications [Conte *et al.* 2008, Conte *et al.* 2012] suggest that the closure of the furrow can be attributed to the apico-basal shortening of the invaginated ventral cells. In [Sweeton *et al.* 1991], it is also suggested that the lengthwise cell shortening is responsible for the cell shape change from columnar through trapezoidal to triangular, which transforms the shallow furrow into an invagination. However, they do not reject the case where the widening of the cell base might be the active component and cell shortening is a secondary passive response. On the other hand, [Allena *et al.* 2010] suggest that apical constriction alone suffices to drive invagination, apico-basal elongation not being a prerequisite.

I propose that the mechanism that induces the ventral closure which signifies the end of invagination is the division of the ventral cells once they are internalized. According to [Grosshans & Wieschaus 2000], the most ventrally located cells go into mitosis after the internalization is completed. The effect of the dividing ventral cells on the invagination is explored in Chapter 5 in page 81.

Chapter 5

Modeling the cell division

Contents

5.1 Introduction

In this chapter, I will talk about the final part of my work, the modeling of the cell division and the integration of this method in the model of the Drosophila Melanogaster (Section 4.3 on page 63). The creation of the model of the embryo of the Drosophila Melanogaster is based on a 3D hexahedral Finite Element mesh. Cells are represented as hexahedra with internal passive elastic forces modeling the effect of the cytoskeleton. Cell proliferation for our model corresponds to hexahedral division.

In this scope, we are interested in 3 characteristics of cell division behaviours, related to three questions:

- timing. When does a cell divide?
- intracellular position. Which cells divide (and where in the mesh)?
- direction of the dividing plane (also referred to as cleavage plane). How does a cell divide?

I will begin by introducing the terms of “mesh cutting” and “mesh refinement” and focus on the aspects that are of interest for this thesis. Then, I will present

examples of existing models in bibliography using mesh cutting and refinement to simulate morphogenetic processes. After that, I will illustrate our method for modeling cell proliferation in a very simple mesh composed of 3 hexaherons. Finally, the integration of the method to the model of the embryo of the Drosophila Melanogaster is explained along with insight on its effect on the ventral closure and possible perspectives.

5.2 Mesh Cutting

The term "mesh cutting" refers to modifying an existing mesh by moving or adding new nodes to a cutting entity and modifying the connectivity of the mesh. One important issue that a mesh cutting technique needs to address is element removal and remeshing, in other words, the way the the cutting operation is implemented (Figure 5.1). Mesh cutting is often used in computer graphics applications, where a virtual tool, also called cutting tool, is used to create a fracture or an incision in an object of a given geometrical mesh. Two common methods are:

- **removing intersected elements**. The elements that intersect the cutting tool are completely removed (see Figure 5.1(a)).
- **re-meshing intersected elements**. The path traversed by the tool through the intersected elements is recreated by remeshing the intersected elements, forming a gap in the mesh (see Figure 5.1(b)).

The first method has the advantage of avoiding the creation of new elements, thereby simplifying the overall operation. However, it has the drawback of creating cuts that might be visually disturbing, especially on irregular meshes. The second method has the additional cost of computing the intersection path, but provides a better representation of the path traversed by the cutting tool.

Other major issues that a mesh cutting method needs to address are:

- the definition of the cut path,
- the number of new elements created,
- when re-meshing is performed (depending on the position and the direction of the cutting tool),
- representation of the cutting tool.

The first and last point are not important in the scope of this work. The reader may refer to [Bruyns *et al.* 2002] for more detailed information concerning these issues. For our simulations, the important part is the remeshing of a specific region of a mesh at a given time.

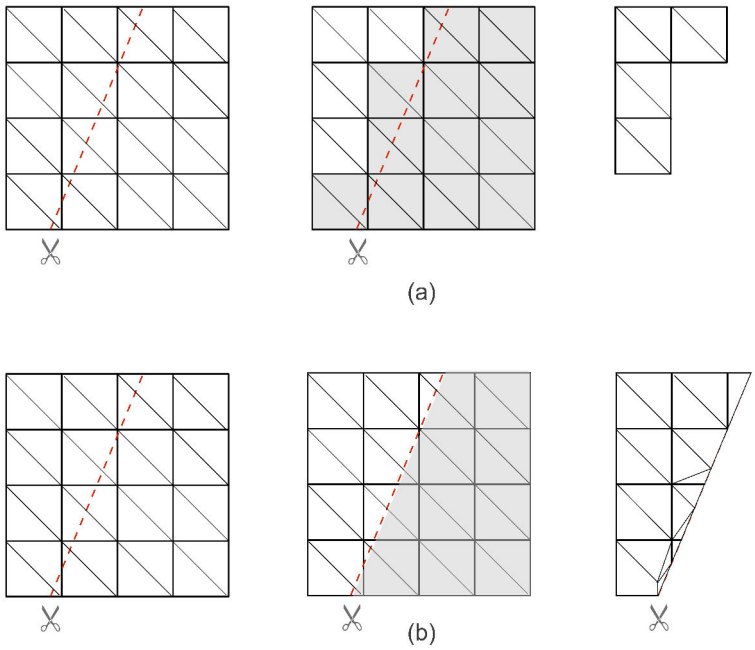

Figure 5.1: *Simple schematic showing the two common implementations of the cutting operation: (a) Removing intersected elements (b) Re-meshing intersected elements*

5.3 Mesh Refinement and the Discontinuity Problem

Adaptive mesh refinement is a method of changing the accuracy of a solution in certain regions of the mesh. Simply put, for a hexahedral mesh, the hexahedra at an area of interest are refined in order to better control the behaviour of the mesh at this area (reduce the numerical error of the calculations).

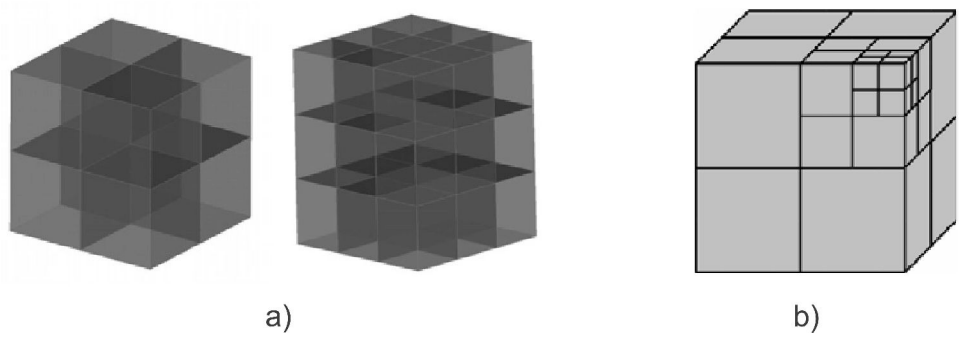

Figure 5.2: *Refinement of an individual hexahedron [Paudel et al. 2012]. a) 2-refinement and 3-refinement of a hexahedron. b) Adaptation of hexahedron by introducing hanging nodes at edge centers.*

As shown in Figure 5.2(a), 3-refinement splits an existing hexahedron three

times along an edge, and 2-refinement splits an existing hexahedron twice along an edge [Paudel *et al.* 2012]. 3-refinement is simple to implement but risks to over-refine a region of interest. 2-refinement has more constraints on it's implementation but can often provide well controlled refined regions.

Adaptive procedures try to automatically refine, coarsen, or relocate a mesh and/or adjust the basis to achieve a solution yhat provides a specified accuracy in an optimal fashion [1]. Common procedures studied to date include:

- local refinement and/or coarsening of a mesh (h-refinement),
- relocating or moving a mesh (r-refinement),
- locally varying the polynomial degree of the basis of the mesh (p-refinement).

The most popular technique among the three is h-refinement. Refinement of an element of a structured quadrilateral-element mesh by bisection requires mesh lines running to the boundaries to retain the four-neighbor structure. This strategy is simple to implement and has been used with finite difference computation. However, it clearly refines more elements than necessary. The customary way of avoiding the excess refinement is to introduce irregular nodes where the edges of a refined element meet at the midsides of a coarser one 5.2(b). However, the introduction of irregular nodes may cause problems of discontinuity on the mesh at the edge of refined areas as shown in Figure 5.3.

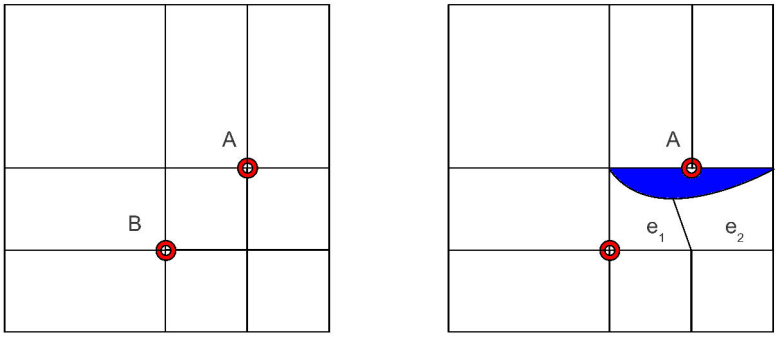

Figure 5.3: *Problem of discontinuity in the method of introducing irregular nodes at the edge centers of a very simple mesh. Suppose points A and B are points where irregular nodes have been placed. If for some reason, the elements e_1 and e_2 are forced to bend their top edges, then the result is an area that is totally empty (blue area in Figure 5.3).*

A lot of methods are available in the litterature for mesh refinement. For our simulations, the effect of physics is important, so we will concentrate on h-refinement. The geometrical discontinuity problem will be neglected for now because of lack of time.

[1] Joseph E. Flaherty, class lecture for "Adaptive Finite Element Techniques", Rensselaer Polytechnic Institute

5.4 Modeling Cell Division in Morphogenesis

In this section, I will present an overview of the biomechanical models developed to study cell division and proliferation in morphogenetic processes.

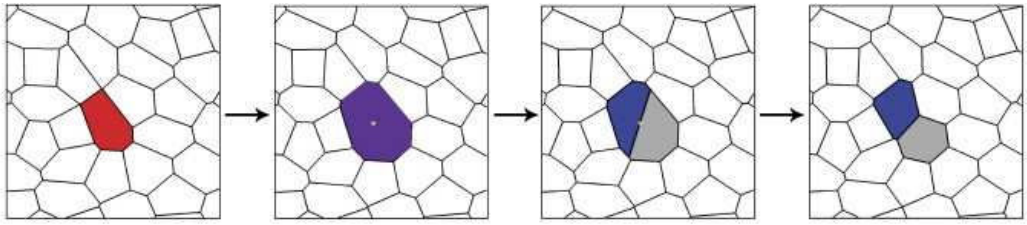

Figure 5.4: *Cell division in the vertex model [Farhadifar et al. 2007]. The preferred area of a randomly chosen cell is increased and the network is relaxed. A new cell boundary is introduced with a random orientation. Both new cells are assigned the initial preferred area, and the resulting network is again relaxed. The yellow dot indicates the average vertex position of the original cell through which the new boundary is initially formed.*

[Honda *et al.* 1984] were probably the first ones to attempt to model with a computer simulation the way in which cell number increases in a living tissue. They simulated the process of cell division on the blastular wall of the starfish, *Asterina pectinifera* using a geometrical model made of polygonal cells to determine the direction of cell division. In 1993, [Mombach *et al.* 1993] presented a simulation of the growth of a two-dimensional biological cellular system in which the cells experience mitosis whenever the area-to-perimeter ratio reaches a critical value.

[Brodland & Veldhuis 2002] performed finite element-based simulations to explore mitosis, and how mitosis, cell shape and epithelia reshaping depend on each other. *Cleavage plane* is defined as the axis along which any cell division occurs. They concluded that, stress and strain applied on a group of cells, can reshape the cells in such a way that their mitosis cleavage planes are aligned. Their simulations also show that mitoses with suitably aligned cleavage planes can drive epithelium reshaping. Their results are based on the formulation presented in [Chen & Brodland 2000]: the forces generated by circumferential microfilament bundles, microtubules, contraction of the cell membrane and its associated proteins and cell-cell adhesions, are resolved into an equivalent interfacial tension. To incorporate mitosis into the computer model they had to incorporate the rate of cell division M (the fraction of the current number of cells that divide per time τ), where

$$\tau = \frac{\gamma}{\rho t} 2\mu\delta \tag{5.1}$$

with δ and ρ the thickness and density of the epithelium respectively, μ the viscosity of the cells, t the time and γ the interfacial tension.

To understand how physical cellular properties and proliferation determine cell-

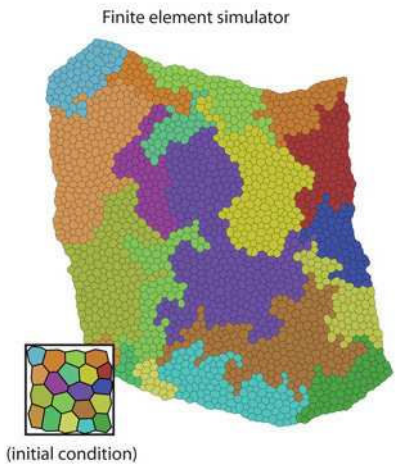

Figure 5.5: *The finite element simulator models cellular mechanics, division, and rearrangement [Gibson et al. 2010]. The simulator captures mechanics in terms of a net, interfacial tension, which is modeled using rod-like finite elements. Division likelihoods are informed by the empirically measured values.*

packing geometries, [Farhadifar *et al.* 2007] used a 2D vertex model for the epithelial junctional network in which cell packing geometries correspond to stable and stationary network configurations. A vertex model is a type of statistical mechanics model in which the Boltzmann weights are associated with a vertex in the model. A Boltzmann weight or factor determines the relative probability of a particle to be in a state i in a multi-state system in thermodynamic equilibrium at temperature T. Cells were represented as polygons with cell edges defined as straight lines connecting vertices, see Figure 5.4. The model takes into account three contributions to the potential energy E of a particular configuration of the epithelial junctional network: area elasticity, line tension along apical junctions, and contractility. The proliferation is numerically simulated and different network morphologies that depend on physical parameters are generated as a result.

The vertex models are further discussed and analyzed in [Staple *et al.* 2010], as well as the method they use to implement cell division. Broadly, the steps followed are:

- Initially the network is in a force-balanced state,
- a cell α is selected to divide,
- the cell α is bisected into two daughter cells by inserting a new cell bond with a random orientation that passes through the geometric center of the cell α,
- the system is relaxed to a force-balanced state.

[Hamant *et al.* 2008] created a 2D model of the *Arabidopsis* (a small flowering

plant) shoot apex to prove that morphogenesis depends on the microtubule cytoskeleton, which in turn is regulated by mechanical stress. They created a model incorporating mechanisms such as elastic wall mechanics, wall growth, cellular mechanical anisotropy (microfibrils), stress feedback, growth and proliferation. They defined a microtubule direction within each cell where the stiffness of the wall material increases as the wall becomes more parallel to the direction of the cortical microtubules, thus introducing mechanical anisotropy. Stress feedback is introduced by updating the microtubule directions to align along maximal stress directions, which for one cell is measured by the directional weighted average of its wall stresses.

[Gibson *et al.* 2010] used mechanical simulations to show that cell topology biases cleavage plane orientation in monolayer cell sheets. More precisely, the polygonal shapes of individual cells can systematically affect the long axis orientations of their adjacent mitotic neighbors in both plants and animals. This effect can be explained by fundamental packing constraints. They created a finite element model (Figure 5.5) to argue that the fraction of n-sided polygons in the junctional network can be determined by simple topological rules describing allocation of neighbor cells after division.

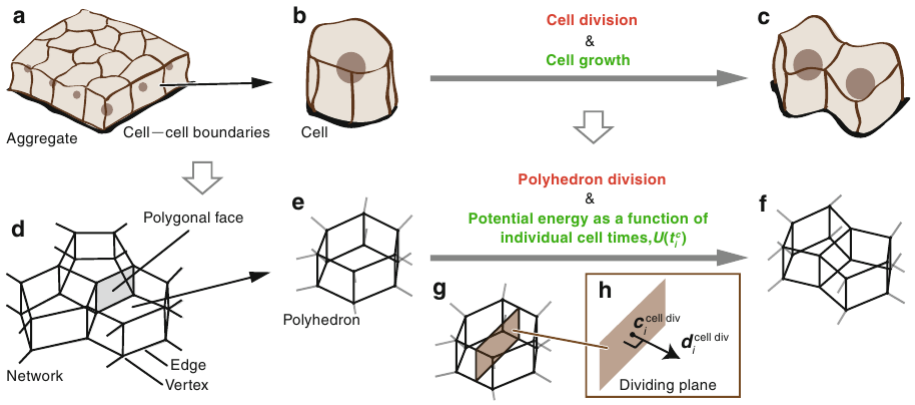

Figure 5.6: *Modeling cell proliferation based on a RNR framework [Okuda et al. 2013a]. (a,b,c) Two deforming daughter cells accompanied by cell growth, normally tightly packed in a cell aggregate where they adhere cell-cell boundaries. (d,e,f,g,h) Network representing the aggregate in a RNR model framework. Cells are compartmentalized by polygonal faces (gray facet) that represent cell-cell boundaries. A single cell is represented by a single polyhedron. Cell growth (increase in cell volume during the cell cycle) is expressed by potential energy that is a function of individual cell times within their respective cell cycles. Cell division (increase in cell number after a cell cycle) is represented by dividing a polyhedron at a dividing plane where a new polygonal face is introduced (brown area).*

[Okuda *et al.* 2013a] attempted to determine the general effects of proliferative cell behaviours on tissue morphogenesis at a scale of multiple cells. The cell proliferation was based on a 3D Reversible Network Reconnection (RNR) model framework.

A RNR model is a vertex model where the rearrangement of multi-object aggregates is defined by a rule of changing topological patterns called "network reconnections" [Okuda *et al.* 2013b]. An individual cell division was expressed by dividing a polyhedron at a planar surface. Cell division behaviours were characterized by three quantities: timing, intracellular position, and direction of the dividing plane. Furthermore, cell growth was expressed by potential energy as a function of individual cell times within their respective cell cycles (see Figure 5.6).

Although a lot of models have been created to simulate cell proliferation for morphogenetic processes, most of them are 2D. Some 3D models have already been implemented, but, to our knowledge, none of them is based on the Finite Element Method. Consequently, the next step for this work is to model cell division in a 3D hexahedral Finite Element mesh.

5.5 Model of the Cell Division

In this section, I present the method I implemented to model cell division. In biology, the dividing cell is usually referred to as the mother cell and the offspring are referred to as the daughter cells. We use this formalism for our elements as well, the dividing element is called mother element and the new divided elements are called daughter elements. I have had to face two main challenges:

- preserving the elasticity and the physics in the mesh after the division (although the geometry has suffered important topological changes),
- the inheritance of the initial stress situation of the mother element to the daughters.

The idea is that the daughter elements are smoothly integrated into the mesh without discontinuity and they attempt to acquire the initial stress state of their mother. I will start by a very simple example of 3 hexahedra, where the basics of the method will be explained and then I will focus on the integration of the cell division in a complex mesh, such as the 3D hexahedral Finite Element mesh of the embryo of the drosophila melanogaster presented in Chapter 4 on page 45.

5.5.1 Hexahedral Division

In general, we can say that the mitotic procedure of an individual eucaryotic cell conforms to the following path:

- The cell arrives at a dividing state (for instance when it receives a signal ordering it to divide or by growing over a certain level).
- The mother cell is split into two daughter cells (for our simulation, we are going to assume that the two offspring have the same size).

- The two new cells are temporarilly linked and share a common surface (the cleavage plane).

- The daughter cells inherit their mother's properties.

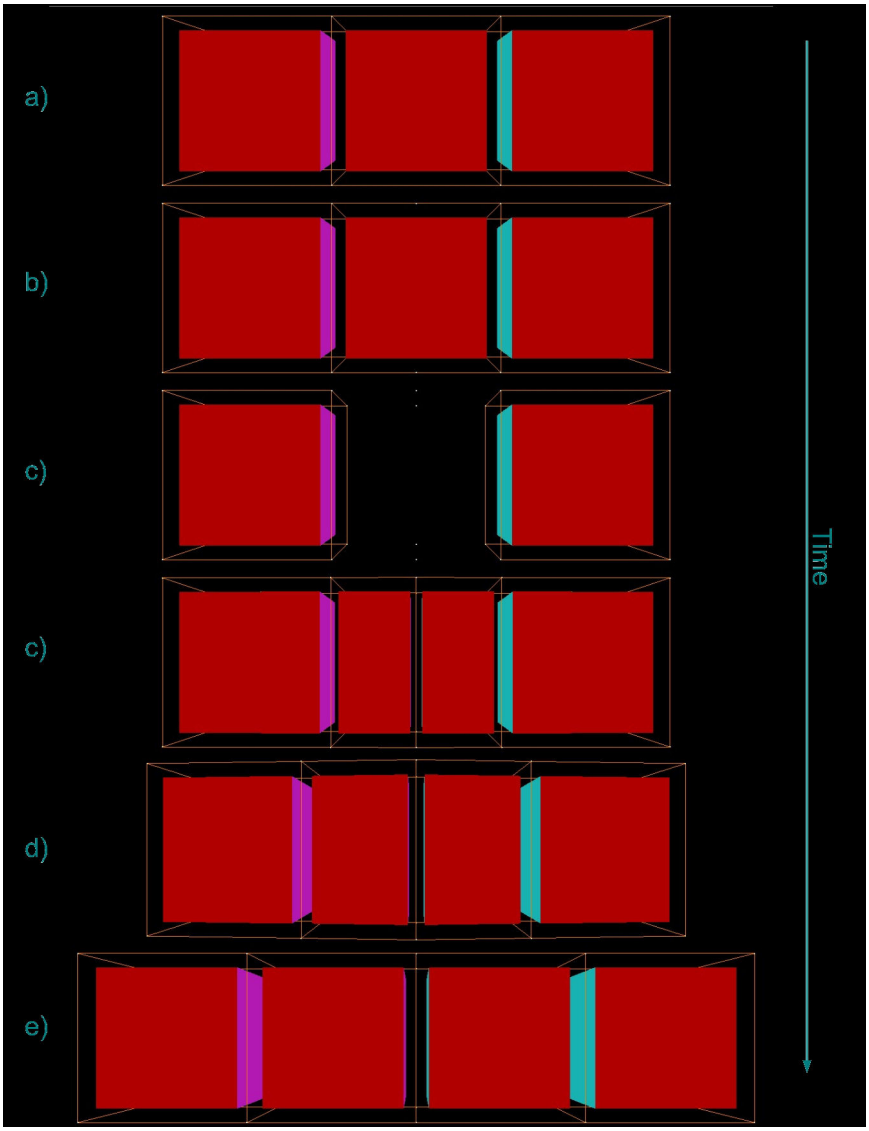

Figure 5.7: *Stages of an individual hexahedral division in a simple 3-hexahedron mesh. a) The hexahedra in their initial rest state. b) The points that define the position of the cut in the mesh are positioned. c) The mother middle hexahedron is removed. d) The two daughter hexahedra are placed in the mesh. e) The daughter hexahedra start to "inflate" in order to acquire the original unstressed shape of their mother. f) The hexahedra have acquired the same form as their mother, signalling the end of the process.*

The main challenges that we had to address when dividing an hexahedral element participating in the topology of a Finite Element mesh are:

- to determine the direction of the division (cut),
- to make sure that the two new elements are well defined and placed in the topology,
- to make sure that they are close/linked to each other (share a facet or nodes of the mesh).

As a consequence, the new cells will have the same elasticity and follow the same constitutive equation as the mother hexahedron.

The process of the division of a single hexahedron is shown in Figure 5.7. In this simple example, we choose to divide the middle hexahedron in a very simple mesh made of 3 hexahedra. A simple linear constitutive law defines the elasticity of the mesh with a rather small Young modulus of $E = 1000Pa$ and a commonly used Poisson ratio of $v = 0.3$. The values of the Young Modulus and the Poisson ratio were chosen to be the same as in the model of the Drosophila Melanogaster embryo [Conte *et al.* 2008, Maniotis *et al.* 1997, Bidhendi & Korhonen 2012]. The only existing forces are the elasticity forces of the Finite Element Method; there are no external forces (e.g. no gravity and no superimposed forces from the user). The direction of the division plane is vertical to the main axis of the mesh.

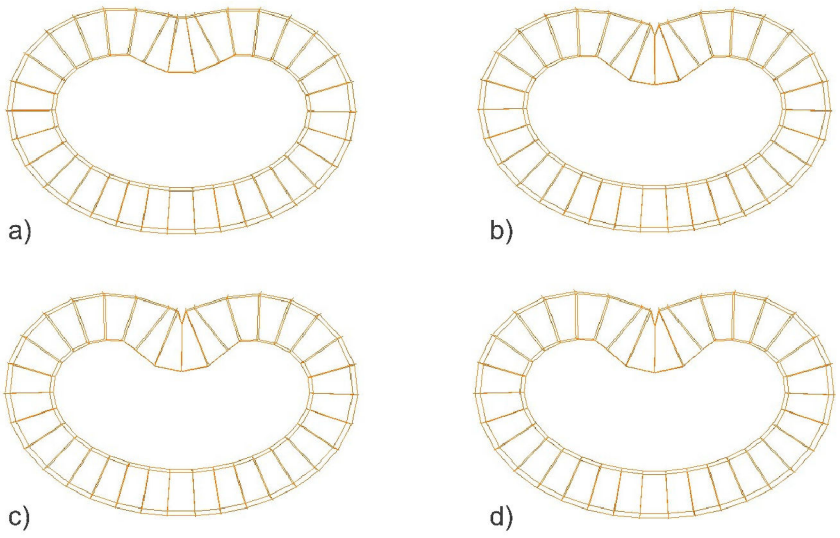

Figure 5.8: *Cross-sections of the stages of the ventral cells of the embryo undergoing division after the internalization has ended. a)* $t = 5.4$. *The model before the division of the most ventral hexahedra. b)* $t = 5.6$. *The model after the division of the most ventral hexahedra. c)* $t = 8.1$. *The invagination continues at a very slow pace. d)* $t = 10$. *The ventral hexahedra have reached maximum depth.*

The consecutive steps implemented for the hexahedral division are the following:

1. Determine the hexahedron(s) to divide and the direction of the division plane which corresponds to the cleavage plane.

2. For each hexahedron to divide, add new nodes on each of the 4 intersections between the division plane and the hexahedra edges.

3. Remove the selected mother hexahedron(s).

4. Create the daughter hexahedra in the mesh.

5. "Inject" to the daughter hexahedra the same physics as in the mother hexahedron (constitutive law, undeformed shape, Young modulus, Poisson ratio...).

The consequence of step 5 is to initialize the daughter cells with an initial stress. This means that the daughter hexahedra are not in mechanical equilibrium when created. The resolution of the physical laws post-division will make the daughter hexahedra try to acquire the un-stressed state of their mother (i.e. try to reach the same initial shape and size as their mother).

From a strictly biological point of view, it may seem strange as implementation. One could argue that, what we propose is "vanishing" a cell from a tissue and placing two other cells at its place. It is important to note that steps 2, 3 and 4 are artificial steps, pragmatically needed in the algorithm from a geometry perspective. They do not correspond to any real stage of mitosis.

From a biomechanical point of view, we had to choose between two solutions: either use a mesh-cutting technique (see Section 5.2) with a manually defined cutting path, or implement the method mentioned above. The method we chose has three advantages:

- The initial and residual stresses are preserved and the growth of the daughter hexahedra is influenced by them. This way we can monitor the growth of an hexahedron and the effects of its environment on it.

- Each hexahedron can be treated separately from the others. We can determine which hexahedron will divide and when, thus the division doesn't have to be following a certain path defined by a cutting tool

- Following the second advantage, although not implemented during the course of this thesis, we can imagine an automated element division, where the hexahedra will divide when they meet specific criteria. The criterion of a certain threshold for the $area/perimeter$ ratio of cells in a 2D model was already suggested in [Mombach *et al.* 1993]. Extended in 3D, this criterion would be the $surface/volume$ ratio.

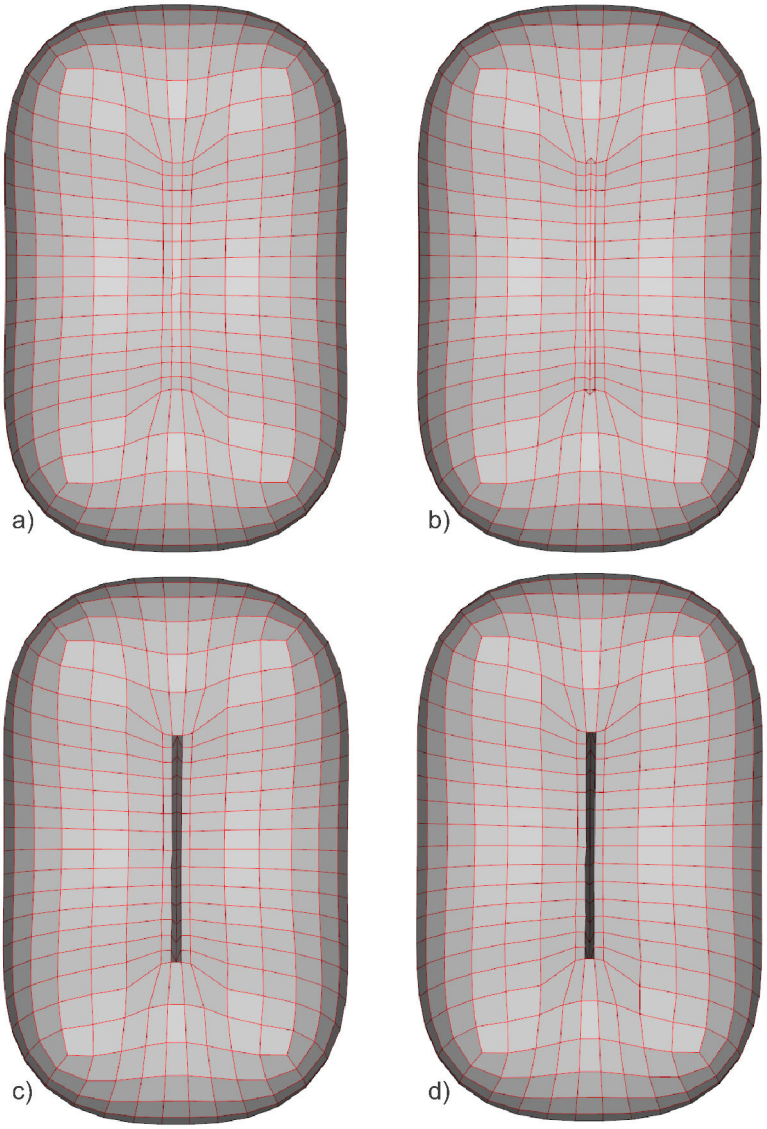

Figure 5.9: *View of the ventral hexahedra dividing and going further inside the embryo. The time of each stage corresponds to the time in Figure 5.8. a) $t = 5.4$. The model before the division of the most ventral hexahedra. b) $t = 5.6$. The model after the division of the most ventral hexahedra. c) $t = 8.1$. The ventral hexahedra continue to internalize. d) $t = 10$. The ventral hexahedra have reached maximum depth and have almost disappeared into the interior of the embryo.*

5.5.2 Framework

The simulations of the 3D biomechanical models of cell division are performed by SOFA[2] [Allard *et al.* 2007, Faure *et al.* 2007] (an open-source Simulation Open

[2]http://www.sofa-framework.org

Framework Architecture).

Two specific plugins were designed and added to the SOFA framework:

1. a plugin that performs steps 2, 3 and 4 of the hexahedral division (adding the new nodes, remove the selected mother hexahedra, create the daughter hexahedra)

2. a plugin that performs step 5 (inject to the daughter hexahedra the same physics as their mother)

Step 1 is done manually for now. The hexahedra to divide and the direction of the division plane are determined before the start of the simulation.

5.5.3 Integration of the hexahedral division in the model of the embryo of the Drosophila Melanogaster

In this section, I will show how I integrated the method of hexahedral division presented in Section 5.5.1 in the FEM model of the Drosophila Melanogaster presented in Section 4.3 on page 63.

As mentioned in Section 4.4 on page 80, the "bean-shaped" model of the ventral furrow invagination, although it simulates efficiently the internalization of the most ventrally located cells, it is not capable of simulating the last step of invagination, the ventral closure. In other scientific work [Sweeton *et al.* 1991, Brodland *et al.* 2010, Conte *et al.* 2012] it is suggested that ventral furrow invagination arises from a combination of apical constriction and apical-basal shortening forces in the mesoderm. I suggest that the closing of the furrow can be explained by the division of the most ventrally located cells, once internalized, in a vertical to the main axis of the embryo direction. The idea is that fact that the daughter cells will try to acquire the shape of their mother will make them push the invagination to go even deeper, thus pulling further the neighboring cells located at the borders of the prospective mesoderm.

In Figure 5.8, we show consecutive instances of the invagination process with the division of the most ventrally located cells. The divisions take place when the internalization of the ventral cells (see Section 4.3 on page 63) has been completed. It is obvious that the cell division "boosts" the internalization of the ventral cells. The results of the simulations can be viewed on the 3D mesh in Figure 5.9.

In Figure 5.10 we show a comparison of the two simulations of the ventral furrow invagination: with and without cell division. We use two cross-sections of the two models so that the difference is more easily understood. We are interested in two paricular distances:

- the vertical distance between the uppermost node of the mesh and the node at the depth of the furrow (h and h' in Figure 5.10). From now on, we will refer to this distance as the height of the invagination.

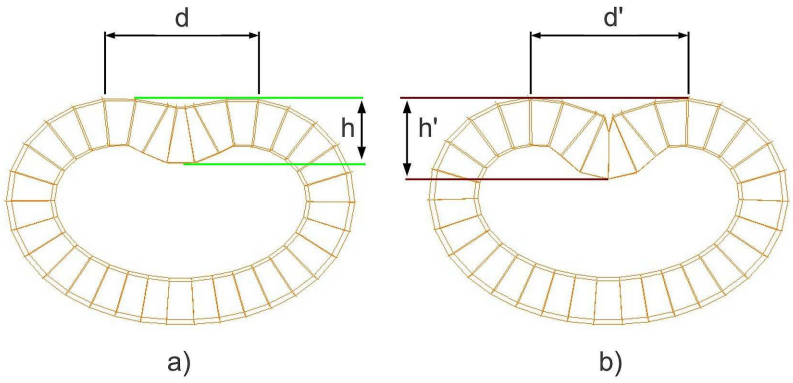

Figure 5.10: *Comparison of the latest stage of the simulated invaginations without (a) and with (b) cell division. Notice that the invagination height h' is bigger for the simulation with cell division than the invagination height h for the simulation without cell division. In addition, the distance between the two uppermost nodes d' is slightly smaller than d.*

- the distance between the two uppermost nodes of the mesh (d and d' in Figure 5.10).

The height of the invagination h for the simulation without cell division is $46.4\mu m$ while the height h' for the simulation with cell division is $60.3\mu m$. On the other hand, for the simulation without cell division the distance $d = 71.5\mu m$ while for the simulation with cell division $d' = 70.8\mu m$.

We notice that the integration of the cell division process increases significantly the height of the invagination by $13.9\mu m$ and that the distance between the two uppermost nodes is slightly smaller ($0.7\mu m$) for the simulation with cell division. The height of the invagination in Figure 5.10(b) as well as the disappearance from our view of the ventral cells in Figure 5.9 seem to explain the observations in Figure 2.14 on page 21 of the ventral cells eventually disappearing from microscopic observation towards the interior of the Drosophila embryo.

Although, the difference of the distances between the two uppermost nodes is not substancial, it is a result that shows that our hypothesis has reliable basis and it needs further testing. The division, not only of the most ventrally located cells, but, of their neighbors that internalize as well, has to be implemented. Furthermore, the ventral cells may undergo multiple divisions and this is also an assumption that needs to be studied.

5.6 Conclusion

In this chapter, I presented a method to divide hexahedra of an FEM hexahedral mesh. The method is based on the Finite Element Method developed in the SOFA framework (Simulation Open Framework Architecture). The integration of the

method on the FEM model of the Drosophila Melanogaster embryo was explained. Although the resulting configuration does not manage to reproduce efficiently the invagination of the ventral furrow, we consider the idea to be promising and further testing is required. In addition, cell division exists in multiple morphogenetic processes like posterior midgut invagination (see Section 2.9.3 on page 19) and germ band extension (see Section 2.9.4 on page 20), so this first implementation can be extended and integrated to biomechanical models simulating these procedures as well.

Chapter 6

General Conclusion and Perspectives

Contents

6.1 Contributions of this thesis

This thesis focuses on the study from a biomechanical point of view of the morphogenetic process of Ventral Furrow Invagination in the embryo of the Drosophila Melanogaster. The main questions that gave birth to this thesis are:

- "What is the role of apical constriction in the invagination?"
- "Once the internalization of the ventral cells is complete, what is the factor that drives ventral closure?"

To answer these questions we have created two "a minima" biomechanical models of invagination: a physically based discrete model and a model based on the Finite Element Method.

6.1.1 Physically based Discrete Biomechanical Model of the Invagination

The first contribution of this thesis is the creation of a discrete biomechanical model of the embryo of the Drosophila Melanogaster. The cells are defined as physical objects with three characteristics: incompressibility, elasticity and contractility. Active contractile forces are used to model the contriction of the ventral cells caused

by the myosin excess on their apex and passive elastic forces are used to model the effect of the cytoskeleton on cell shape and behaviour. Apart from the simulation of the invagination, the model is used to monitor individual cell characteristics as the apical $surface/volume$ ratio for a cell located at the ventral layer (which is considered to be an indicator of when a cell needs to divide).

6.1.2 Biomechanical Model of the Invagination based on the Finite Element Method

The second contribution of this thesis is the creation of a biomechanical model of the embryo of the Drosophila Melanogaster based on the Finite Element Method. The cells are modeled as easily deformable parallelepiped elements in a hexahedral mesh. The robust physical background the FEM offers allows for efficient validation of the model with characteristics (Poisson ration, Young Modulus) that can be directly linked to the properties of the cells. The model is also used to predict characteristics of the process of invagination like the depth of the furrow and the velocity of invaginating cells. By comparing the simulation of the "bean-shaped" model of the Drosophila embryo to a spherical model following exactly the same principles, we conclude that the geometry is a crucial factor for invagination.

6.1.3 Modeling the cell division

Although both biomechanical models of the embryo of the Drosophila Melanogaster efficiently predict the internalization of the ventral cells starting from the extremities and propagating to the medial area, they are unable to reproduce the ventral closure. We hypothesized that the factor missing from the simulation of the invagination is the proliferation of the ventral cells once internalized. For this purpose, we developed a method modeling cell division, by dividing hexahedra in a mesh and integrated it to the model.

6.2 Perspectives and Future Work

As mentioned in Chapter 2.9.1, ventral furrow invagination is driven by the myosin diffusion along the ventral area of the embryo. In this thesis, the myosin diffusion is neglected (we supposed that it diffuses so rapidly that it can be considered uniformly distributed along the ventral area). The myosin contraction appears in the transition of the energy equilibrium (the gradient of the global elastic energy is descending while the global mechanical energy is preserved). A model based on continuum mechanics integrating reaction-diffusion equations for the myosin is still an open problem.

This work focuses on the study of Ventral Furrow Invagination in the embryo of the Drosophila Melanogaster. We have shown that it is possible to simulate this

process with a simple "a minima" model. An important next step is to validate the robustness of the principles used in this model by simulating other morphogenetic processes as well. Posterior Midgut Invagination (see Section 2.9.3 on page 19) and Germ Band Extension (see Section 2.9.4 on page 20) are two very good candidates as the cells are in the same undifferentiated state.

The idea of the Drosophila ventral closure after internalization, being due to the proliferation of the ventral cells, although promising, needs a lot of testing to be validated. In our model, only one cell division cycle is performed. We can suggest that the implementation of multiple cell cycles could greatly aid the invaginating cells to form a deeper indentation. This way, the cells on the top of the ventral side of the embryo that will eventually stick together and close the furrow will be pulled closer to each other much faster.

In addition, an automated method for modeling cell proliferation can be visualized, where the cells will divide once a specific criterion has been met. In our case, this criterion could be the cell $surface/volume$ ratio. If this ratio overcomes a certain threshold, depending on the process modeled, the cells will divide.

Biomechanical modeling is a scientific area with great potential, because it can help to predict the outcome of biological and genetic experiments. This way, "in vivo" research can be efficiently guided and accelerated, which is very important especially concerning the study of diseases like cancer. Modeling and predicting the behavior of cancer cells could help the prediction of the appearance of a malignant tumor or the understanding of the way these cells need to be treated. In addition, understanding morphogenetic processes on a cellular level could be very important in various ways. For instance, let us think about the example of a lizard which has just had his tail cut off. The tail is going to regenerate due to a mechanism that is not yet understood. Understanding the cellular mechanisms involved in the regeneration of the cells of the lizard's tail could maybe mean that we are not far from reproducing the procedure to humans. This could mean that, eventually, amputated people could have the chance to have their limbs regenerated.

The biomechanical models of morphogenesis so far are focused on animals and plants. In the long term, we can imagine a fully automated method to model the whole early development of an organism. This way, we should be able to predict, for example, the outcome of a genetic anomaly and how it will affect the phenotype of the organism. If these prediction methods are compatible with future genetic treatment, it should be possible to predict and cure severe genetic disorders like Down or Klinefelter syndromes.

The moral aspect of the perspectives of this research is not to be taken lightly however. "Do we have the right to genetically treat an organism that has not already been born?" "What if, in some turn of events, we decide to just preserve one phenotype which is considered the "best" and dispose of all the rest?" These questions, although far from the scope of this thesis, should always be kept in mind. Diversity is a term that defines humankind, as much as all organisms, and it should

be preserved.

Appendix A

Dynamics and Elasticity

In this annex, I explain the principles controlling the dynamics in the physically-based discrete model and the model based on the finite element method presented in Chapter 4.

A.1 Physically Based Discrete Model

For every instant and for each particle, the second law of Newton: $\mathbf{F} = m\ddot{\mathbf{X}}$ is considered, where the left side of the equation is the sum of forces apllied on the particle, whereas the right side is mass of the particle multiplied with its acceleration [Promayon 2013].

$$\begin{cases} \dot{\mathbf{X}} = \mathbf{V} \\ \dot{\mathbf{V}} = \frac{\mathbf{F}}{m} \end{cases} \tag{A.1}$$

where $\mathbf{V}$ is the vector of the velocity. To simplify the resolution of this system, we assembly the equations of all the particles in order to create a global system where the forces, the positions, the velocities and the accelerations are gathered. In each stage of the resolution (time-step), we use the following algorithm:

1. calculation of forces of each particle,
2. resolution of the global differential equation ($t \rightarrow t + dt$),
3. application of the constraints.

Examples of forces applied on a particle are:

- Elastic forces reacting to a local deformation (produced by a non-uniform movement of the neighbouring particles).
- Contracting forces moving closer the neighbouring particles through internal tension.

As soon as the displacement driven by forces is calculated, the effect of the constraints is calculated by direct projection according to the constraint gradient [Promayon 1997]. There are two types of constraints:

- Local constraints applied on isolated particles. For instance, imposed null displacement can be handled as a local constraint applied on targeted particles.

- Global constraints applied on a group of particles. For instance, incompressibility (Section 4.2.1) can be handled as a a direct projection constraint (see Section 4.2.1)

A.1.1 Dynamics of an elastic model

The modeling of the elasticity is based on a method developed by [Marchal 2006]. The formulation of the elasticity relies on the two basic principles of shape memory and the notion of a particle attractor.

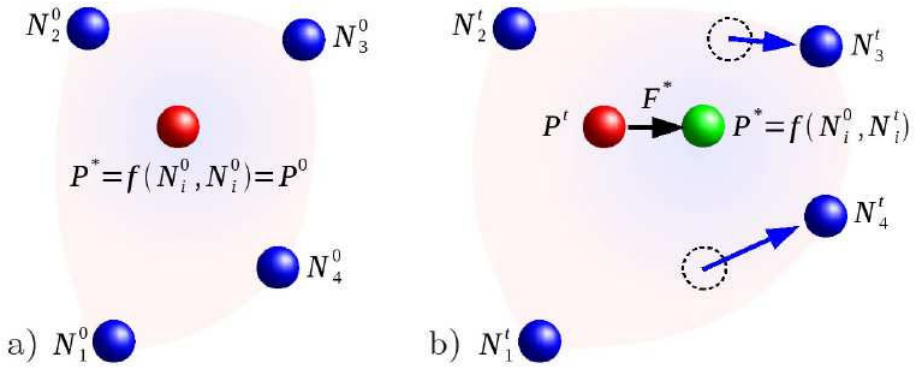

Figure A.1: *Let's consider the particle P and its neighbours N_i at time 0 (a) and at time t after a certain deformation. In the rest shape (a), the shape attractor is defined as $P^* = P^0$. Suppose that the particles N_3 and N_4 displace differently causing a local deformation (b). The deformation is taken into account by the shape function f, the position of the attractor P^* no longer coincides with P. Thus, a memory shape force F^* is created which dynamically pulls P towards P^*, by trying to locally minimize the energy of the deformation.*

Let P the position of a given particle and $N_i, i \in [1...n]$, the positions of n neighbours of this particle. The idea is to express the position P^* of this particle's attractor as a function of its n neighbours. The possible combinations of three particles among the n neighbour particles are taken into account (the triplets formed by three aligned particles are rejected). Each triplet $\langle N_i, N_j, N_k \rangle$ with $i \neq j \neq k$ and $i, j, k \in [1...n]$ form a triangle Δ with a normal n_Δ. The position P_Δ of the particle with regard to the triplet $\langle N_i, N_j, N_k \rangle$ is given by the following equation:

$$P_\Delta = Q_\Delta + \beta_\Delta \frac{n_\Delta}{\|n_\Delta\|} \tag{A.2}$$

where Q_Δ is the projection of P on $\langle N_i, N_j, N_k \rangle$ according to the normal n_Δ and β_Δ the distance between P and Q_Δ. Thus, P^* is defined as the isobarycenter of all the positions P_Δ resulting from the m valid positions formed by the neighbours of

the given particle:

$$P^* = \frac{1}{m} \sum_{\Delta=1}^{m} (Q_\Delta + \beta_\Delta \frac{n_\Delta}{\|n_\Delta\|}) \tag{A.3}$$

A shape memory force F^* is generated between the current position of the particle and the position of its attractor:

$$F^* = k_\varepsilon (P^* - P) \tag{A.4}$$

where k_ε is the elasticity coefficient. Finally, the shape memory force is redistributed to each of the neighbour particles that participated to the calculation of the attractor.

A.1.2 Constraints and Loads

A generic load is defined by the particles it targets, its type, its direction and a list of value-events defined in a given unit [Chabanas & Promayon 2004]. The loads can be divided into two categories:

- **Boundary conditions** consist in null displacements of the particles fixed (see the particles highlighted in blue in Figure 7 in the **Simulation** paragraph in Section 4.2.2).
- **Imposed displacements** consist in forced non-displacement of target particles along a given direction (the particles highlighted in red in Figure 7 cannot move along the z-axis in the **Simulation** paragraph in Section 4.2.2).

A.2 Finite Elements

A solid is discretized using n sample points $p_j, j \in [1, n]$. Each point has fixed coordinates x_j with respect to the object and moving coordinates u_j with respect to the world coordinate system, along with mass m_j velocity $\dot{u}_j$ and acceleration $\ddot{u}_j$. The object space is partitioned in finite elements (cells) based on the sampling points. Each element applies forces to its sampling points according to their positions and velocities and the properties of the medium. Hooke's law $\sigma = D\varepsilon$ is used to model linear elasticity, where vector σ models the local constraints (non-isotropic internal pressures) within the medium, vector ε models the local deformation (compression and shear in all directions) and the $6x6$ matrix D models the stiffness and incompressibility of the medium. The deformation ε of an element is related to the coordinates u of its sampling points by the relation:

$$\Delta\varepsilon = B\Delta u \tag{A.5}$$

where vector Δu represents the displacement of the vertices of an element and the $12x6$ matrix B, called strain-displacement matrix, encodes the geometry of the

element. The force applied by the deformed element to its sampling points is given by

$$f = B^T \sigma \tag{A.6}$$

Putting it all together, we obtain a linear relationship between force and displacement:

$$\Delta f = B^T D B \Delta u \tag{A.7}$$

The matrix $K = B^T D B$ is called the stiffness matrix of the element. The mesh force f_j applied on a sampling point p_j is computed by summing the forces applied by all elements the point belongs to. A similar relation on velocities can be used to model damping.

A.2.1 Newton's and Euler's laws

Newton's law on linear acceleration relates the acceleration of a system to the external forces applied to it:

$$\sum_j m_j \ddot{u}_j = \sum_j f_j^{ext} \tag{A.8}$$

where f_j^{ext} is the external force applied to sampling point p_j. It can be applied on a single particle, on an element as well as on the whole object. The violation of this law would allow an isolated object to linearly accelerate. Euler's law on angular acceleration relates the angular acceleration of a system to the net torque applied to it:

$$\sum_j u_j \times m_j \ddot{u}_j = \sum_j u_j \times f_j^{ext} \tag{A.9}$$

The violation of this law would allow an isolated object to angularly accelerate.

A.2.2 Implicit time integration

To dynamically interact with the FEM system, the following second order differential equation is solved globally:

$$\mathbf{M}\ddot{\mathbf{u}} + \mathbf{C}\dot{\mathbf{u}} + \mathbf{K}\mathbf{u} = \mathbf{f} \tag{A.10}$$

where matrix $\mathbf{M}$ models mass, $\mathbf{C}$ models damping and $\mathbf{K}$ models stiffness, $\mathbf{u}$ corresponds to displacements between initial position $\mathbf{x}_0$ and actual position $\mathbf{x}$, and $\mathbf{f}$ corresponds to forces, for all the vertices. The global matrices are computed by summing up the contributions of each element to its vertices. This operation is called the assembly.

A.2.3 Rotational invariance

The linear equation A.7 is insensitive to translations but inaccurate for large rotations of the elements. To solve this problem we have to decompose the displacement in one rigid rotation combined with a deformation [Nesme *et al.* 2005]. Equation A.7 becomes:

$$\Delta f = R^t B^T D B R \Delta u \tag{A.11}$$

where the matrix R encodes the rotation of a local frame attached to the element with respect to its initial orientation.

To eliminate rotation problems, we compute the 3×3 transformation matrix for each element using 3 of its edges:

$$J = [{e^0}_1 \quad {e^0}_2 \quad {e^0}_3]^{-1}[e_1 \quad e_2 \quad e_3] \tag{A.12}$$

where ${e^0}_i$ are the initial edge vectors and e_i are the current ones. Matrix J is then decomposed in order to extract separately a rigid rotation R applied to the element and a deformation E. We used polar decomposition, which is described in the next section.

A.2.4 Polar Decomposition

The polar decomposition of a square matrix computes the nearest orthogonal frame to the given column axes. As such it provides the ideal decomposition of the displacement matrix J. The strain values can be derived as shown in the following formula.

$$\begin{aligned} J &= R_p E_s \\ E_s = {R_p}^{-1} J &= \begin{bmatrix} 1+\varepsilon_{xx} & \varepsilon_{xy} & \varepsilon_{xz} \\ \varepsilon_{xy} & 1+\varepsilon_{yy} & \varepsilon_{yz} \\ \varepsilon_{xz} & \varepsilon_{yz} & 1+\varepsilon_{zz} \end{bmatrix} \end{aligned} \tag{A.13}$$

Bibliography

[Allard *et al.* 2007] J. Allard, S. Cotin, F. Faure, P.D. Bensoussan, F. Poyer, C. Duriez, H. Delingette and L. Grisoni. *SOFA - an Open Source Framework for Medical Simulation.* In Medicine Meets Virtual Reality, MMVR 15, 2007. (Cited in page 92.)

[Allena & Aubry 2010] R. Allena and D. Aubry. *A novel technique to parametrize shell-like deformations inside biological membranes.* Computational Mechanics, pages 1–15, 2010. (Not cited.)

[Allena *et al.* 2010] R. Allena, A.S. Mouronval and D. Aubry. *Simulation of multiple morphogenetic movements in the Drosophila embryo by a single 3D finite element model.* Journal of the Mechanical Behavior of Biomedical Materials, vol. 3, no. 4, pages 313 – 323, 2010. (Cited in pages 42 and 80.)

[Bard 1981] J.B.L. Bard. *A model for generating aspects of zebra and other mammalian coat patterns.* Journal of Theoretical Biology, vol. 93, no. 2, pages 363 – 385, 1981. (Cited in page 37.)

[Bidhendi & Korhonen 2012] A.J. Bidhendi and R.K. Korhonen. *A Finite Element Study of Micropipette Aspiration of Single Cells: Effect of Compressibility.* Computational and Mathematical Methods in Medicine, vol. 2012, pages 1–15, 2012. (Cited in page 90.)

[Bower 2012] A.F. Bower. Applied mechanics of solids. CRC Press, 2012. (Cited in page 28.)

[Bownes 1975] M. Bownes. *A photographic study of development in the living embryo of Drosophila melanogaster.* Journal of embryology and experimental morphology, vol. 33, pages 789–801, 1975. (Not cited.)

[Brodland & Veldhuis 2002] G.W. Brodland and J.H. Veldhuis. *Computer simulations of mitosis and interdependencies between mitosis orientation, cell shape and epithelia reshaping.* Journal of Biomechanics, vol. 35, no. 5, pages 673 – 681, 2002. (Cited in page 85.)

[Brodland *et al.* 2010] G.W. Brodland, V. Conte, P.G. Cranston, J. Veldhuis, S. Narasimhan, M.S. Hutson, A. Jacinto, F. Ulrich, B. Baum and M. Miodownik. *Video force microscopy reveals the mechanics of ventral furrow invagination in Drosophila.* Proceedings of the National Academy of Sciences, 2010. (Cited in page 93.)

[Bruyns *et al.* 2002] C.D. Bruyns, S. Senger, A. Menon, K. Montgomery, S. Wildermuth and R. Boyle. *A survey of interactive mesh-cutting techniques and a new method for implementing generalized interactive mesh cutting using virtual tools.* The Journal of Visualization and Computer Animation, vol. 13, no. 1, pages 21–42, 2002. (Cited in page 82.)

[Chabanas & Promayon 2004] M. Chabanas and E. Promayon. *Physical Model Language: Towards a Unified Representation for Continuous and Discrete Models.* In S. Cotin and D. Metaxas, editeurs, Medical Simulation, volume 3078 of *Lecture Notes in Computer Science*, pages 256–266. Springer Berlin Heidelberg, 2004. (Cited in pages 25 and 103.)

[Charlton *et al.* 1994] D.J. Charlton, J. Yang and K. K. Teh. *A Review of Methods to Characterize Rubber Elastic Behavior for Use in Finite Element Analysis.* Rubber Chemistry and Technology, vol. 67, no. 3, pages 481–503, 1994. (Cited in pages 29 and 30.)

[Chen & Brodland 2000] H.H. Chen and G.W. Brodland. *Cell-Level Finite Element Studies of Viscous Cells in Planar Aggregates.* Journal of Biomechanical Engineering, vol. 122, no. 4, pages 394–401, 2000. (Cited in page 85.)

[Chen *et al.* 1997] C.S. Chen, M. Mrksich, S. Huang, G.M. Whitesides and D.E. Ingber. *Geometric Control of Cell Life and Death.* Science, vol. 276, no. 5317, pages 1425–1428, 1997. (Cited in page 23.)

[Conte *et al.* 2008] V. Conte, J.J. Munoz and M. Miodownik. *A 3D finite element model of ventral furrow invagination in the Drosophila melanogaster embryo.* Journal of the Mechanical Behavior of Biomedical Materials, vol. 1, pages 188–198, 2008. (Cited in pages 42, 43, 80 and 90.)

[Conte *et al.* 2012] V. Conte, F. Ulrich, B. Baum, J. Munoz, J. Veldhuis, W. Brodland and M. Miodownik. *A Biomechanical Analysis of Ventral Furrow Formation in the Drosophila Melanogaster Embryo.* PLoS ONE, vol. 7, no. 4, 2012. (Cited in pages 80 and 93.)

[Cooper 2000] G.M. Cooper. The cell: A molecular approach. 2nd edition. Sinauer Associates, 2000. (Cited in pages 10 and 11.)

[Costa & Balaniuk 2001] I.F. Costa and R. Balaniuk. *LEM-an approach for real time physically based soft tissue simulation.* In Robotics and Automation, 2001. Proceedings 2001 ICRA. IEEE International Conference on, volume 3, pages 2337–2343 vol.3, 2001. (Cited in page 33.)

[da Silva & Vincent 2007] S.M. da Silva and J.P. Vincent. *Oriented cell divisions in the extending germband of Drosophila.* Development, vol. 134, pages 3049–3054, 2007. (Cited in pages 19 and 20.)

[Davidson *et al.* 1995] L.A. Davidson, M.A. Koehl, R. Keller and G.F. Oster. *How do sea urchins invaginate? Using biomechanics to distinguish between mechanisms of primary invagination.* Development, vol. 121, pages 2005–2018, 1995. (Cited in pages 40 and 41.)

[Davidson *et al.* 1999] L.A. Davidson, G.F. Oster, R. Keller and M.A. Koehl. *Measurements of mechanical properties of the blastula wall reveal which hypothesized mechanisms of primary invagination are physically plausible in the sea urchin Strongylocentrotus purpuratus.* Developmental biology, vol. 209, pages 221–238, 1999. (Cited in page 41.)

[Dawes-Hoang *et al.* 2005] R.E. Dawes-Hoang, K.M. Parmar, A.E. Christiansen, C.B. Phelps, A.H. Brand and E.F. Wieschaus. *Folded gastrulation, cell shape change and the control of myosin localization.* Development, vol. 132, pages 4165–4178, 2005. (Cited in page 17.)

[Delingette *et al.* 1999] H. Delingette, S. Cotin and N. Ayache. *A hybrid elastic model allowing real-time cutting, deformations and force-feedback for surgery training and simulation.* In Computer Animation, 1999. Proceedings, pages 70–81, 1999. (Cited in pages 33 and 34.)

[Demongeot *et al.* 2011] J. Demongeot, A. Henrion-Caude, A. Lontos and E. Promayon. *General architecture of a genetic regulatory network. Applications to embryologic control.* In T. Lenaerts, M. Giacobini, H. Bersini, P. Bourgine, M. Dorigo and R. Doursat, editeurs, ECAL'11, Advances in Artificial Life, Proceedings of the Eleventh European Conference on the Synthesis and Simulation of Living Systems, pages 1–8. MIT Press, Cambridge, MA, 2011. (Cited in pages 48 and 57.)

[Demongeot *et al.* 2012] J. Demongeot, J. Gaudart, A. Lontos, J. Minsta, E. Promayon and M. Rachdi. *Zero-diffusion domains in reaction-diffusion morphogenetic & epidemiologic processes.* International Journal of Bifurcation and Chaos, vol. 22, no. 2, February 2012. (Cited in page 63.)

[Deram 2012] A. Deram. *Environnement Générique pour la Validation de Simulations Medicales.* PhD thesis, Université de Grenoble, October 2012. (Cited in page 34.)

[Dominguez & Holmes 2011] R. Dominguez and K.C. Holmes. *Actin Structure and Function.* Annu Rev Biophys, vol. 40, pages 169–186, 2011. (Cited in page 8.)

[Driquez *et al.* 2011] B. Driquez, A. Bouclet and E. Farge. *Mechanotransduction in mechanically coupled pulsating cells: transition to collective constriction and mesoderm invagination simulation.* Phys Biol, vol. 8, pages 169–186, 2011. (Cited in page 39.)

[Eymard *et al.* 1999] R. Eymard, M. Gutnic and D. Hilhorst. *The finite volume method for Richards equation*. Computational Geosciences, vol. 3, no. 3-4, pages 259–294, 1999. (Cited in page 32.)

[Farhadifar *et al.* 2007] R. Farhadifar, J.-C. Röper, B. Aigouy, S. Eaton and F. Jülicher. *The Influence of Cell Mechanics, Cell-Cell Interactions, and Proliferation on Epithelial Packing*. Current Biology, vol. 17, no. 24, pages 2095 – 2104, 2007. (Cited in pages 85 and 86.)

[Faure *et al.* 2007] F. Faure, J. Allard, S. Cotin, P. Neumann, P.J. Bensoussan, C. Duriez, H. Delingette and L. Grisoni. *SOFA: A modular yet efficient simulation framework*. In Surgetica 2007: Computer-Aided Medical Interventions: tools and applications, 2007. (Cited in page 92.)

[Forest & Demongeot 2008] L. Forest and J. Demongeot. *A General Formalism for Tissue Morphogenesis Based on Cellular Dynamics and Control System Interactions*. Acta Biotheoretica, vol. 56, no. 1-2, pages 51–74, 2008. (Cited in pages 38 and 39.)

[Forgacs & Newman 2005] G. Forgacs and S.A. Newman. Biological physics of the developing embryo. Cambridge University Press, 2005. (Not cited.)

[Fouard *et al.* 2012] C. Fouard, A. Deram, Y. Keraval and E. Promayon. Camitk: a modular framework integrating visualization, image processing and biomechanical modeling, pages 323–354. Springer Berlin Heidelberg, 2012. (Not cited.)

[Fracchia *et al.* 1990] F.D. Fracchia, P. Prusinkiewicz and M.J.M. de Boer. *Animation of the Development of Multicellular Structures*. In Nadia Magnenat-Thalmann and Daniel Thalmann, editeurs, Computer Animation '90, pages 3–19. Springer Japan, 1990. (Cited in page 26.)

[Fullilove & Jacobson 1971] S.L. Fullilove and A.G. Jacobson. *Nuclear elongation and cytokinesis in Drosophila montana*. Developmental Biology, vol. 26, no. 4, pages 560 – 577, 1971. (Cited in page 14.)

[Galle *et al.* 2005] J. Galle, M. Loefflerâ and D. Drasdo. *Modeling the Effect of Deregulated Proliferation and Apoptosis on the Growth Dynamics of Epithelial Cell Populations In Vitro*. Biophysical Journal, vol. 88, pages 62–75, 2005. (Not cited.)

[Gibson *et al.* 2010] W.T. Gibson, J.H. Veldhuis, B. Rubinstein, H.N. Cartwright, N. Perrimon, G.W. Brodland, R. Nagpal and M.C. Gibson. *Control of the Mitotic Cleavage Plane by Local Epithelial Topology*. Cell, vol. 144, pages 427–438, 2010. (Cited in pages 86 and 87.)

[Gierer & Meinhardt 1972] A. Gierer and H. Meinhardt. *A theory of biological pattern formation.* Kybernetik., vol. 12, pages 30–39, 1972. (Cited in page 37.)

[Grosshans & Wieschaus 2000] J. Grosshans and E. Wieschaus. *A genetic link between morphogenesis and cell division during formation of the ventral furrow in Drosophila.* Cell, vol. 101, pages 523–531, 2000. (Cited in pages 3 and 80.)

[Grumbling *et al.* 2006] G. Grumbling, V. Strelets and The FlyBase Consortium. *FlyBase: anatomical data, images and queries.* Nucleic Acids Research, vol. 34, no. suppl 1, pages D484–D488, 2006. (Cited in page 16.)

[Gumbiner 2005] B.M. Gumbiner. *Regulation of cadherin-mediated adhesion in morphogenesis.* Nat Rev Mol Cell Biol., vol. 6, pages 622–634, 2005. (Not cited.)

[Hamant *et al.* 2008] O. Hamant, M.G. Heisler, H. Jönsson, P. Krupinski, M. Uyttewaal, P. Bokov, F. Corson, P. Sahlin, A. Boudaoud, E.M. Meyerowitz, Y. Couder and J. Traas. *Developmental Patterning by Mechanical Signals in Arabidopsis.* Science, vol. 322, no. 5908, pages 1650–1655, 2008. (Cited in page 86.)

[Hauth *et al.* 2003] M. Hauth, O. Etzmuß and W. Straßer. *Analysis of numerical methods for the simulation of deformable models.* The Visual Computer, vol. 19, no. 7, pages 581–600, 2003. (Cited in page 35.)

[Honda *et al.* 1984] H. Honda, H. Yamanaka and M. Dan-Sohkawa. *A computer simulation of geometrical configurations during cell division.* Journal of Theoretical Biology, vol. 106, no. 3, pages 423 – 435, 1984. (Cited in page 85.)

[Huang & Ingber 1999] S. Huang and D.E. Ingber. *The structural and mechanical complexity of cell-growth control.* Nat Cell Biol, vol. 1, no. 5, pages 131–E138, 1999. (Cited in page 23.)

[James & Pai 1999] D.L. James and D.K. Pai. *ArtDefo: accurate real time deformable objects.* In Proceedings of the 26th annual conference on Computer graphics and interactive techniques, SIGGRAPH '99, pages 65–72, New York, NY, USA, 1999. ACM Press/Addison-Wesley Publishing Co. (Cited in page 33.)

[Johnston & Nusslein-Volhard 1992] D.S. Johnston and C. Nusslein-Volhard. *The origin of pattern and polarity in the Drosophila embryo.* Cell, vol. 68, no. 2, pages 201 – 219, 1992. (Cited in page 17.)

[Kam *et al.* 1991] Z. Kam, J.S. Minden, D.A Agard, J.W. Sedat and M. Leptin. *Drosophila gastrulation: analysis of cell shape changes in living embryos by three-dimensional fluorescence microscopy.* Development, vol. 112, pages 365–370, 1991. (Cited in page 19.)

[Karr & Alberts 1986] T.L. Karr and B.M. Alberts. *Organization of the cytoskeleton in early Drosophila embryos.* J Cell Biol, vol. 102, pages 1494–1509, 1986. (Not cited.)

[Kernevez *et al.* 1979] J.P. Kernevez, G. Joly, M.C. Duban, B. Bunow and D. Thomas. *Hysteresis, oscillations, and pattern formation in realistic immobilized enzyme systems.* Journal of Mathematical Biology, vol. 7, no. 1, pages 41–56, 1979. (Cited in page 37.)

[Koehl 1990] M.A.R. Koehl. *Biomechanical approaches to morphogenesis.* seminars in Developmental Biology, vol. 1, pages 367–378, 1990. (Cited in page 36.)

[Kotadia *et al.* 2010] S. Kotadia, J. Crest, U. Tram, B. Riggs and W. Sullivan. *Blastoderm Formation and Cellularisation in Drosophila melanogaster.* Encyclopedia of Life Sciences, 2010. (Cited in page 14.)

[Lecuit & Wieschaus 2000] T. Lecuit and E. Wieschaus. *Polarized insertion of new membrane from a cytoplasmic reservoir during cleavage of the Drosophila embryo.* J Cell Biol, vol. 150, pages 849–860, 2000. (Cited in page 13.)

[Leptin & Grunewald 1990] M. Leptin and B. Grunewald. *Cell shape changes during gastrulation in Drosophila.* Development, vol. 110, pages 73–84, 1990. (Not cited.)

[Leptin 1999] M. Leptin. *Gastrulation in Drosophila: the logic and the cellular mechanisms.* EMBO J, vol. 18, no. 12, page 3187â3192, 1999. (Cited in pages 15 and 17.)

[Lindenmayer & Rozenberg 1979] A. Lindenmayer and G. Rozenberg. *Parallel generation of maps: Developmental systems for cell layers.* In Volker Claus, Hartmut Ehrig and Grzegorz Rozenberg, editeurs, Graph-Grammars and Their Application to Computer Science and Biology, volume 73 of *Lecture Notes in Computer Science*, pages 301–316. Springer Berlin Heidelberg, 1979. (Cited in page 26.)

[Lodish *et al.* 2000] H. Lodish, A. Berk, SL Zipursky, P. Matsudaira, D. Baltimore and J. Darnell. Molecular cell biology. 4th edition. W. H. Freeman, 2000. (Cited in page 9.)

[Mahowald 1963] A.P. Mahowald. *Ultrastructural differentiations during formation of the blastoderm in the Drosophila melanogaster embryo.* Developmental Biology, vol. 8, no. 2, pages 186 – 204, 1963. (Cited in page 13.)

[Maniotis *et al.* 1997] A.J. Maniotis, C.S. Chen and D.E. Ingber. *Demonstration of mechanical connections between integrins, cytoskeletal filaments, and nucleoplasm that stabilize nuclear structure.* Proceedings of the National Academy of Sciences, vol. 94, no. 3, pages 849–854, 1997. (Cited in page 90.)

[Marchal *et al.* 2006] M. Marchal, E. Promayon and J. Troccaz. *Simulating Prostate Surgical Procedures with a Discrete Soft Tissue Model*. In I. Navazo C. Mendoza, editeur, Eurographics Workshop in Virtual Reality Interactions and Physical Simulations, VriPhys06, pages 109–118, 2006. (Cited in page 46.)

[Marchal 2006] M. Marchal. *Modélisation des tissus mous dans leur environnement pour l'aide aux gestes médico-chirurgicaux*. PhD thesis, Université Joseph Fourier, 2006. (Cited in page 102.)

[Marieb & Hoehn 2010] E. Marieb and K. Hoehn. Human Anatomy & Physiology. Benjamin Cummings, 8 édition, 2010. (Cited in page 6.)

[Martin *et al.* 2008] A.C. Martin, M. Kaschube and E.F. Wieschaus. *Pulsed contractions of an actin-myosin network drive apical constriction.* Nature, vol. 457, pages 495–499, 2008. (Cited in pages 2, 18, 20, 21, 39 and 48.)

[Martin *et al.* 2010] A.C. Martin, M. Gelbart, R. Fernandez-Gonzalez, M. Kaschube and E.F. Wieschaus. *Integration of contractile forces during tissue invagination.* J Cell Biol, vol. 188, pages 735–49, 2010. (Cited in page 39.)

[Mazumdar & Mazumdar 2002] A. Mazumdar and M. Mazumdar. *How one becomes many: blastoderm cellularization in Drosophila melanogaster.* Bioessays, vol. 24, pages 1012–1022, 2002. (Cited in page 13.)

[McMahon *et al.* 2008] A. McMahon, W. Supatto, S.E. Fraser and A. Stathopoulos. *Dynamic Analyses of Drosophila Gastrulation Provide Insights into Collective Cell Migration*. Science, vol. 322, no. 5907, pages 1546–1550, 2008. (Not cited.)

[Miller & Kiehart 1995] K.G. Miller and D.P. Kiehart. *Fly division.* J Cell Biol, vol. 131, pages 1–5, 1995. (Cited in page 14.)

[Miyoshi & Takai 2008] J. Miyoshi and Y. Takai. *Structural and functional associations of apical junctions with cytoskeleton*. Biochimica et Biophysica Acta (BBA) - Biomembranes, vol. 1778, no. 3, pages 670–691, 2008. (Not cited.)

[Mombach *et al.* 1993] J.C. Mombach, R.M. de Almeida and J.R. Iglesias. *Mitosis and growth in biological tissues.* Physical review. E, Statistical physics, plasmas, fluids, and related interdisciplinary topics, vol. 48, pages 598–602, 1993. (Cited in pages 85 and 91.)

[Mooney 1940] M. Mooney. *A Theory of Large Elastic Deformation.* Journal of Applied Physics, vol. 11, page 582â592, 1940. (Cited in page 30.)

[Munoz *et al.* 2007] J.J. Munoz, K. Barrett and M. Miodownik. *A deformation gradient decomposition method for the analysis of the mechanics of morphogenesis.* Journal of biomechanics, vol. 40, pages 1372–1380, 2007. (Cited in pages 41 and 42.)

[Needham 1936] J. Needham. *Order and Life*, 1936. (Cited in page 37.)

[Nesme *et al.* 2005] M. Nesme, M. Marchal, E. Promayon, M. Chabanas, Y. Payan and F. Faure. *Physically realistic interactive simulation for biological soft tissues.* Recent Research Developments in Biomechanics, vol. 2, pages 1–22, 2005. (Cited in page 105.)

[Oda & Tsukita 2000] H. Oda and S. Tsukita. *Real-time imaging of cell-cell adherens junctions reveals that Drosophila mesoderm invagination begins with two phases of apical constriction of cells.* Journal of Cell Science, vol. 114, pages 493–501, 2000. (Not cited.)

[Odell *et al.* 1980] G. Odell, G. Oster, B. Burnside and P. Alberch. *A mechanical model for epithelial morphogenesis.* Journal of Mathematical Biology, vol. 9, no. 3, pages 291–295, 1980. (Cited in page 40.)

[Odell *et al.* 1981] G.M. Odell, G. Oster, P. Alberch and B. Burnside. *The mechanical basis of morphogenesis: I. Epithelial folding and invagination.* Developmental Biology, vol. 85, no. 2, pages 446 – 462, 1981. (Cited in pages 39 and 40.)

[Okuda *et al.* 2013a] S. Okuda, Y. Inoue, M. Eiraku, Y. Sasai and T. Adachi. *Modeling cell proliferation for simulating three-dimensional tissue morphogenesis based on a reversible network reconnection framework.* Biomechanics and Modeling in Mechanobiology, vol. 12, no. 5, pages 987–996, 2013. (Cited in page 87.)

[Okuda *et al.* 2013b] S. Okuda, Y. Inoue, M. Eiraku, Y. Sasai and T. Adachi. *Reversible network reconnection model for simulating large deformation in dynamic tissue morphogenesis.* Biomechanics and Modeling in Mechanobiology, vol. 12, no. 4, pages 627–644, 2013. (Cited in page 88.)

[Paudel *et al.* 2012] G. Paudel, S.J. Owen and S.E. Benzley. *Hexahedral Mesh Refinement Using an Error Sizing Function.* In WilliamRoshan Quadros, editeur, Proceedings of the 20th International Meshing Roundtable, pages 143–159. Springer Berlin Heidelberg, 2012. (Cited in pages 83 and 84.)

[Petitot 2011] J. Petitot. *The Morphogenetic Models of René Thom.* In Paul Bourgine and Annick Lesne, editeurs, Morphogenesis, pages 273–281. Springer Berlin Heidelberg, 2011. (Cited in page 37.)

[Picinbono *et al.* 2000] G. Picinbono, H. Delingette and N. Ayache. *Real-Time Large Displacement Elasticity for Surgery Simulation: Non-Linear Tensor-Mass Model.* In Third International Conference on Medical Robotics, Imaging And Computer Assisted Surgery: MICCAI 2000, pages 643–652, October 2000. (Cited in page 34.)

[Pouille & Farge 2008] Philippe-Alexandre Pouille and Emmanuel Farge. *Hydrodynamic simulation of multicellular embryo invagination.* Physical Biology, vol. 5, no. 1, page 015005, 2008. (Not cited.)

[Promayon *et al.* 2003] E. Promayon, J.L. Martiel and P. Tracqui. *Physically-Based 3D Simulations of Cell Deformations and Migrations.* In W. Alt, M. Chaplain, M. Griebel and J. Lenz, editeurs, Polymer and Cell Dynamics - Multiscale Modeling and Numerical Simulations, pages 125–138. Birkhäuser, December 2003. (Cited in page 46.)

[Promayon 1997] E. Promayon. *Modélisation et Simulation de la Respiration.* PhD thesis, Université Joseph Fourier, 1997. (Cited in page 101.)

[Promayon 2013] E. Promayon. *Modéliser les cellules comme des objets déformables 3D couplant biomécanique et chimie.* chapitre 15, pages 133–154. Éditions Matériologiques, September 2013. (Cited in page 101.)

[Prusinkiewicz & Lindenmayer 1990] P. Prusinkiewicz and A. Lindenmayer. The algorithmic beauty of plants. Springer-Verlag New York, Inc., New York, NY, USA, 1990. (Cited in page 26.)

[Reuter & Leptin 1994] R. Reuter and M. Leptin. *Interacting functions of snail, twist and huckebein during the early development of germ layers in Drosophila.* Development, vol. 120, pages 1137–1150, 1994. (Cited in page 17.)

[Rodriguez *et al.* 1994] E.K. Rodriguez, A. Hoger and A.D. McCulloch. *Stress-dependent finite growth in soft elastic tissues.* Journal of biomechanics, vol. 27, pages 455–467, 1994. (Cited in page 41.)

[Rolland-Lagan *et al.* 2003] A.G. Rolland-Lagan, J.A Bangham and E. Coen. *Growth dynamics underlying petal shape and asymmetry.* Nature, vol. 422, pages 161–163, 2003. (Cited in page 26.)

[Rudge & Haseloff 2005] T. Rudge and J. Haseloff. *A Computational Model of Cellular Morphogenesis in Plants.* In MathieuS. CapcarrÃÂ¨re, AlexA. Freitas, PeterJ. Bentley, ColinG. Johnson and Jon Timmis, editeurs, Advances in Artificial Life, volume 3630 of *Lecture Notes in Computer Science*, pages 78–87. Springer Berlin Heidelberg, 2005. (Cited in page 27.)

[Schejter & Wieschaus 1993] E.D. Schejter and E. Wieschaus. *Functional Elements of the Cytoskeleton in the Early Drosophila Embryo.* Annual Review of Cell Biology, vol. 9, pages 67–99, 1993. (Not cited.)

[Schnakenberg 1979] J. Schnakenberg. *Simple chemical reaction systems with limit cycle behaviour.* J Theor Biol., vol. 81, pages 389–400, 1979. (Cited in page 37.)

[Seher *et al.* 2007] T.C. Seher, M. Narasimha, E. Vogelsang and M. Leptin. *Analysis and reconstitution of the genetic cascade controlling early mesoderm morphogenesis in the Drosophila embryo.* Mechanisms of Development, vol. 124, no. 3, pages 167 – 179, 2007. (Cited in page 17.)

[Sherrard *et al.* 2010] K. Sherrard, F. Robin, P. Lemaire and E. Munro. *Sequential activation of apical and basolateral contractility drives ascidian endoderm invagination.* Current biology, vol. 20, pages 1499–510, 2010. (Cited in page 39.)

[Spahn & Reuter 2013] P. Spahn and R. Reuter. *A Vertex Model of Drosophila Ventral Furrow Formation.* PLoS ONE, vol. 8, no. 9, 2013. (Not cited.)

[Spirov 1993] A.V. Spirov. *The Change of Initial Symmetry in the Pattern-form Interaction Model of Sea Urchin Gastrulation.* Journal of Theoretical Biology, vol. 161, no. 4, pages 491 – 504, 1993. (Cited in page 38.)

[Staple *et al.* 2010] D.B. Staple, R. Farhadifar, J.-C. Röper, B. Aigouy, S. Eaton and F. Jülicher. *Mechanics and remodelling of cell packings in epithelia.* The European Physical Journal E, vol. 33, no. 2, pages 117–127, 2010. (Cited in page 86.)

[Sweeton *et al.* 1991] D. Sweeton, S. Parks, M. Costa and E. Wieschaus. *Gastrulation in Drosophila: the formation of the ventral furrow and posterior midgut invaginations.* Development, vol. 112, pages 775–789, 1991. (Cited in pages 16, 17, 18, 19, 80 and 93.)

[Tayyab *et al.* 2011] M. Tayyab, A. Lontos, E. Promayon and J. Demongeot. *Modelling and Image Processing of Constriction and Proliferation in the Gastrulation Process of Drosophila melanogaster.* In Proc. IEEE Workshops of Int Advanced Information Networking and Applications (WAINA) Conf 2011, pages 473–477, 2011. (Cited in page 57.)

[Tepass & Hartenstein 1994] U. Tepass and V. Hartenstein. *The Development of Cellular Junctions in the Drosophila Embryo.* Developmental Biology, vol. 161, pages 563–596, 1994. (Not cited.)

[Terzopoulos *et al.* 1987] D. Terzopoulos, J. Platt, A. Barr and K. Fleischer. *Elastically deformable models*. SIGGRAPH Comput. Graph., vol. 21, no. 4, pages 205–214, 1987. (Cited in page 32.)

[Tram *et al.* 2001] U. Tram, B. Riggs and W. Sullivan. Cleavage and gastrulation in drosophila embryos. John Wiley & Sons, Ltd, 2001. (Cited in page 14.)

[Turing 1952] A.M. Turing. *The Chemical Basis of Morphogenesis*. Philosophical Transactions of the Royal Society of London. Series B, Biological Sciences, vol. 237, no. 641, pages 37–72, 1952. (Cited in page 37.)

[Waddington 1942] C.H. Waddington. *Observations on the Forces of Morphogenesis in the Amphibian Embryo*. Journal of Experimental Biology, vol. 19, no. 3, pages 284–293, 1942. (Cited in page 1.)

[Waddington 1952] C.H. Waddington. The epigenetics of birds. Cambridge Univ. Press, 1952. (Cited in page 37.)

[Wang *et al.* 2013] M.X. Wang, Y.J. Li, P.Y. Lai and C.K. Chan. *Model on cell movement, growth, differentiation and de-differentiation: Reaction-diffusion equation and wave propagation*. The European Physical Journal E, vol. 36, no. 6, pages 1–18, 2013. (Cited in page 38.)

[Watters 2005] C. Watters. *Video Views and Reviews: Cytokinesis: A Phenomenon Overlooked Too Often*. Cell Biology Education, vol. 4, no. 1, pages 10–18, 2005. (Cited in pages 12 and 13.)

[Wolpert 1969] L. Wolpert. *Positional information and the spatial pattern of cellular differentiation*. Journal of Theoretical Biology, vol. 25, no. 1, pages 1 – 47, 1969. (Cited in page 37.)

[Wyczalkowski *et al.* 2012] M.A. Wyczalkowski, Z. Chen, B.A. Filas, V.D. Varner and L.A. Taber. *Computational models for mechanics of morphogenesis*. Birth Defects Research Part C: Embryo Today: Reviews, vol. 96, no. 2, pages 132–152, 2012. (Cited in page 23.)

[Young *et al.* 2009] P.E. Young, R.C. Pesacreta and D.P. Kiehart. *Dynamic changes in the distribution of cytoplasmic myosin during Drosophila embryogenesis.* Development, vol. 111, pages 1–14, 2009. (Cited in page 14.)

[Zienkiewicz & Taylor 2000] O.C. Zienkiewicz and R.L. Taylor. Finite element method (5th edition). Elsevier, 2000. (Cited in page 30.)

Résumé

L'embryon de la Drosophila Melanogaster subit une série des mouvements cellulaires pendant son développement. La gastrulation est le processus qui décrit la différentiation des futurs tissus à l'intérieur de l'embryon. La gastrulation commence par la formation du sillon ventral, un processus connu sous le nom de "Ventral Furrow Invagination". Pendant ce processus, les cellules de la blastoderme positionnées dans la région ventrale de l'embryon, aplatissent et contractent leur surface apicale jusqu'à ce qu'elles deviennent prismatiques. Ce changement de forme cellulaire aboutit à un enfoncement au niveau de la région ventrale, le sillon ventral, qui est ensuite totalement intériorisé.

Nous focalisons notre étude sur les mécanismes qui conduisent à l'invagination. Les questions principales auxquelles ce travail de thèse essaie de répondre sont: "Quel est le rôle de la contraction apicale des cellules ventrales dans l'invagination?" et "Quel est le mécanisme qui conduit à la clôture ventrale, une fois les cellules ventrales intériorisées?".

Nous essayons de répondre à ces questions d'un point de vue biomécanique. Dans ce but, un maillage 3D de l'embryon de la Drosophila Melanogaster a été créé. Basés sur ce maillage, deux modèles biomécaniques "a minima" de l'embryon de la Drosophila ont été créés: un modèle physique discret et un modèle basé sur la Méthode des Eléments Finis. Les résultats des simulations des deux modèles montrent que la géométrie joue un rôle décisif dans l'intériorisation des cellules ventrales.

Les deux modèles ont permis de simuler l'intériorisation des cellules ventrales mais se trouvent incapables de simuler la clôture ventrale. Notre hypothèse est que la clôture ventrale peut s'expliquer par l'intéraction des forces développées à l'intérieur de l'embryon, une fois que les cellules ventrales commencent à proliférer. Nous proposons une méthode pour diviser des éléments dans un maillage d'éléments finis et ensuite nous expliquons l'intégration de cette méthode dans le modèle des Eléments Finis pour l'embryon de la Drosophila Melanogaster.

Mots-Clés: Biomécanique, Simulation, Méthode des Eléments Finis, Modèle Physique Discret, Mouvements Cellulaires et Déformations, Division Cellulaire.

Abstract

The embryo of the Drosophila Melanogaster undergoes a series of cell movements during its early development. Gastrulation is the process describing the segregation of the future internal tissues into the interior of the developing embryo. Gastrulation starts with the formation of the ventral furrow, a process commonly known as the ventral furrow invagination. During this process, the most ventrally located blastoderm cells flatten and progressively constrict their apical sides until they are wedge shaped. As a result of these cell-shape changes, the blastoderm epithelium first forms an indentation, the ventral furrow, which is then completely internalized.

We focus on the study of the mechanisms that drive the invagination. The main questions that gave birth to this thesis are: "What is the role of the apical constriction of the ventral cells in the invagination?" and "Once the ventral cells are internalized, what is the mechanism that drives the ventral closure?"

We attempt to answer to these two questions from a biomechanical point of view. For this purpose, a 3D mesh of the embryo of the Drosophila Melanogaster has been created. Based on this mesh, two "a minima" biomechanical models of the Drosophila embryo have been created, a physically based discrete model and a model based on the Finite Element Method. The results of the simulations in both models show that the geometry of the embryo plays a crucial role in the internalization of the ventral cells.

The two models efficiently simulate the internalization of the ventral cells but are incapable of reproducing the ventral closure. We hypothesize that the ventral closure can be explained by the interplay of forces developed in the embryo once the internalized ventral cells undergo cell division. We propose an approach to divide elements in a Finite Element Mesh and we integrate it to the Finite Element Model of the Drosophila Melanogaster.

Key-words: Biomechanics, Simulation, Finite Element Method, Physically Based Discrete Model, Cellular Movements and Deformations, Cell Division.